Microbially induced sulphur and carbonate authigenesis in Messinian sulphate-rich strata

Dissertation zur Erlangung des Doktorgrades in den Naturwissenschaften

– Dr. rer. nat. –

vorgelegt

im Fachbereich Geowissenschaften der Universität Bremen

von

Diplom-Geowissenschaftlerin Simone Ziegenbalg

– Januar 2011 –

Tag des öffentlichen Kolloquiums

02. März 2011

Gutachter der Dissertation

Prof. Dr. Jörn Peckmann

Dr. Timothy G. Ferdelman

Prüfer

Prof. Dr. Kai-Uwe Hinrichs

Prof. Dr. Wolfgang Bach

Weitere Mitglieder der Kommission

Dr. Dorothee Wilhelms-Dick

Kevin Becker

…das Geheimnis eines Steines,

außen grau und unscheinbar,

weiß er doch in seinem Inneren

ein Kristall sternenklar…

Gerhard Schöne

*(aus „Die sieben Gaben“)**

PREFACE

The thesis presented here was financed by the German Research Foundation through the International Graduate College Proxies in Earth History ("EUROPROX"), which provided not only my scholarship but also financed the two sampling campaigns in Sicily, my participation on national and international scientific meetings, my attendance on topic-related and soft skill courses, my stay abroad for three weeks at the department of sedimentology of the Vrije Universteit Amsterdam as well as half a year at the department of geodynamics and sedimentology of the University of Vienna and offered me a pleasant and effective time for doing my PhD.

TABLE OF CONTENTS

ABSTRACT

Authigenic carbonates accompanied by native sulphur are present within sulphate-rich deposits all around the world, for example associated to salt dome cap rocks or the evaporitic succession of the Messinian salinity crisis in the Mediterranean. Several authors proposed the involvement of sulphate reducing bacteria in carbonate and sulphur authigenesis, but the pathways of sulphur and carbonate formation are still under discussion and the organisms involved in these diagenetic processes could not be determined so far. Because numerous abandoned sulphur mines still demonstrate the former economic importance of native sulphur for this island, Sicilian sulphur deposits were selected to study the genesis of authigenic carbonate and sulphur. The results are presented in **the first and second manuscript**:

Microbial sulphate reduction results in large sulphur isotope fractionation between the sulphate source and the produced sulphide, reflected in fractionation of up to 60‰ between sulphate and sulphur in the Sicilian samples. The observed variability in carbon and oxygen isotopic composition of the carbonates between the five sampled locations was unexpected. Although the reduction of sulphate led in all locations to deposition of authigenic carbonate and accompanying native sulphur, two distinct modes of that process are differentiable. A) During epigenesist (late-diagenetic) gypsum or anhydrite was dissolved by meteoric waters, providing a sulphate source for bacteria to oxidize mainly crude oil carbon, resulting in carbonates depleted in ^{13}C ($\delta^{13}C$: as low as −29‰) and characterized by low $\delta^{18}O_{carbonate}$ values. B) During syngenesis (early-diagenetic) dissolved sulphate was consumed to oxidize organic carbon, mainly methane, resulting in highly ^{13}C-depleted carbonates ($\delta^{13}C$: as low as −52‰). High $\delta^{18}O$ values and pseudomorphs after lenticular gypsum within the carbonate reveal evaporitic conditions, which is verified by lipid biomarkers namely tetrahymanol, extended archaeol and possibly phytanylglycerol monoethers as well as non-isoprenoidal macrocyclic glycerol diethers. The presence of ^{13}C-depleted archaeal lipids such as PMI and *sn*2-hydroxyarchaeol as well as ^{13}C-depleted molecular fossils of sulphate-reducing bacteria (e.g., *iso*- and *anteiso*-fatty acids) in these syngenetic carbonates led to the conclusion that these carbonates are induced by sulphate-dependent anaerobic oxidation of methane (AOM) and that AOM functions also in hypersaline settings.

The third manuscript describes the application of a modern X-ray diffractometer combined with focussing X-ray optics and a large 2-dimensional detector (μ-XRD^2), which allows the determination of minute minerals directly on uncovered thin section. In contrast to conventional XRD and electron microscopy including EDX, that method allowed the identification of peculiar hair-like crystals in a

sulphur-bearing anhydrite sample from Sicily as gypsum whiskers. These delicate crystals are successfully protected against destruction by embedding in native sulphur. Whisker crystals had not been described before in such settings, according to available literature. Furthermore the study emphasises the utility of μ-XRD^2 for sedimentological studies.

Lacustrine settings are usually low in sulphate and therefore not thought to be influenced by sulphate reduction. Nevertheless, native sulphur accompanied by diagenetic carbonate is present in the lacustrine Hellín basin in southeastern Spain, as reported in **the fourth manuscript**. Here microbial sulphate reduction is crucial for the sulphur precipitation as well, revealed by low sulphur isotope values of the native sulphur (as low as −17‰). The accompanying carbonate, mainly dolomite, is characterized by lamination, which partly resembles biomat structures, and by spheroidal dolomite crystals which indicate a microbial origin, corroborated by low $\delta^{13}C$ values (as low as −11‰). Most interestingly the oxidation of sulphide, which resulted from sulphate reduction, to native sulphur, was most likely carried out by sulphur bacteria, indicated by spheroidal structures bedded in sulphur, which resemble *Thiomargarita* sp. or *Achromatium* sp.. This is important as the oxidation of sulphide to sulphur is still puzzling in most of the sulphur deposits and so far no method is available to clearly solve that question.

KURZFASSUNG

Schwefelführende authigene Karbonate kommen weltweit in vielen sulfatreichen Ablagerungen vor, zum Beispiel in den Deckgesteinen von Salzstöcken oder in den evaporitischen Ablagerungen der Messinischen Salinitätskrise rund um das Mittelmeer. Der Einfluss sulfatreduzierender Mikroorganismen auf die Karbonat- und Schwefelbildung wurde in mehreren Studien an Hand von petrographischen und stabilen Isotopendaten dargelegt. Der Zeitpunkt und Ablauf der Sulfatreduktion konnte jedoch bisher noch nicht abschließend geklärt werden. Ebenso wurden die beteiligten Mikroorganismen bisher nicht näher bestimmt. In Sizilien weisen dutzende verlassene Schwefelminen darauf hin, dass der Schwefelabbau bis zu Beginn des letzten Jahrhunderts in Sizilien eine große Bedeutung hatte. Fünf Lokationen, alle auf dem Gebiet oder in der Nähe ehemaliger Schwefelminen wurden ausgewählt, um die Genese der authigenen Karbonate und des Schwefels zu untersuchen. Die Ergebnisse sind in den Manuskripten eins und zwei dargestellt.

Mikrobielle Sulfatreduktion führt zu einer starken Fraktionierung der Schwefelisotope zwischen der Sulfatquelle und dem produzierten Sulfid. Das spiegelt sich in einer Fraktionierung von bis zu 60‰ zwischen Sulfat und Schwefel in den Sizilianischen Proben wieder. Die Variabilität in der Kohlenstoff- und Sauerstoffisotopie der Karbonate zwischen den einzelnen Lokationen war unerwartet groß. Obwohl Sulfatreduktion in allen Lokationen zur Bildung von authigenem Karbonat und Schwefel führte, lassen sich zwei verschiedene Entstehungswege unterscheiden. A) Während der Epigenese (spät-diagenetisch) werden Gips oder Anhydrite durch meteorische Wässer gelöst und stehen somit den Mikroorganismen als Sulfatquelle zur Verfügung um organischen Kohlenstoff, z.B. Rohöl, zu oxidieren. Die daraus resultierenden Karbonate sind charakterisiert durch eine Abreicherung an ^{13}C und niedrige $\delta^{18}O$-Werte ($\delta^{13}C \geq -29‰$; $\delta^{18}O \geq -4‰$). B) Während der Syngenese nutzen die Mikroorganismen im Porenwasser gelöstes Sulfat um hauptsächlich Methan zu oxidieren. Das führt zur Bildung von sehr stark an ^{13}C-abgereichertem Karbonat ($\geq -52‰$). Hohe $\delta^{18}O$ Werte ($\leq +8‰$) und Pseudomorphosen nach Gips in den Karbonaten zeigen evaporitische Bedingungen an. Lipid-Biomarker (Tetrahymanol, verlängertes Archaeol, sowie höchstwahrscheinlich auch Phytanylglycerol-Monoether und makrozyklische Glycerol-Diether) bestätigen die Existenz von salzliebenden Mikroorganismen während der Karbonatbildung. Der Nachweis von Archaeenlipiden mit niedrigen $\delta^{13}C$-Werten ($\geq -105‰$), wie zum Beispiel PMI und *sn*2-Hydroxyarchaeol, sowie molekularen Fossilien sulfatreduzierender Bakterien mit ähnlich niedrigen $\delta^{13}C$-Werten in den syngenetisch-gebildeten Karbonaten führt zu der Schlussfolgerung, dass die Karbonatbildung durch den Prozess der sulfatabhängigen anaeroben Methanoxidation (AOM) induziert wurde und das AOM auch in hypersalinaren Milieus ablaufen kann.

Das dritte Manuskript beschreibt die Anwendung eines modernen Röntgendiffraktometers in Kombination mit einer fokussierenden Röntgenoptik und einem großen zweidimensionalen Detektor (μ-XRD^2). Diese Technik erlaubt die Untersuchung von sehr kleinen Mineralen direkt auf dem Dünnschliff. Verglichen mit herkömmlicher Röntgendiffraktometrie, sowie der Analyse mit Elektronenmikroskop und energiedispersiver Röntgenspektroskopie war nur diese neue Methode in der Lage feine haarartige Kristalle in schwefelführenden Anhydritproben aus Sizilien als Gips-Whisker zu identifizieren. Diese filigranen Kristalle sind durch ihre Einbettung in Schwefel effektiv geschützt. Bisher wurden solche Gips-Whisker in evaporitischen Ablagerungen nicht beschrieben. Darüber hinaus unterstreicht diese Arbeit die Bedeutung der Mikro-XRD^2 für sedimentologische Studien.

Elementarer Schwefel und diagenetische Karbonate aus dem lakustrinen Hellín Becken im Südosten Spaniens sind im vierten Manuskript beschrieben. Weil lakustrine Milieus normalerweise niedrige Sulfatkonzentrationen aufweisen, spielt die bakterielle Sulfatreduktion hier meist eine untergeordnete Rolle. Im Hellín Becken allerdings dienen im Untergrund befindliche Triassische Gipse als Sulfatquelle. Niedrige Schwefelisotope des Schwefels (≥ −17‰) zeigen das Sulfatreduzierer an der Schwefelbildung beteiligt waren. Das Karbonat, hauptsächlich Dolomit, zeigt eine biomattenartige Lamination. Spheroidale Dolomitkristalle legen ebenso einen mikrobiellen Ursprung nahe. Das wird untermauert durch niedrige δ^{13}C Werte (≥ −11‰). Die Oxidation von Sulfid zu Schwefel erfolgte höchstwahrscheinlich durch Schwefelbakterien, da es sich bei den im Schwefel eingebetteten spheroidalen Strukturen höchstwahrscheinlich um fossilisierte Zellen von *Thiomargarita* sp. oder *Achromatium* sp. handelt. Das ist von großer Bedeutung, da für die meisten Schwefelvorkommen nach wie vor ungeklärt ist, auf welchem Weg das Sulfid zu Schwefel oxidiert wird.

1 - INTRODUCTION

1.1 Sulphur

1.1.1 Sulphur and the sulphur cycle

Sulphur is the fourteenth most abundant element in the Earth's crust. It mainly occurs as sulphide or sulphate with valence states -2 and +6 respectively, but it is also present as native sulphur (S^0) or intermediately in valence states of +2 and +4. This variability in valence states allows its participation in various reactions and makes sulphur an important redox partner for biochemical processes. Sulphate is the second most abundant anionic complex in seawater (behind chloride) with average concentrations of about 2649 ppm. If oxygen is depleted due to mineralization of organic matter in the water column or the upper sediment, other electron acceptors takes up the role of oxygen as principal electron acceptor, namely nitrate, manganese and iron. Mainly sulphate reducing bacteria undertake the task from aerobic heterotrophic organisms under anaerobic conditions, due to the ubiquitous presence of sulphate in sea- and pore-water (e.g., Jørgensen, 1982; Ferdelman et al., 1999). Sulphate reducing bacteria are able to oxidise organic matter including crude oil compounds (Rueter et al., 1994; Heider et al., 1999; Rabus, 2005 and references therein). The sulphate is reduced to sulphide, and bicarbonate is produced according to the following net-equation ([I]; e.g., Coleman and Raiswell, 1995).

[I] $2CH_2O + SO_4^{2-} \rightarrow 2HCO_3^- + H_2S$

Sulphate-reducing bacteria, which are able to use methane as carbon source directly, are not known so far. The process of sulphate-dependent anaerobic oxidation of methane (AOM) mediated by a consortium of methanotrophic archaea and sulphate-reducing bacteria couples the oxidation of methane with sulphate reduction according to the following net-equation ([II]; e.g., Hoehler et al., 1994; Boetius et al., 2000).

[II] $CH_4 + SO_4^{2-} \rightarrow HCO_3^- + HS^- + H_2O$

Sulphate is abiologically reduced by thermochemical sulphate reduction (TSR) in settings characterized by temperatures above 80°C (mainly between 100 and 140°C; Machel et al., 1995; Worden et al., 1995, 1997; Machel 2001).

Subsequently sulphide is either precipitated as metal sulphide, if sufficient metal ions are available, or it is oxidized biologically or abiologically to native sulphur or further to sulphate. Purple sulphur bacteria oxidize hydrogen sulphide by anaerobic photosynthesis to native sulphur which is stored as small globules inside the cells (Madigan and Martinko, 2009). Chemolithotrophic sulphur-oxidizing bacteria or so called colourless sulphur bacteria, e.g., the spherical *Achromatium* and *Thiomargarita* or the filamentous *Beggiatoa*, oxidize hydrogen sulphide to native sulphur with oxygen or nitrate (Schulz and Jørgensen, 2001). Like the photosynthetic sulphur bacteria, they store native sulphur within the cell and may further oxidize it to sulphate if sulphide is temporary not sufficiently available (Ferdelman et al., 1997; Schulz and Jørgensen, 2001). Without the activity of microorganisms sulphur is suggested to be produced by synproportionation, which is the reaction of hydrogen sulphide with sulphate (Feely and Kulp, 1957). Davis et al., (1970) queries however, that synproportionation occurs at temperatures below 70°C. Instead, these authors suggested abiological sulphide oxidation with oxygen leading to sulphur precipitation.

1.1.2 Application of sulphur and oxygen isotopes in sulphur species

Sulphur has four stable isotopes ^{32}S, ^{33}S, ^{34}S, ^{36}S with relative abundances of 94.99%, 0.75%, 4.25% and 0.01%, respectively (De Laeter et al., 2003). For studies concerning isotope fractionation between naturally occurring sulphur containing phases, the ^{32}S and ^{34}S isotopes are mainly considered. Recently, higher precision techniques increase the importance of ^{33}S and ^{36}S (e.g., Ono, 2008). Sulphur isotopic composition is given in δ-notation according to the following equation relative to the standard material, a troilite (i.e., iron monosulphide) from the Cañon Diabolo meteorite (Cañon Diabolo troilite, CDT; Ding et al., 2001):

[III] $$\delta^{34}S_{CDT}\ (‰) = [(^{34}S/^{32}S)_{sample} / (^{34}S/^{32}S)_{CDT} - 1] * 10^3$$

The CDT was recently substituted by Vienna-CDT, which is based on the new sulphide reference material IAEA-S-1 (De Laeter et al., 2003). The ratio between the isotopic compositions of two phases A and B (R_A and R_B) is given as fractionation factor α, which is defined as:

[IV] $$\alpha_{A-B} = R_A / R_B$$

The isotope enrichment or separation factor ε describes the differences between the isotopic compositions of two phases in per mill, given as:

[V] $$\varepsilon = \alpha - 1 * 1000$$

It has long been known that sulphate reducing bacteria are able to fractionate sulphur isotopes (e.g., Jones and Starkey, 1957; Harrison and Thode, 1958; Kaplan and Rittenberg, 1964). They

preferentially use sulphate containing the light sulphur isotope and reduce it to sulphide, resulting in an enrichment of light sulphur isotopes in the reduced sulphur species relative to the sulphate. A fractionation of up to 46‰ between sulphide and the sulphate source in culture studies was suggested to be the upper limit of bacterial sulphate reduction (Kaplan and Rittenberg, 1964; Kemp and Thode, 1968; Habicht and Canfield, 1996). Sedimentary sulphide, however, is even more depleted compared to marine sulphate in some locations (e.g., Fry et al., 1991; Wortmann et al., 2001). Some authors recommend an oxidative step to be responsible for these high fractionation effects, namely the disproportionation (Jørgensen, 1990; Canfield and Thamdrup, 1994; Habicht and Canfield, 2001). Sulphur-disproportionating bacteria use various sulphur intermediates as native sulphur, sulphite or thiosulphate to produce contemporaneously both oxidized and reduced sulphur species (Canfield and Thamdrup, 1994; Cypionka et al., 1998; Finster et al., 1998; Habicht et al., 1998; Böttcher et al., 2001). If followed by sulphide oxidation, a cycling is initiated which may cause huge fractionation between the sulphate-source and reduced sulphur species (Jørgensen, 1990; Canfield and Thamdrup, 1994). Nevertheless, a recent model by Brunner and Bernasconi (2005) proposed that bacterial sulphate reduction alone can achieve a fractionation as high as 70‰.

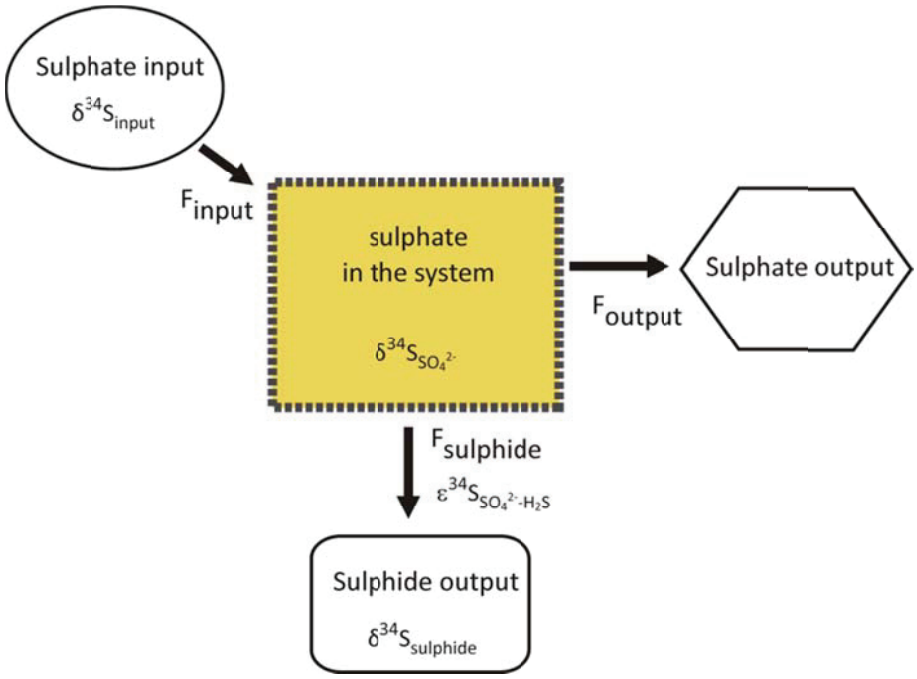

Fig. 1-1 Sulphur fluxes in and out of a system of interest (by courtesy of Ben Brunner, Bremen)

The expression of isotope fractionation effects by sulphate reduction in sulphur bearing phases (i.e., sulphates, sulphides, native sulphur) strongly depends on the sulphur fluxes in and out of the system of interest, where the sulphate reduction takes place (Figure 1-1). If the rate of sulphate reduction is similar to the flux of sulphate into the investigated system ($F_{sulphide} \approx F_{input}$), the sulphur isotopic composition of the resulting sulphide is similar to that of the sulphate source ($\delta^{34}S_{sulphide} \approx$

$\delta^{34}S_{input}$). Fractionation during sulphate reduction enriches the sulphate in the system in ^{34}S compared to the sulphate source ($\delta^{34}S_{SO_4^{2-}} > \delta^{34}S_{input}$). If though the rate of sulphate reduction is much smaller than the influx of sulphate into that system ($F_{sulphide} < F_{input}$), fractionation between sulphate and sulphide is large, leading to ^{34}S-depleted sulphide ($\delta^{34}S_{sulphide} < \delta^{34}S_{SO_4^{2-}}$). The sulphur isotopic composition of the sulphate in the system is nearly unchanged compared to the sulphate source ($\delta^{34}S_{SO_4^{2-}} \approx \delta^{34}S_{input}$). The fractionation during sulphate reduction ($\varepsilon^{34}S_{SO_4^{2-}-H_2S}$) can therefore be estimated by the difference in sulphur isotopic composition between the produced sulphide and the sulphate present in the system. To study the genesis of native sulphur deposits, it is worthwhile to analyse the isotopic composition of sulphate entering the system, sulphate in the system and the produced sulphide.

Evaporitic gypsum or anhydrite may provide the sulphur isotopic composition of the sulphate source. The sulphur isotopic composition of sulphide can be derived from the sulphur isotopic composition of native sulphur, if not preserved in form of pyrite or other sulphide minerals. There is only a small fractionation effect during bacterial oxidation from sulphide to native sulphur (Fry et al., 1986). The sulphur isotope exchange between native sulphur and sulphide is rapid (Fossing, 1995) and comprises only a small isotope equilibrium fractionation (Ohmoto and Rye, 1979). As the sulphate in the system cannot be measured directly, the $\delta^{34}S$ of carbonate associated sulphate (CAS) is applied as proxy here. CAS occurs in trace amounts in carbonates. There it substitutes carbonate ions in the crystal lattice (Pingitore et al., 1995). Although the concentration of CAS in the carbonates may be influenced, the sulphur isotopic composition is found to be stable also in case of diagenetic processes (Lyons et al., 2004; Gill et al., 2008). Therefore, CAS is a valuable and elegant proxy of the sulphur isotopic composition of sulphate present in the sea or pore water contemporaneous to carbonate precipitation.

The oxygen isotopes of sulphate species are given in δ-notation, calculated relative to the standard Vienna-Standard mean ocean water (V-SMOW) corresponding to equation [III]. Similar to $\delta^{34}S$, the $\delta^{18}O$ of sulphate also mirrors bacterial sulphate reduction since both fractionation processes are positively correlated. Sulphate reducing bacteria preferentially utilize sulphate with ^{16}O, leading to ^{18}O-enrichment in the residual dissolved sulphate (Lloyd, 1968; Mizutani and Rafter, 1973; Böttcher et al., 1998, 1999; Brunner et al., 2005). Gypsum and anhydrite, which precipitate from a solution that is influenced by intense microbial sulphate reduction, are therefore characterized by elevated $\delta^{34}S$ and $\delta^{18}O$ values.

1.2 Authigenic carbonates

The influence of microorganisms on carbonate precipitation has long been proposed. In laboratory experiments the activity of sulphate-reducing bacteria increased the bicarbonate and carbonate concentration and therewith the alkalinity (Abd-el-Malek and Rizk, 1962a, b). Some authors remark that the ability of dissimilatory sulphate reduction to precipitate carbonate is dependent on the presence and behaviour of the produced sulphide (Castanier et al., 2000, Soetaerd et al., 2007). If sulphide is neither used by e.g., sulphide oxidizing microorganisms nor precipitated as metal-sulphides or degassed, it leads to a decrease in pH and hence inhibits carbonate precipitation (Castanier et al., 2000; cf., Soetaerd et al., 2007). Nevertheless culture studies of sulphate reducing bacteria substantiated their crucial role in the production of bicarbonate and subsequent carbonate precipitation in a variety of environments (Van Lith et al., 2003; Dupraz et al., 2004; Aloisi et al., 2006). For the sulphur bearing settings I suppose that the transformation of sulphide into native sulphur likewise prevents the lowering in pH, and consequently permits carbonate precipitation. Sulphate-dependent AOM, however, in any case favours carbonate authigenesis as this process in general increases the alkalinity (Soetaerd et al., 2007).

The influence of microbial processes on carbonate authigenesis is reflected by the carbon isotopic composition of the carbonate minerals. The $\delta^{13}C_{carbonate}$ is dependent on the pool of carbon from which the carbonate precipitated. Marine dissolved inorganic carbon (DIC) is characterized by a $\delta^{13}C$ of approximately +1‰ (Kroopnick et al., 1972). This value fits quite well to $\delta^{13}C$ values measured for a number of different marine carbonates ($\delta^{13}C$: −3 to +2‰; Craig, 1953). If heterotrophic processes produce additional bicarbonate, the $\delta^{13}C_{carbonate}$ will be shifted towards the carbon isotopic composition of the carbon sources, which are typified by specific $\delta^{13}C$ ranges. Marine organic matter shows a characteristic depletion in ^{13}C compared to DIC by about 20 to 25‰ ($\delta^{13}C$ for marine plankton from mid-latitudes: −25 to −20‰; Sackett et al., 1965). The majority of crude oils is even more depleted in ^{13}C ($\delta^{13}C$: −30 to −26‰; Eckelmann et al., 1962). Methane is the most depleted carbon compound with $\delta^{13}C$ of −50 to −20‰ for thermogenic and −110 to −50‰ for biogenic methane (Whiticar, 1999). Carbonate, which resulted from the oxidation of methane by AOM, is characterized by $\delta^{13}C$ values as low as −76‰ (Campbell, 2006).

Stable isotope composition of carbonates and sulphur compounds can be considered as indirect biological markers of biological processes. Compared to that, lipid biomarkers are direct biological markers of biosynthetic origin. Depending on their taxonomic specificity and their preservation potential, they can be regarded as molecular fossils. Some of them are even stable enough to outlast hundreds of Millions of years (e.g., Brocks et al., 2003). Lipid biomarkers also provide information about environmental parameters as temperature, salinity, pH, and nutrients, to which the organisms

are adapted to. Additionally they can be applied to identify chemical processes, in which the organisms participate (see table 1-1). Lipid biomarkers are potentially well preserved in authigenic carbonates. Here they offer information about the organisms which induced the carbonate precipitation and moreover they archive the microbial ecosystem that was active contemporaneous to authigenesis (e.g., Peckmann and Thiel, 2004; Birgel et al., 2006a, 2008b).

Table 1-1: Examples of lipid biomarkers and their putative source organisms.

Lipid	Putative source	Reference
Pentamethylicosane (PMI)	halophilic methanogenic archaea	Holzer et al., 1979; Tornabene et al., 1979
PMI, ^{13}C-depleted	methanotrophic archaea	Elvert et al., 1999; Peckmann et al., 1999b, 2009; Thiel et al., 1999, 2001; Pancost et al., 2000; Birgel et al., 2008b
Crocetane, ^{13}C-depleted	methanotrophic archaea	Elvert et al., 1999; Thiel et al., 1999; Blumenberg et al., 2004
Archaeol	archaea, e.g., halophilic methanogenic archaea	Tornabene and Langworthy, 1979; De Rosa and Gambacorta, 1988; Kates, 1993; Koga et al., 1993, 1998
Archaeol, ^{13}C-depleted	methanotrophic archaea, *Methanosarcinales*	Hinrichs et al., 1999
Hydroxyarchaeol, ^{13}C-depleted	methanotrophic archaea	Hinrichs et al., 1999, 2000; Pancost et al., 2000; Blumenberg et al., 2004; Niemann and Elvert, 2008
Extended archaeol (O-phytanyl-O-sesterterpanyl glycerolether)	halophilic archaea	Teixidor et al., 1993
Monoalkyl glycerolethers (MAGEs), Dialkyl glycerolethers (DAGEs)	sulphate reducing bacteria	Hinrichs et al., 2000; Orphan et al., 2001a; Pancost et al., 2001a; Werne et al., 2002
iso- and *anteiso*-$C_{15:0}$ and $C_{17:0}$ fatty acid	sulphate reducing bacteria	Taylor and Parkes, 1983; Edlund et al., 1985; Dowling et al., 1986; Hinrichs et al., 2000; Orphan et al., 2001a; Rütters et al., 2001, 2002; Elvert et al., 2003; Könneke and Widdel, 2003; Pape et al., 2005; Birgel et al., 2006a; Niemann and Elvert, 2008
iso-$C_{16:0}$ fatty acid	sulphate reducing bacteria	Taylor and Parkes, 1983; Dowling et al., 1986; Coleman et al., 1993; Könneke and Widdel, 2003; Londry et al., 2004; Hinrichs et al., 2000; Elvert et al., 2003

Molecular fossils are especially useful to detect recent and ancient bacterial sulphate reduction as well as sulphate-dependent AOM as both sulphate-reducing bacteria and methane-oxidizing archaea produce specific lipids (see table 1-1; e.g., Taylor and Parkes, 1985; Hinrichs et al., 1999; Thiel et al., 1999; Rütters et al., 2002; Elvert et al., 2003; Peckmann and Thiel, 2004; Niemann and Elvert, 2008). Lipids derived from microorganisms involved in AOM are furthermore characterized by a significant depletion in ^{13}C due to the uptake of methane (e.g., Elvert et al., 1999; Hinrichs et al., 1999; Thiel et al., 1999; Peckmann and Thiel, 2004 and references therein).

1.3 Authigenic sulphur and carbonate deposits with focus on Sicily and Spain

Biogenic native sulphur deposits are widely distributed on earth (Fig. 1-2). They are usually associated to authigenic carbonates and occur always in sulphate rich settings or strata. Most prominent areas of sulphur deposits are the Gulf of Mexico area, with its various salt domes (Fig. 1-2, no. 3a,b and 4; e.g., Feely and Kulp, 1957; Davis and Kirkland, 1979; Ruckmick et al., 1979) and the Mediterranean area (Fig. 1-2, no. 5, 8, 9, 12; e.g., Rouchy et al., 1998; Nissenbaum and Kaplan, 1966; Nissenbaum 1980; Hunt, 1915; Dessau et al., 1962; Decima et al., 1988). While in the Gulf of Mexico area sulphur formation is closely related to the formation and diagenesis of salt dome cap rocks, in the Mediterranean area it is bound to evaporitic deposits of the Messinian.

The Messinian salinity crisis, one of the most important evaporitic events in earth history, had huge impact on the Mediterranean area. The deposition of the Lower Evaporites marks the onset of the crisis at 5.9 Ma (Krijgsman et al., 1999), which was initiated by a progressive separation of the Mediterranean Sea from the Atlantic Ocean (e.g., Duggen et al., 2003; Jolivet et al., 2006), superimposed by eccentricity-controlled regional climate changes (Krijgsman et al., 1999, 2007). The subsequent development of restricted and evaporative conditions led to the deposition of complete evaporitic series, including carbonates, sulphates, halite and bittern salts in the deep Mediterranean basins (Hsü et al., 1973a) as well as in Sicily (Decima and Wezel, 1973). In Sicily the transition from pre-evaporitic conditions towards pronounced evaporitic conditions is marked by a diatomite unit (Tripoli). The carbonate, which is described as first, basal evaporitic deposit is named ‘Calcare di Base’. It is overlain by huge amounts of Messinian gypsum. The sulphur-bearing limestone (‘Calcare Solfifero’) is described as subunit of the basal limestone or resting on top of it (Dessau et al., 1962; Decima et al., 1988).

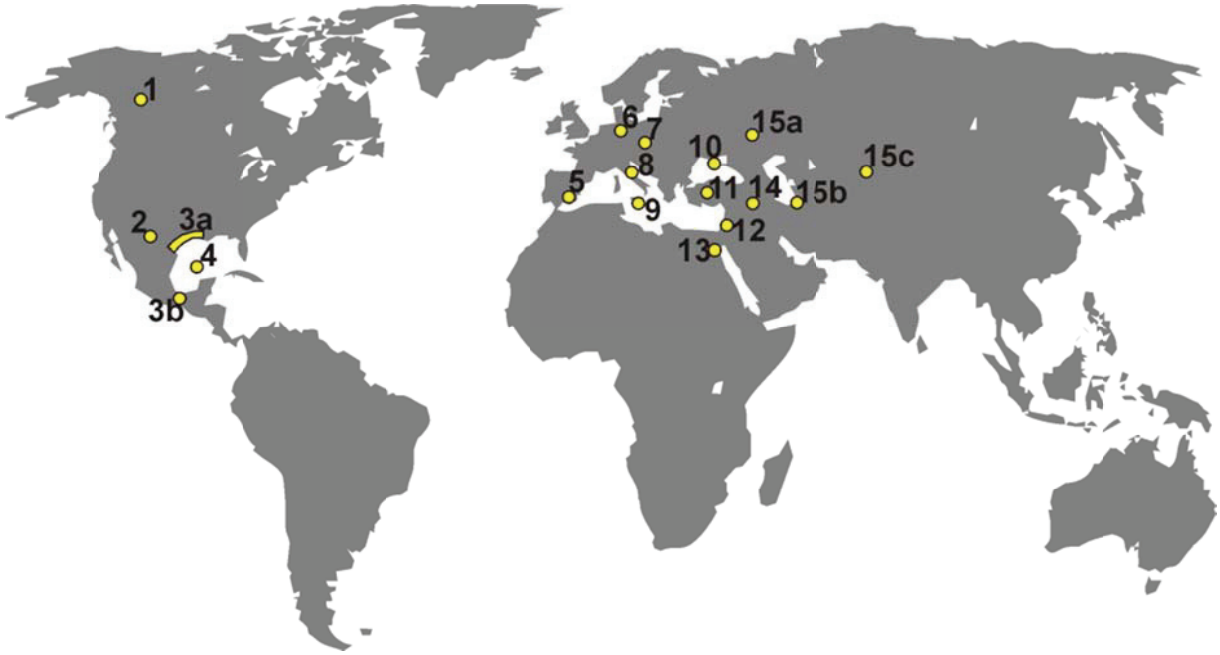

Fig. 1-2 Global distribution of described biogenic sulphur deposits; 1) Western Canadian Sedimentary Basin of Alberta and British Columbia: Hora and Hamilton, 1992; 2) Permian Rocks of the Delaware Basin, West Texas, Culberson County, Castile, Salado and Rustler Formation: Davis and Kirkland, 1970; Kirkland and Evans, 1976; Davis and Kirkland, 1979; Ruckmick et al., 1979; Klemmick, 1992; Salisbury, 1992; Wallace and Crawford, 1992; 3a, b) Salt dome cap rocks along the northern and southern coast of the Gulf of Mexico: Feely and Kulp, 1957; Davis and Kirkland, 1979; Ruckmick et al., 1979; Samuelson, 1992; 4) Challenger Knoll salt dome: Davis and Kirkland, 1979; 5) Messinian basins in southern Spain (Lorca, Hellín, Teruel): Servant-Vildary et al., 1990; Anadón et al., 1992; Rouchy et al., 1998; Ortí et al., 2010; 6) Salt diapir of Weenzen, Germany: Schneider and Nielsen, 1965; 7) Northern Carpathian foredeep in Poland; Cis-Carpathian area, Ukraine: Ivanov, 1968; Pawlowski et al., 1979; Niec,1992, Böttcher and Parafiniuk, 1998; Gasiewicz, 2000; 8) Northern Apennines, Perticara: Roveri et al., 2006; 9) Sicily: Hunt, 1915 ; Dessau et al., 1962 ; Decima et al., 1988; 10) Kerch Peninsula, Ukraine: Lein et al., 1975; 11) Turkey : Tekin et al., 1999; Tekin, 2006; 12) the southeastern coast of the Mediterranean Sea, southern Israel (e.g., Beeri) and northern Egypt (Sinai peninsula): Nissenbaum and Kaplan, 1966; Nissenbaum 1980; Druckmann et al., 1994; Burhan et al., 2002; 13) Ras Gemsa peninsula, Egypt: Schnellmann 1959; Youssef, 1989; 14) Stratabound deposits of northern Iraq, e.g., Mishraq: Barker et al., 1979; Jassim et al., 1999; 15a,b,c) some of the sulphur deposits situated in the area of the former USSR: Ivanov, 1968 a) Vodino deposits, Russia, b) Krasnovodsk, Turkmenistan, c) Shor-Su, Usbekistan

Referring to a first detailed laboratory study of sulphate reducing bacteria by Beyerinck (1895), Hunt (1910) suggested for the first time a bacterial origin for the Sicilian sulphur deposits (Fig. 1-2, no. 9). Later this interpretation was applied to many other sulphur deposits. Low $\delta^{34}S$ values of native sulphur and elevated $\delta^{34}S$ values of associated gypsum mirror sulphur isotopic fractionation by sulphate reducing bacteria (e.g., Thode et al., 1954; Feely and Kulp, 1957; Schneider and Nielsen, 1965). Low $\delta^{13}C$ values of sulphur-associated carbonate reveal its origin from ^{13}C depleted carbon derived from the oxidation of organic matter or crude oil (Peckmann et al., 1999a) or even methane (Cheney and Jensen, 1965; Kirkland and Evans, 1976; Böttcher and Parafiniuk, 1998).

Two different models of sulphur and carbonate precipitation are defined (Ruckmick et al., 1979): A) Syngenetic deposition: During sedimentation or early diagenesis sulphate reducing bacteria might

have used sulphate that is dissolved in the sea- or pore-waters, similar to processes in recent sediments (cf., Jørgensen, 1982). Evaporation may have even increased the sulphate concentration. Sulphate reducers oxidize organic detritus (see [I]) or they join anaerobic methanotrophic archaea to mediate sulphate-dependent AOM (see [II]). The methane may therefore derive either from thermogenic sources (cf., Orphan et al., 2004) or from methanogens, active in the sediments below (cf., Hoehler et al., 1994). B) Epigenetic deposition: Much later after burial and subsequent uplift, gypsum, anhydrite or even celestine may be dissolved by meteoric waters, providing sulphate ions for bacterial sulphate reduction (e.g., Feely and Kulp, 1957; Davis and Kirkland, 1970; Böttcher and Parafiniuk, 1998; Peckmann et al., 1999a; Tekin et al., 1999). Hereby they oxidize most likely crude oil compounds. The epigenetic model obviously describes the formation of salt dome cap rock sulphur deposits. This model was applied to most of the fossil deposits, while the syngenetic model is assumed to be only true for recent sedimentary systems (Wessel, 1994). In contrast Dessau et al., (1962) favoured a syngenetic origin for most if not all Sicilian sulphur deposits. They describe the sulphur-bearing limestone beds as mainly uniformly bedded, lacking intergrowths between limestone and unreduced sulphate, which would be expected for epigenetic deposits. A most recent paper, however, described the 'Calcare solfifero' to be formed by bacterial reduction of clastic gypsum in a late diagenetic stage (Manzi et al., 2010).

In Spain sulphur-bearing carbonates are present in small marginal Neogene basins characterized by either marine or lacustrine deposits (Fig. 1-2, no. 5). In the marine Lorca basin the microbially induced sulphur and secondary carbonate precipitation is associated with meteoric dissolution of abundant gypsum present in the organic-rich diatomitic succession (Rouchy et al., 1998). Sulphur in the lacustrine Teruel basin is reported to be early diagenetic but derived from the dissolution of primary gypsum and associated to the replacement of sulphate minerals by carbonate (Anadón et al., 1992; Ortí et al., 2010); and thus must be regarded as epigenetic deposit as well. In the Hellín basin, another lacustrine basin, native sulphur was produced from dissolved sulphate during anoxic conditions in the water column (Servant-Vildary et al., 1990). In contrast to Lorca and Sicily for example no marine evaporites are precipitated during the Messinian in that lacustrine basin. Instead, the sulphate for both gypsum precipitation and bacterial sulphate reduction derived from the weathering of Triassic gypsum located in the basement (Servant-Vildary et al., 1990; Utrilla et al., 1992).

2 - Objectives and outline of the thesis

Native sulphur deposits have been intensively studied in the first half of the last century, a time when natural sulphur deposits were economically important and sulphur mines were in use. Nowadays sulphur is a by-product of natural gas and petroleum refining. The sulphur mines are closed, but the scientific investigation of native sulphur is again of rising interest as meanwhile methods evolved like the analysis of molecular fossils and compound-specific carbon isotope measurements, which are proposed to increase the understanding of the genesis of native sulphur deposits. The microbially driven sulphur cycle is not only one of the most important element cycles in marine sediments but also a very ancient one (Wagner et al., 1998; Canfield and Raiswell, 1999, Shen et al., 2001; Shen and Buick, 2004). Shen et al. (2001) suggested that microbial sulphate reduction was active as early as 3.47 Ga. The biogenic native sulphur deposits present on earth are obviously very impressive signs of the huge impact of sulphur cycling in the geological record. However, although there are many recent studies about bacterial sulphate reduction in all types of sediments, the native sulphur deposits were currently not investigated in such a detail. Research on the microbial community involved in sulphur and carbonate precipitation by application of lipid biomarker methods are scarce (Peckmann et al., 1999a; Burhan et al., 2002).

Since Sicily used to be the world's leading sulphur producer at the beginning of the last century, which is still visible by means of numerous sulphur mines, we decided to examine the Sicilian sulphur deposits for a new study on microbial sulphur deposition. For the present study, five locations in Sicily, all related to former sulphur mines, were studied. Samples were subjected to a multiproxy study, including petrography, stable carbon, oxygen and sulphur isotopes as well as lipid biomarker studies and compound specific carbon isotope analyses to achieve the following main objectives of the presented theses:

- Verify the biogenicity of both native sulphur and authigenic carbonate, concerning all indirect and direct biomarkers as described above and determine the microorganisms, which are responsible for sulphur and carbonate precipitation, including their metabolic pathways and carbon sources.
- Solve the controversy about the pathway and timing of precipitation of the Sicilian sulphur and carbonate deposits: are they either syngenetic as proposed by Dessau et al. (1992) or epigenetic as proposed by others (Ruckmick et al., 1979; Manzi et al., 2010).
- Describe the microbial ecosystem, in which these processes occurred.
- Compare authigenic sulphur and carbonate deposits of marine and lacustrine origin.

These objectives are addressed in four manuscripts presented in the following chapters.

Chapter 3:

Formation of secondary carbonates and native sulphur in sulphate-rich Messinian strata, Sicily. Ziegenbalg SB, Brunner B, Rouchy JM, Birgel D, Pierre C, Böttcher ME, Caruso A, Immenhauser A, Peckmann J, *Sedimentary Geology* **227** 37-50.

In a first overview the five sampling locations and the petrography of the samples were described. The biogenicity of the native sulphur was proven by means of strong sulphur and oxygen isotope fractionation between carbonate associated sulphate and sulphate minerals on the one hand and native sulphur on the other hand. The microbial impact on the authigenesis of the carbonates is obvious by means of low $\delta^{13}C$ values. Most surprising was the variability in $\delta^{13}C_{carbonate}$ and $\delta^{18}O_{carbonate}$ between the different locations. Leading to the conclusion that dependent on the location I) the carbon sources for bacterial sulphate reduction varied from organic matter and crude oils to highly ^{13}C-depleted methane and II) sulphur and carbonate were deposited during syn- and epigenesis, which is also displayed by the petrography. While syngenesis occurred within restricted, hypersaline conditions, mirrored by enrichment in ^{18}O and pseudomorphs after lenticular gypsum within the carbonate, epigenetic deposits are characterized by meteoric dissolution of gypsum, as revealed by low $\delta^{18}O$ values.

I performed and interpreted the petrographical analyses, prepared samples for XRD and electron-microscopy analyses as well as for the determination of elemental and isotopic composition. I interpreted the XRD-, element-, electron-microscope and $\delta^{13}C_{carbonate}$ and $\delta^{18}O_{carbonate}$ data. I interpreted the $\delta^{34}S_{sulphur\ and\ sulphate}$ and $\delta^{18}O_{sulphate}$ data with support of Ben Brunner and wrote the manuscript with the help of Jörn Peckmann and Ben Brunner and with editorial comments of all co-authors.

Chapter 4:

Anaerobic oxidation of methane in hypersaline Messinian environments revealed by ^{13}C-depleted molecular fossils. Ziegenbalg SB, Birgel D, Hoffmann-Sell L, Pierre C, Rouchy JM, Peckmann J, to be submitted to *Chemical Geology*.

Lipid biomarkers and compound specific carbon isotopes from samples of two selected locations from Sicily were analyzed and compared to another site of Messinian deposits in the northern Apennines, where carbonate was deposited under similar restricted conditions. Results verify the conclusions of the first manuscript, that sulphate reducing bacteria are involved in the precipitation

of the carbonates. Furthermore the results elucidate the process by which methane derived carbon was incorporated into the carbonate, namely the sulphate-dependent anaerobic oxidation of methane. This study reveals that sulphate-dependent AOM was occurring in hypersaline conditions.

I prepared samples for analyses, performed laboratory work of the Sicilian samples with the help of Daniel Birgel, processed and interpreted the data with supported by Daniel Birgel and wrote the manuscript supported by Daniel Birgel and Jörn Peckmann, and with editorial comments of all co-authors.

Chapter 5:

Gypsum whiskers in Messinian evaporites identified by μ-XRD^2. Ziegenbalg SB, Berthold C, Kappler A, Peckmann J, *Facies*, DOI 10.1007/s10347-010-0237-x.

Delicate hair-like minerals present in samples from one of the former described locations were identified as gypsum whiskers with a new sophisticated method, the μ-XRD^2. This technique allows the non-destructive determination of the mineralogy of small crystals within their context directly on the thin section. Not even the unevenness of the thin sections, due to the prior dissolution of native sulphur interfered with the measurements, making that technique a useful tool not only for our studies.

I prepared samples for XRD, electron-microscopy and μ-XRD^2 analyses, interpreted the data, with support of Christoph Berthold concerning the μ-XRD^2 data and wrote the manuscript with the help of Jörn Peckmann and editorial comments of all co-authors.

Chapter 6:

Authigenesis of native sulphur and dolomite in a lacustrine evaporitic setting (Hellín Basin, Late Miocene, SE Spain). Lindtke J, Ziegenbalg SB, Brunner B, Rouchy J-M, Pierre C, Peckmann J, *Geological Magazine* (accepted).

As sulphate reduction usually occurs in marine settings due to the ubiquitous presence of sulphate, it was of high interest to investigate a biogenic sulphur deposit in a lacustrine basin, where sulphate is typically rare. Sulphur isotope values of native sulphur are low compared to the sulphate source, which is derived from the weathering of Triassic gypsum, providing evidence that the precipitation of native sulphur is induced by sulphate reducing bacteria. Sulphate present in the samples is secondary derived from the oxidation of native sulphur, partially accompanied by replacement of carbonates by gypsum. The presence of putative fossilized spherical bacteria,

enclosed in native sulphur, indicate that the oxidation of sulphide, produced by bacterial sulphate reduction, to native sulphur might be performed by sulphide oxidizing bacteria like *Achromatium* sp..

I contributed to the interpretation of petrographical and stable isotope data, helped substantially preparing the outline and writing the manuscript, and gave editorial comments.

3 - FIRST MANUSCRIPT

Formation of secondary carbonates and native sulphur in sulphate-rich Messinian strata, Sicily

S.B. Ziegenbalg[1], B. Brunner[2], J.M. Rouchy[3], D. Birgel[1], C. Pierre[4], M.E. Böttcher[5], A. Caruso[6], A. Immenhauser[7], J. Peckmann[1]

[1] MARUM, Universität Bremen, 28359 Bremen, Germany

[2] Max-Planck-Institut für Marine Mikrobiologie, 28359 Bremen, Germany

[3] Département Histoire de la Terre, Muséum National d'Histoire Naturelle, 75005 Paris, France

[4] CNRS-UMR 7159, LOCEAN, Univ. P. et M. Curie, 75252 Paris Cedex 05, France

[5] Leibniz Institut für Ostseeforschung Warnemünde, 18119 Warnemünde, Germany

[6] Dipartimento di Geologia e Geodesia, Università degli Studi di Palermo, 90123 Palermo, Italy

[7] Ruhr-Universität Bochum, Institut für Geologie, Mineralogie und Geophysik, 44801 Bochum, Germany

Corresponding author: Jörn Peckmann (joern.peckmann@univie.ac.at)

Keywords: authigenic carbonate, native sulphur, microbial sulphate reduction, Messinian salinity crisis, Sicily

Abstract

Microbially formed authigenic carbonates accompanied by native sulphur are present in the 'Calcare Solfifero' below a thick succession of gypsum deposited during the Messinian salinity crisis in Sicily. We sampled these carbonates and associated sulphur in five former sulphur mines to subject them to a detailed petrographic and geochemical study in order to explore their different modes of formation. Native sulphur formed in conjunction with microbial sulphate reduction, which is reflected in its depletion in ^{34}S ($\delta^{34}S$ values as low as −2‰ vs. V-CDT) and an enrichment of ^{34}S in the residual sulphate ($\delta^{34}S$ values as high as +61‰). The oxidation of organic matter by sulphate reduction increased alkalinity, inducing precipitation of secondary carbonate minerals. A set of authigenic limestones lacking sulphate minerals, but characterized by pseudomorphs after gypsum and high $\delta^{18}O$ values (as high as +9‰ vs. V-PDB) reflects syngenetic mineral formation within evaporitic settings. Low $\delta^{13}C$ values (as low as −52‰ vs. V-PDB) reveal that these carbonate phases formed by microbial sulphate reduction coupled to the oxidation of biogenic methane. Another set of

authigenic carbonates that replaced sulphate minerals is typified by low $\delta^{18}O$ values (as low as −4‰). These carbonates formed epigenetically during later diagenesis following compaction. Dissolution of gypsum or anhydrite by meteoric waters delivered sulphate for microbial sulphate reduction. Low carbon isotope values of these carbonates (−29 to −5‰) indicate that carbonate was derived from the oxidation of crude oil and possibly minor methane, partly involving different degrees of admixture of dissolved carbonate from other sources. Although the studied rocks with their vast amounts of secondary carbonate minerals and sulphur seem to indicate a similar genesis at first glance – having formed by biogeochemical transformations of sulphate and hydrocarbons – this study reveals that these processes can occur at different times in variable geological environments.

3.1 Introduction

Evaporites are often locally associated with native sulphur deposits and diagenetic carbonate minerals. Examples include cap rock deposits like those of the salt-domes along the coast of the Gulf of Mexico (Thode et al., 1954; Feely and Kulp, 1957) or the Permian salt dome of the Hils syncline, northern Germany (Schneider and Nielsen, 1965), but also strata-bound deposits like those from the western margin of the Gulf of Suez, Egypt (Schnellmann, 1959; Pierre and Rouchy, 1988), the Castile Formation, Texas (Davis and Kirkland, 1970), the Polish Carpathian foredeep (Pawlowski et al., 1979; Böttcher and Parafiniuk, 1998), northern Iraq (Barker et al., 1979; Jassim et al., 1999), or Zechstein strata of Germany (Peckmann et al., 1999). There are several other occurrences of native sulphur and associated carbonates worldwide (Wessel, 1994), whose origin has not been investigated to date. The examples of the paragenesis of evaporites, native sulphur, and diagenetic carbonate minerals in the Messinian of Sicily belong to the strata-bound type (Wessel, 1994). The Sicilian sulphur and secondary carbonates are intercalated in the thick evaporitic succession that formed during the Messinian salinity crisis. Numerous abandoned sulphur mines reflect the former economic importance and the vast masses of native sulphur in Sicily (Hunt, 1915).

Microbial sulphate reduction is considered to be the key process for the precipitation of native sulphur and accompanying carbonates in evaporitic lithologies (Feely and Kulp, 1957; Davis and Kirkland, 1970; Anadón et al., 1992; Böttcher and Parafiniuk, 1998; Peckmann et al., 1999). Sulphate-reducing bacteria use sulphate to oxidize organic matter, including crude oil (Feely and Kulp, 1957; Rueter et al., 1994; Aeckersberg et al., 1998; Heider et al., 1999; Rabus, 2005), which leads to the production of reduced sulphur species such as hydrogen sulphide (Feely and Kulp, 1957; Sagemann et al., 1999) and an alkalinity increase (Abd-El-Malek and Rizk, 1963a). This alkalinity increase is responsible for the precipitation of carbonate minerals (Abd-El-Malek and Rizk, 1963b), mainly calcite (Machel, 2001), but also aragonite and dolomite (Pierre and Rouchy, 1988; Anadón et al.,

1992; Böttcher and Parafiniuk, 1998; Peckmann et al., 1999). Hydrogen sulphide is either abiologically or biologically oxidized to native sulphur (Machel, 1992), but the exact mechanisms are still unknown.

Ruckmick et al. (1979) classified rocks containing biogenic sulphur into bioepigenetic and biosyngenetic deposits. Most of the above-mentioned examples are attributed to the bioepigenetic pathway (see Wessel, 1994). According to this scenario, meteoric waters dissolve gypsum or anhydrite, which serve as sulphate source for microbial sulphate reduction. This only happens after burial and subsequent uplift of the host rocks, often hundreds of millions of years after deposition (e.g., Feely and Kulp, 1957; Schneider and Nielsen, 1965; Davis and Kirkland, 1979; Hentz and Henry, 1989). An epigenetic origin is obvious for salt dome cap rocks (Schneider and Nielsen, 1965; Davis and Kirkland, 1979). Stratabound deposits have also been described as products of epigenesis, e.g. the Late Permian Salado and Castile Formations (Davis and Kirkland, 1970; 1979; Hentz and Henry, 1989). Dissolution of halite and sulphate minerals by meteoric waters is thought to have increased the porosity, permitting the influx of crude-oil bearing waters from underlying formations, which then fuelled microbial sulphate reduction (e.g., Kirkland and Evans, 1976; Davis and Kirkland, 1979). Based on the observation that hydrogen sulphide is still present in waters from sulphur wells near salt dome cap rocks, Feely and Kulp (1957) inferred that microbial sulphate reduction is not necessarily terminated in these sulphate rocks, depending on the presence of anoxic conditions, meteoric waters, and a source of reduced carbon.

With respect to some previously described occurrences (Dessau et al., 1962; Gasiewiecz, 2000), carbonate precipitation and sulphur authigenesis are suggested to be induced in a fashion similar to the epigenetic pathway, but during sedimentation and very early diagenesis (biosyngenetic pathway; Ruckmick et al., 1979; Wessel, 1994). Interestingly, high-Mg calcite and dolomite formation induced by sulphate-reducing bacteria is a well studied phenomenon in modern hypersaline lakes and lagoons (e.g., Vasconcelos et al., 1995; Dupraz et al., 2004). In these environments, however, no accumulation of native sulphur has been described. Active production of native sulphur was reported from lagoonal lakes in Cyrenaica, Libya (Butlin and Postgate, 1954; Thode et al., 1954). In these lagoonal lakes, hydrogen sulphide is produced locally by microbial sulphate reduction and dissolved sulphide is apparently oxidized by anoxygenic phototrophic bacteria (Butlin and Postgate, 1954). It seems likely, however, that regional springs contribute additional sulphide (Ivanov, 1968). To date, only few ancient occurrences of native sulphur and associated secondary carbonates, like the Miocene deposits from the Polish Carpathian foredeep, have been attributed to biosyngenetic processes (Gasiewicz, 2000). A bacterial origin of the Sicilian sulphur deposits was first put forward at the beginning of the 20th century by Hunt (1915). The isotope data on sulphur and carbonates from

Sicilian sulphur mines presented by Dessau et al. (1962) confirmed this suggestion. These authors favoured biosyngenetic formation of the Sicilian sulphur deposits. This assumption was challenged later on (e.g., Ruckmick et al., 1979; Wessel, 1994), but the problem was never addressed by a detailed study of the secondary mineral phases.

Here, we analyse samples of sulphur-bearing limestones from five abandoned mines of Sicily in order to reconstruct the genesis of native sulphur and associated carbonates, using petrography, element patterns, as well as carbon (C), oxygen (O), and sulphur (S) stable isotope signatures. Our data confirm the microbial origin of the secondary minerals and reveal that timing and modes of authigenesis are more variable than previously recognized.

3.2 Geological context

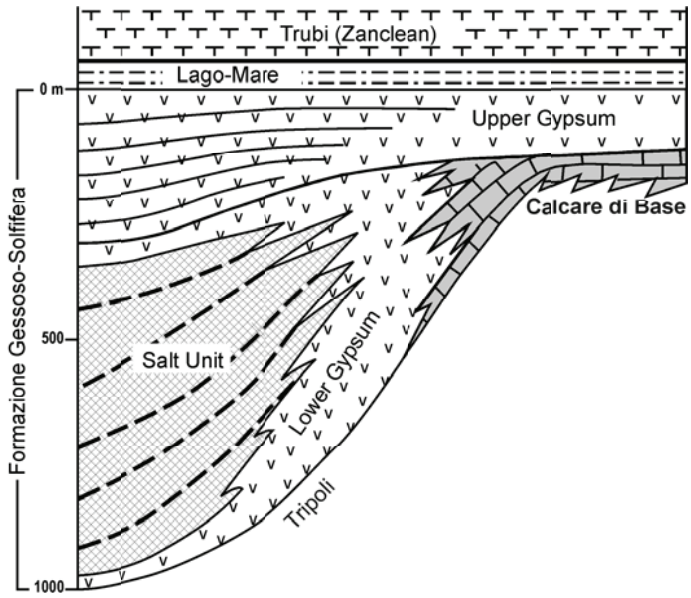

Fig. 3-1 Interpretative cross-section through the Central Sicilian Basin illustrating the stratigraphic position of the Calcare di Base, modified after Rouchy and Caruso (2006).

The sulphate-bearing strata of Sicily resulted from one of the greatest evaporitic events in Earth history, the so-called Messinian salinity crisis. Several scenarios of the onset, timing, and development of this crisis have been controversially discussed during the last decades (see Rouchy and Caruso, 2006; Briand, 2007; Roveri et al., 2008 a). Deposition of the Lower Evaporites marks the onset of the salinity crisis at 5.96 Ma (Krijgsman et al., 1999). This onset was caused by the sea level drop induced by the cut off of the Mediterranean Sea from the Atlantic Ocean (e.g., Krijgsman et al., 1999; Duggen et al., 2003 and references therein). The development of restricted conditions led to the deposition of an evaporitic series including evaporitic carbonate, sulphate, halite, and bitter salts in the deepest Messinian basins (Hsü et al., 1973) as well as in the Central Sicilian Basin (e.g., Decima and Wezel, 1973).

During the Messinian (Late Miocene) the Mediterranean area was segmented into several interconnected basins, largely varying in size. The Caltanissetta or Central Sicilian Basin in the middle to southern part of Sicily was tectonically separated into several sub-basins (Butler et al., 1995). The Neogene stratigraphic succession of Sicily includes Messinian evaporites of the so-called 'Formazione Gessoso-Solfifera' (gypsum-sulphur formation; Fig. 3-1). The transition from the pre-evaporitic diatomite formation (Tripoli Formation) to the overlying evaporites is marked by two types of limestone. The first type is named 'Calcare di Base' (basal limestone), which was studied by McKenzie (1985a) and Decima et al. (1988). This unit is formed of massive limestone beds, which usually consist of irregular, peloidal, or clotted micrite to microspar. The beds are separated by layers of laminar limestone, dolomite, calcareous marl, or rarely gypsum. In some places stromatolites occur at the transition from the Tripoli Formation to the Calcare di Base (Oliveri et al., 2010) or at the top of massive Calcare di Base limestone beds (Decima et al., 1988). The total thickness of this unit is quite variable, ranging from 20 to 60 m. The Calcare di Base was interpreted as evaporitic limestone (Decima et al., 1988). Diagenetic alteration resulted in pseudomorphs after gypsum and mouldic pores that were primarily filled with halite crystals.

The 'Calcare Solfifero' (limestone with sulphur) represents a local subunit, which is intercalated in the upper part of the Calcare di Base or is found on top of it (Decima et al., 1988). Sometimes, the Calcare Solfifero is described as an independent unit, which rests on the Calcare di Base or directly on the diatomite unit, where the basal limestone is missing (Dessau et al., 1962). The Calcare Solfifero is a diagenetic limestone. The occurrences of native sulphur are not continuous in this unit, but are confined to some isolated sites (Hunt, 1915). According to Rouchy and Caruso (2006) both types of limestone, the Calcare di Base and the Calcare Solfifero, pass basinwards into the lower gypsum and salt units and are overlain by the upper gypsum units (Fig. 3-1). This stratigraphic relationship, however, is still under discussion (Rouchy and Caruso, 2006; Briand, 2007; Roveri et al., 2008 a). Therefore, we use the term 'Calcare Solfifero' descriptively for the sulphur-containing limestone. The Messinian salinity crisis ended with the deposition of the brackish and freshwater 'Lago-Mare' facies and the subsequent return to marine conditions (Trubi Formation) during the Early Pliocene flooding. The distribution of the upper gypsum and the Lago-Mare facies as well as the conditions under which they were deposited are still discussed (Rouchy and Caruso, 2006; Roveri et al., 2008b; Manzi et al., 2009).

3.3 Samples

For this study, rocks were sampled from five locations (Fig. 3-2). The former carbonate quarry of Monte de Drasi and the former sulphur mine, La Muculufa, are situated in the south of Sicily near

Gela. The abandoned sulphur mine of Cozzo Disi is situated close to the town of Casteltermini. Contrada Gaspa and the former sulphur mine, Monte Capodarso, are located in central Sicily close to Enna and Caltanissetta, respectively. The evaporitic successions at the five locations display a wide variety of lithologies and facies, out of which only rocks with native sulphur or carbonates were sampled.

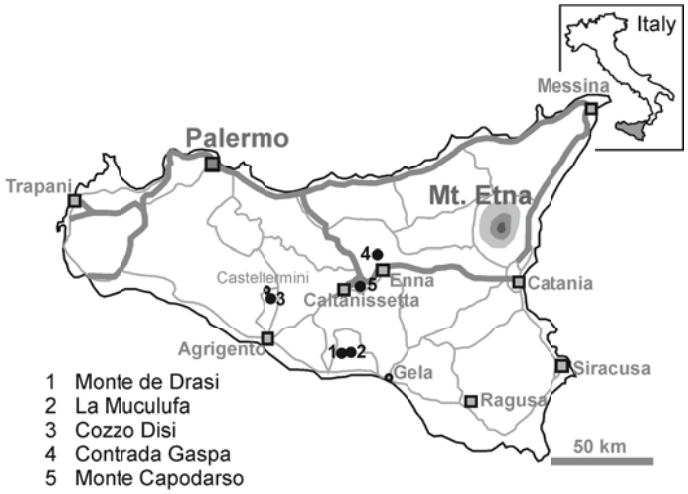

Fig. 3-2 Map of Sicily with the five sample locations.

3.3.1 Monte de Drasi

This outcrop is situated on the slope of the mountain Monte de Drasi, east of the road from Licata to Ravanusa. It represents a former sulphur mine that was subsequently used as a carbonate quarry. The transition from the uppermost cycles of the Tripoli Formation to the Calcare di Base is exposed in this outcrop. The Calcare di Base is a massive peloidal to filamentous limestone crosscut by sulphur-filled veins (Fig. 3-3A, Fig. 3-4A).

3.3.2 La Muculufa

This former quarry is situated on the slope of the mountain Monte Muculufa. Messinian strata crop out close to the abandoned sulphur mine, La Muculufa. The sedimentary sequence is inverted due to tectonic activity. Therefore, Calcare di Base, which is extremely rich in pseudomorphs after halite, overlies gypsum. Both units are covered by approximately 100 m of Tortonian marls. Loose blocks of sulphur-rich celestine associated with carbonate (Fig. 3-3B) were sampled from the base of the gypsum quarry.

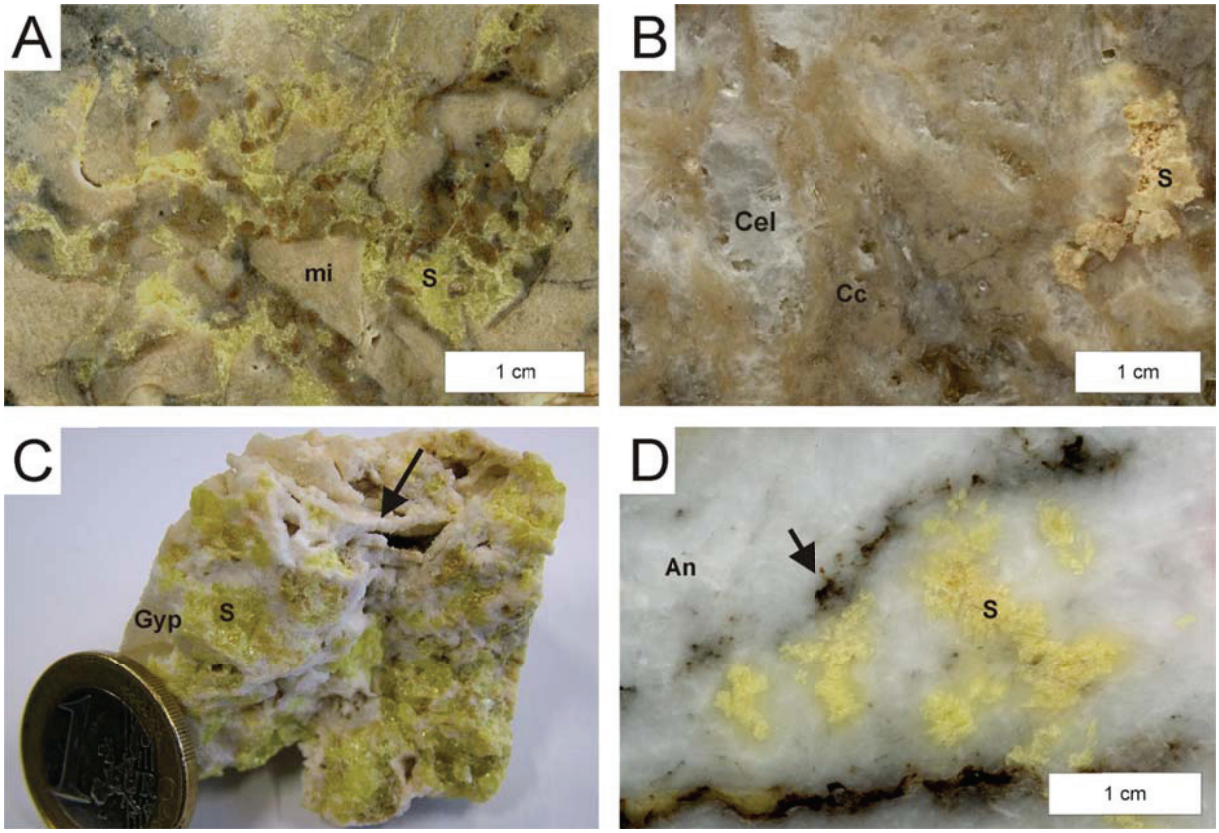

Fig. 3-3 Samples of Calcare Solfifero, i.e., limestone containing native sulphur. An = anhydrite; Cc = calcite; Cel = celestine; Gyp = gypsum; mi = micrite; S = native sulphur. (A) Sulphur in veins between micrite clasts; Monte de Drasi; scanned slab. (B) Sulphur accompanied by micritic and sparitic calcite in celestine matrix; Monte Muculufa; scanned slab. (C) Sulphur, gypsum, and platy aggregations of secondary calcite (arrow); Cozzo Disi; coin = 23.3 mm in diameter. (D) Sulphur and dolomite (arrow) embedded in anhydrite matrix; Monte Capodarso; scanned slab.

3.3.3 Cozzo Disi

The sulphur mine of Cozzo Disi is situated southeast of Casteltermini. In the middle of the last century it was one of the most productive sulphur mines in Sicily. The mine was closed in the 1980s, resulting in flooding of the lower levels. The sulphur-bearing limestone is underlain by marine clays and passes upwards into massive to nodular gypsum beds (Dessau et al., 1962). Samples of micritic to sparitic limestones with some accessory sulphate minerals and native sulphur from deeper, currently not accessible levels of the mine have been provided by private collectors for this study. Apart from that, sulphur-bearing gypsum-carbonate associations (Fig. 3-3C) and limestones have been sampled from the uppermost level, which is currently the only level that can be accessed safely.

3.3.4 Contrada Gaspa

Porous and brecciated Calcare Solfifero was sampled from a limestone cliff, situated close to the street S 230 from Enna to Alimena, between Casa Realmesi and Casa Bastione. The limestone cliff is close to an ancient sulphur mine, which is largely covered by soil and wood. During the onset of the salinity crisis the area of Contrada Gaspa was situated in a local depocenter in a synclinal position,

where more than 80 m of diatomitic laminites of the Tripoli Formation were deposited (Butler et al., 1995). The diatomites are followed by layered limestones of the Calcare di Base passing into the Calcare Solfifero. Laterally these carbonate facies pass into gypsum associated with carbonates. The sampled section consists of diagenetic limestones followed by a thin layer of whitish detrital mudstone capped by yellowish foraminiferal packstone.

3.3.5 Monte Capodarso

The outcrop, situated within the natural reserve, Monte Capodarso e Valle dell Imera Meridionale, north-east of Caltanissetta, is a former sulphur mine. The Tripoli Formation is exposed along the footpath to the mine. In this section it is only 25 m thick (Suc et al., 1995), suggesting a more marginal setting than for the Gaspa location. The sedimentary succession of the mine represents the transition from the upper Tripoli Formation into the Calcare Solfifero. In the uppermost part, cavernous Calcare Solfifero crops out, which is partly covered by powder-like native sulphur and bitumen. Loose blocks of Calcare Solfifero and sulphur-bearing anhydrite (Fig. 3-3D) were sampled from a dumping site in the former mine area.

3.4 Methods

Thin sections were studied with transmitted light and fluorescence microscopy carried out on a Zeiss Axioskop 40 optical microscope (lamp: HBO 50; filters: BP 365/12 FT 395 LP 397 and BP 450-490 FT 510 LP 515). Thin sections were stained with a combined potassium ferricyanide and alizarin red solution, dissolved in 0.1% HCl solution (Füchtbauer, 1988). Feigl's solution was used to test for aragonite (Feigl, 1960). Magnesium content of the carbonate was assessed by the titan-yellow (Clayton yellow) stain (Choquette and Trusell, 1978). A LEO 1530 Gemini and an attached energy dispersive X-ray spectrometer (EDX) Oxford Inca 400 were used for field-emission scanning-electron microscopy (FE-SEM) and qualitative element recognition. Mineralogy was determined by X-ray diffraction performed on a Philips X'Pert Pro MD.

Samples for element and stable isotope analyses were taken from the surface of slabs using a hand-held micro drill. Individual phases, which were distinguished by microscope analysis beforehand, were used for analysis. Mineral powders were dissolved by microwave digestion with a MLS Ethos 1600. Measurements were performed with an inductivity coupled plasma optical emission spectrometer (Perkin-Elmer Optima 3300 equipped with a cross-flow nebulizer). Carbon and oxygen isotope measurements were performed with a Finnigan MAT 251 mass spectrometer using the 'Kiel' carbonate device type 'Bremen'. A Solenhofen limestone was used as in-house standard, which was calibrated against the international standard NBS-19. Analytical standard deviation (1σ) was smaller

than ±0.07‰ for $\delta^{18}O$ values and ±0.05‰ for $\delta^{13}C$ values. Carbon and oxygen isotope ratios for carbonates are given in the δ-notation relative to the Vienna-Peedee-Belemnite (V-PDB) standard. Because of undetermined admixture of minor calcite, oxygen isotope data of dolomite samples were not corrected for their different fractionation compared to calcite during precipitation (McKenzie, 1981) or during the analytical procedure (Sharma and Clayton, 1965).

Table 3-1: Element contents of individual mineral phases.

Sample	Mineralogy	Crystal habit	Ca [%]	Mg [ppm]	Sr [ppm]	Fe [ppm]	Mn [ppm]
Monte de Drasi							
MD-1-a1_E1	calcite	microcrystalline	38	2846	17170	755	103
MD-1-a1_E2	calcite	sparitic	36	2182	38085	630	92
MD-2-d-1_E1	calcite	microcrystalline	37	2500	28147	873	209
MD-2-d-1_E2	calcite	microcrystalline	39	3827	839	326	41
La Muculufa							
LM-d_E1	calcite & celestine	microcr./ acicul.	14	1254	135494	39	109
LM-d_E2	celestine	acicular	1	31	133526	19	3
LM-f_E1	calcite	microcrystalline	36	4606	5767	4332	624
LM-f_E2	celestine	acicular	0	0	246663	13	0
Cozzo Disi							
CD5_E1	calcite	microcrystalline	37	2001	1077	162	310
CD5_E2	calcite	microcrystalline	37	2499	1641	1696	56
CD5_E3	aragonite	prismatic	36	0	7744	28	1
CD7_E1	calcite	radiaxial-fibrous	37	6393	713	152	7
CD7_E2	calcite	scalenohedral	36	8679	16093	90	54
CD7_E3	calcite	microsparitic	34	3559	653	3755	181
CD9_E1	dolomite	microcrystalline	21	108069	185	3067	386
CD9_E2	calcite	microsparitic	36	4121	2364	1209	31
CD9_E3	calcite	scalenohedral	39	3764	664	22	77
CD9_E4	calcite	radiaxial-fibrous	38	5774	458	61	19
CD18_E1	calcite	microcrystalline	34	6505	356	4339	184
CD18_E2	calcite	sparitic	33	3340	459	392	84
CD20_E1	calcite	sparitic	38	2805	205	20	78
CD20_E2	gypsum	selenitic	29	1091	186	10	28
Contrada Gaspa							
GA-f_E1	calcite	microcrystalline	39	2893	479	1557	70
GA-f_E2	calcite	sparitic	39	3022	645	47	26
GA-i_E1	calcite	microcrystalline	39	2465	512	1001	34
Monte Capodarso							
MC-a_E1	anhydrite	acicular	29	1039	1009	2	1
MC-a_E2	anhydrite & dolomite	acicular	25	12270	1175	1454	69
MC-c_E1	calcite	microcrystalline	37	6237	397	3132	322
MC-c_E2	calcite	sparitic	39	6335	979	595	62

For sulphur isotope analysis, anhydrite was dissolved and precipitated as barium sulphate by addition of barium chloride solution. Native sulphur, gypsum, and celestine were directly analyzed for their sulphur isotope composition without pretreatment. For oxygen isotope analysis of sulphate, gypsum, and anhydrite were dissolved in a sodium chloride solution and precipitated as barium sulphate by addition of barium chloride solution. The oxygen isotope composition of celestine was analyzed directly without pretreatment. For the determination of carbonate-associated sulphate,

carbonate samples were powdered and submerged in a sodium chloride solution over night. This treatment removed easily soluble sulphate phases (i.e., gypsum and anhydrite). After washing with deionized water, the sample was dissolved with hydrochloric acid. Liberated carbonate-associated sulphate was precipitated as barium sulphate by addition of barium chloride solution that was further washed and dried.

Sulphur and oxygen isotopes were measured in continuous flow with a Thermo Finnigan Delta V Plus (via Eurovector 3000; Max Planck Institute, Bremen) or a Thermo Delta V (via Thermo flash EA; Thermo Bremen) gas mass spectrometer. For sulphur isotope analysis, samples and V_2O_5 (as a catalyst) were weighed into tin capsules and combusted in an elemental analyzer (Euro Vector 3000) to produce SO_2. For oxygen isotope analysis, barium sulphate was transferred to a silver capsule and thermochemically pyrolized to CO gas in a Thermo-Finnigan Thermal Conversion/Elemental Analyzer (TC/EA; Thermo Fisher Scientific; Gehre and Strauch, 2003). Sulphur isotope composition of sulphur and sulphates and oxygen isotope composition of sulphates are given in the δ-notation relative to the Vienna-Canyon Diablo Troilite (V-CDT) standard and Vienna-Standard Mean Ocean Water (V-SMOW), respectively. International standard NBS-127 and in-house standards were used for the calibration towards the respective mass scales. The standard errors (1) of replicate measurements were less than ±0.3‰ for $\delta^{18}O$ and $\delta^{34}S$ values.

3.5 Results

3.5.1 Petrography

3.5.1.a Monte de Drasi

Abundant sulphur-filled veins crosscut primary filamentous limestones consisting of low-magnesium calcite (Fig. 3-3A). The micritic matrix encloses microspar and spar (Fig. 3-4A) as well as calcitic pseudomorphs after gypsum and halite (Fig. 3-4B). The strontium content of the micritic matrix is exceptionally high (Table 3-1), which is caused by numerous small celestine crystals enclosed in the limestone (Fig. 3-4C). Some samples of limestone contain traces of microcrystalline aragonite. Possibly, recrystallisation of aragonite to calcite provided the strontium for celestine precipitation (cf., Decima et al., 1988). The limestones also enclose minor amounts of gypsum. Veins crosscutting the limestone are filled with sparry calcite or a sequence of microspar, sparry calcite, and elemental sulphur towards the centre of the vein (Fig. 3-4D). Occasionally, celestine is embedded in the sparry calcite. The celestine is either bladed, rhomb-shaped, or appears as fan-shaped crystal aggregates.

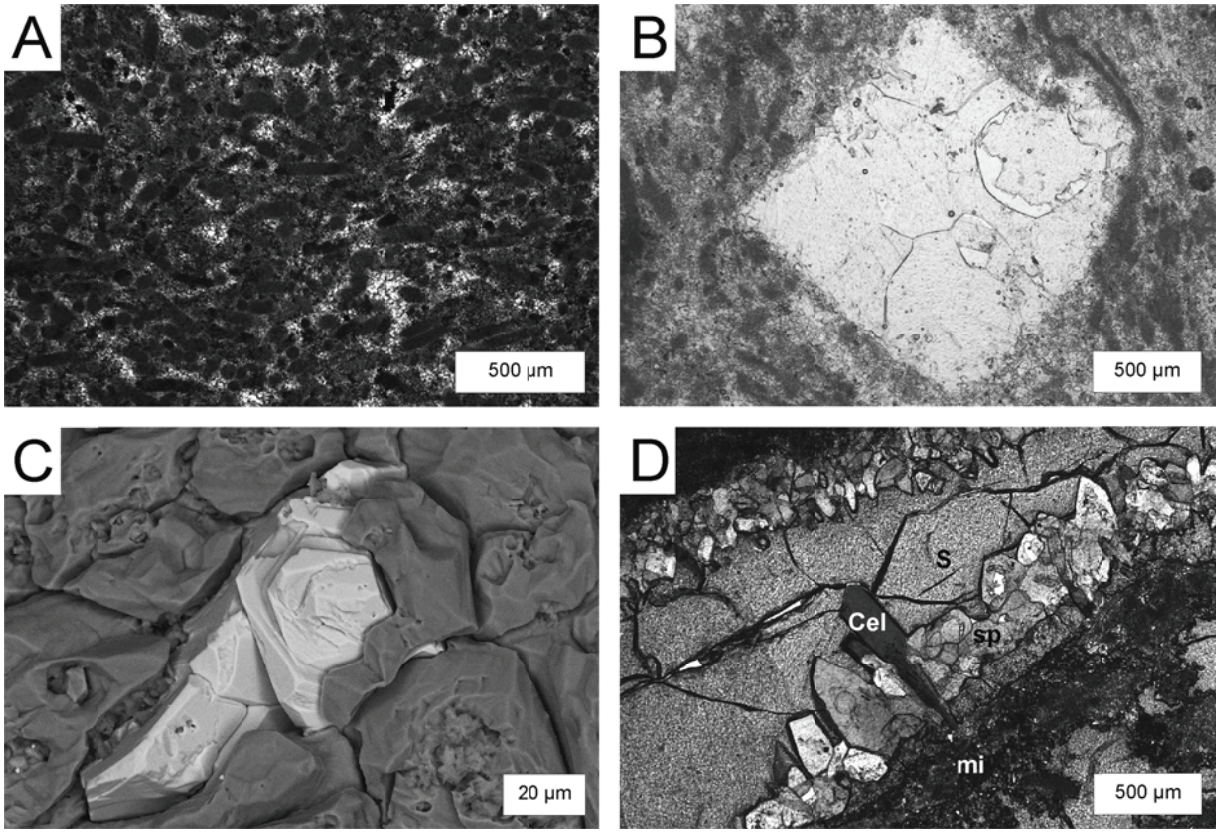

Fig. 3-4 Monte de Drasi. Cel = celestine; mi = micrite; S = native sulphur; sp = calcite spar. (A) Filamentous limestone; plane-polarized light. (B) Spar-filled pseudomorph after halite; plane-polarized light. (C) Celestine crystals bedded in calcite microspar; FE-scanning electron micrograph. (D) Vein within the micritic limestone filled by a sequence of calcite spar, celestine, and native sulphur; cross-polarized light.

3.5.1.b La Muculufa

Samples from this site display a complex fabric. Their lithology is volumetrically dominated by secondary celestine and gypsum. The celestine forms fan-shaped crystal aggregates. Crystals are prismatic to acicular, but rhombic crystal habits occur as well. Celestine crystals of up to 0.5 cm in length project into open voids (Fig. 3-5A). Secondary gypsum appears as a felted mass of crystal needles. The sulphate phases enclose micrite, which is spatially associated with elemental sulphur (Fig. 3-5B). Micrite is accompanied by microspar and spar (Fig. 3-5C). It is organic-rich and shows high contents of iron and manganese (Table 3-1). The sulphur nodules are often corroded at their rims. Minor amounts of chalcedony are finely dispersed in the limestone matrix.

3.5.1.c Cozzo Disi

The limestone samples as well as the gypsum-carbonate associations (Fig. 3-3C) from this site contain large aggregates of native sulphur. Limestones consist of micritic low-Mg calcite and sparry calcite (Fig. 3-6A). The organic-rich micrite is occasionally laminated and encloses spar-filled pseudomorphs after lenticular gypsum. One sample contains few scattered foraminifera (*Orbulina*

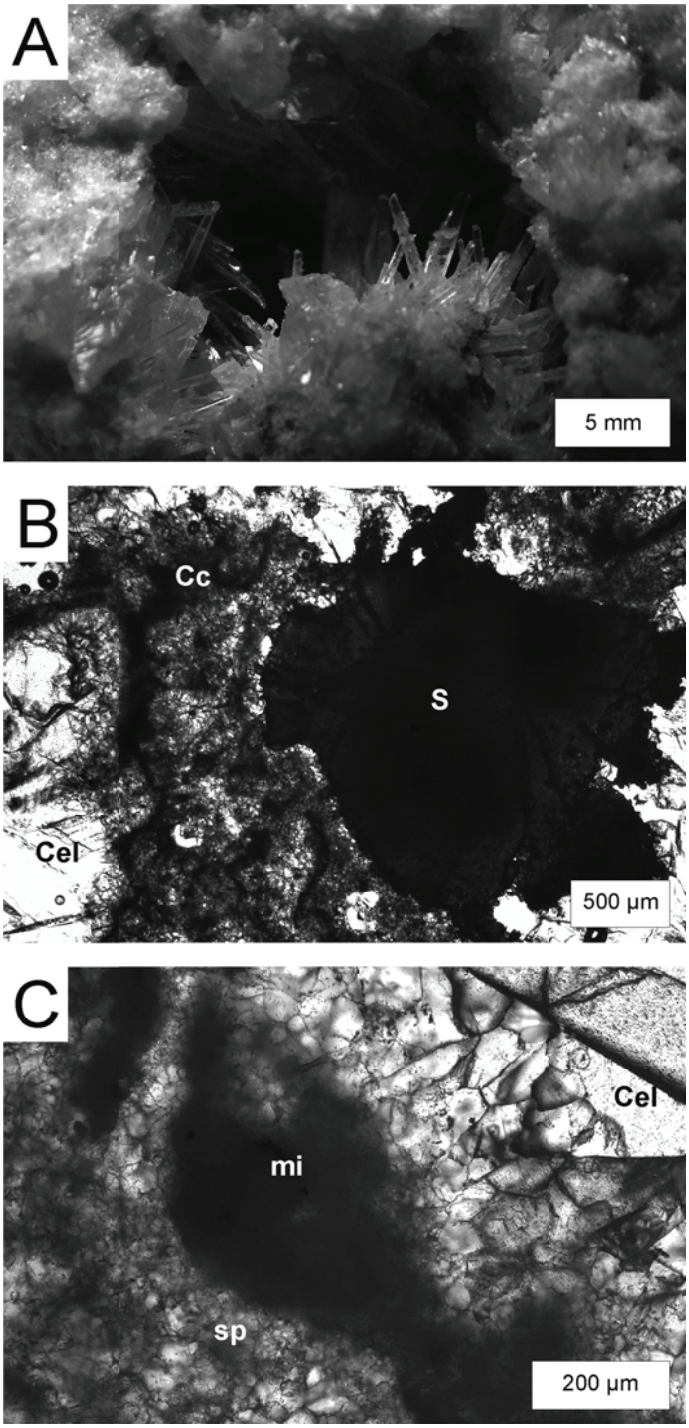

Fig. 3-5 La Muculufa. Cc = calcite; Cel = celestine; mi = micrite; S = native sulphur; sp = spar. (A) Celestine needles growing into a void. (B) Native sulphur nodule associated with calcite enclosed in celestine; plane-polarized light. (C) Closer view of the calcite made of micritic remnants and microspar to spar surrounded by celestine; plane-polarized light.

sp., *Globigerinoides* sp., *Globigerina bulloides*). Microcrystalline dolomite is an accessory mineral phase (Table 3-1). Small celestine crystals in the limestone matrix account for the high strontium contents (Table 3-1). Much of the former pore space is filled by native sulphur (Fig. 3-6A). Within the gypsum-carbonate associations, the carbonate is mostly sparitic, sometimes enclosing micrite. The

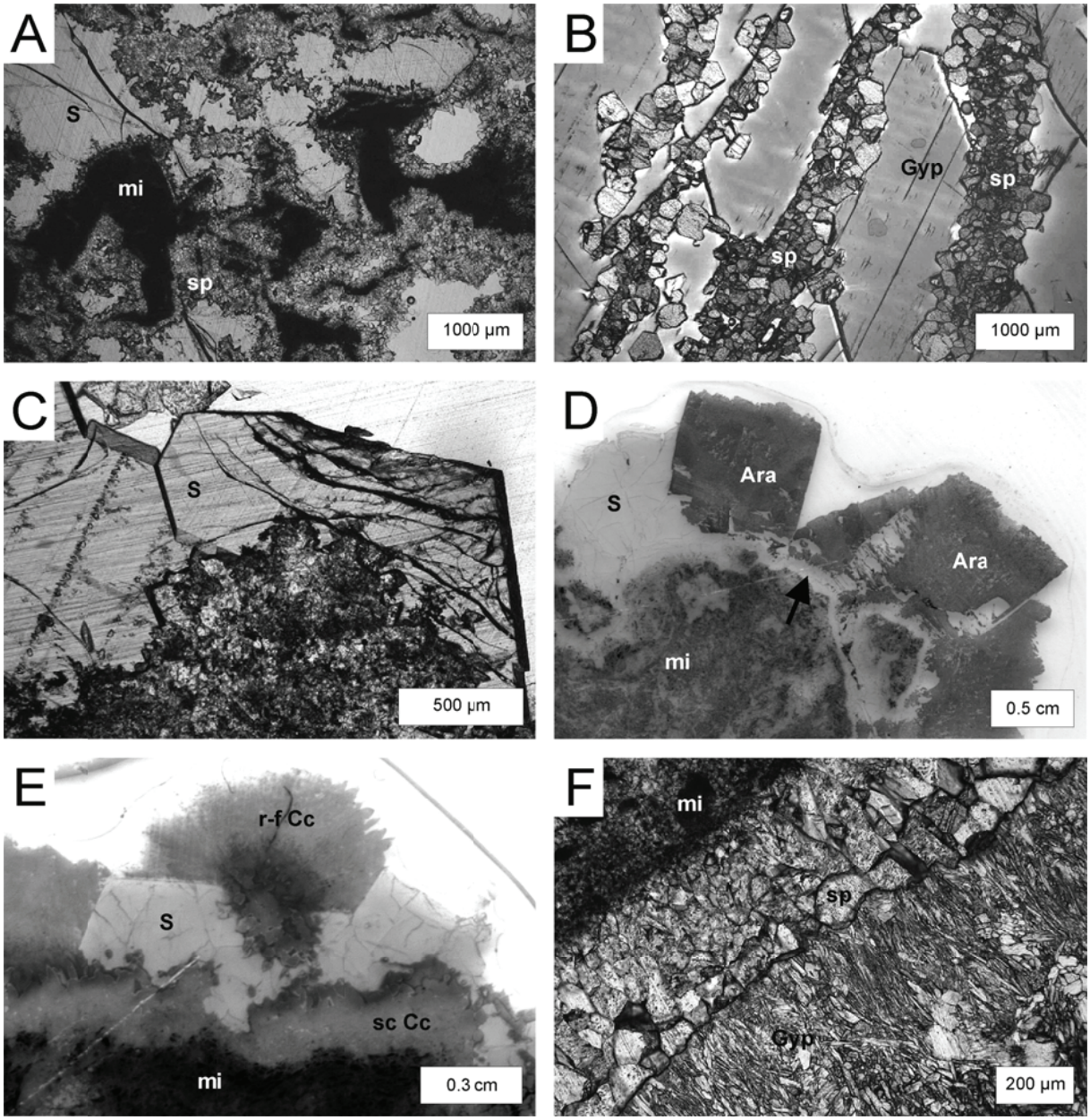

Fig. 3-6 Cozzo Disi. Gyp = gypsum; mi = micrite; r-f Cc = radiaxial fibrous calcite cement; sc Cc = scalenohedral calcite; S = native sulphur; sp = spar. (A) Micrite surrounded by microspar to spar and sulphur as pore-filling; plane-polarized light. (B) Calcite spar partly replacing selenitic gypsum; plane-polarized light. (C) Large idiomorphic sulphur crystals filling veins; plane-polarized light. (D) Vein crossing micrite filled by a succession of scalenohedral calcite (arrow), sulphur and large pseudo-hexagonal aragonite crystals; stained with Feigl's solution; scanned thin section. (E) Vein crossing micrite filled by a succession of scalenohedral calcite, sulphur, and radiaxial fibrous calcite cement; stained with potassium ferricyanide and alizarin red; scanned thin section. (F) Micrite, sparite, and secondary gypsum that appears as small needles in a felted mass; plane-polarized light.

secondary spar formed along crystal margins of primary selenitic gypsum, apparently replacing the sulphate mineral (Fig. 3-6B). This type of replacement resulted in a platy habit of aggregations of secondary calcite crystals (Fig. 3-3C). In places, subsequent dissolution of selenitic gypsum produced a reticulate fabric. Besides filling pore space, sulphur occurs as inclusion-rich nodules enclosed in the limestone and as large, translucent, idiomorphic crystals within veins (Fig. 3-6C). Some limestones

show a succession of micrite, scalenohedral calcite, large crystals of sulphur, and large crystals of pseudo-hexagonal aragonite (Fig. 3-6D). Instead of the latter, radiaxial fibrous calcite cement is the terminal phase of the paragenetic sequence in some other samples (Fig. 3-6E). Secondary gypsum appears as small needles, forming a felted mass (Fig. 3-6F).

3.5.1.d Contrada Gaspa

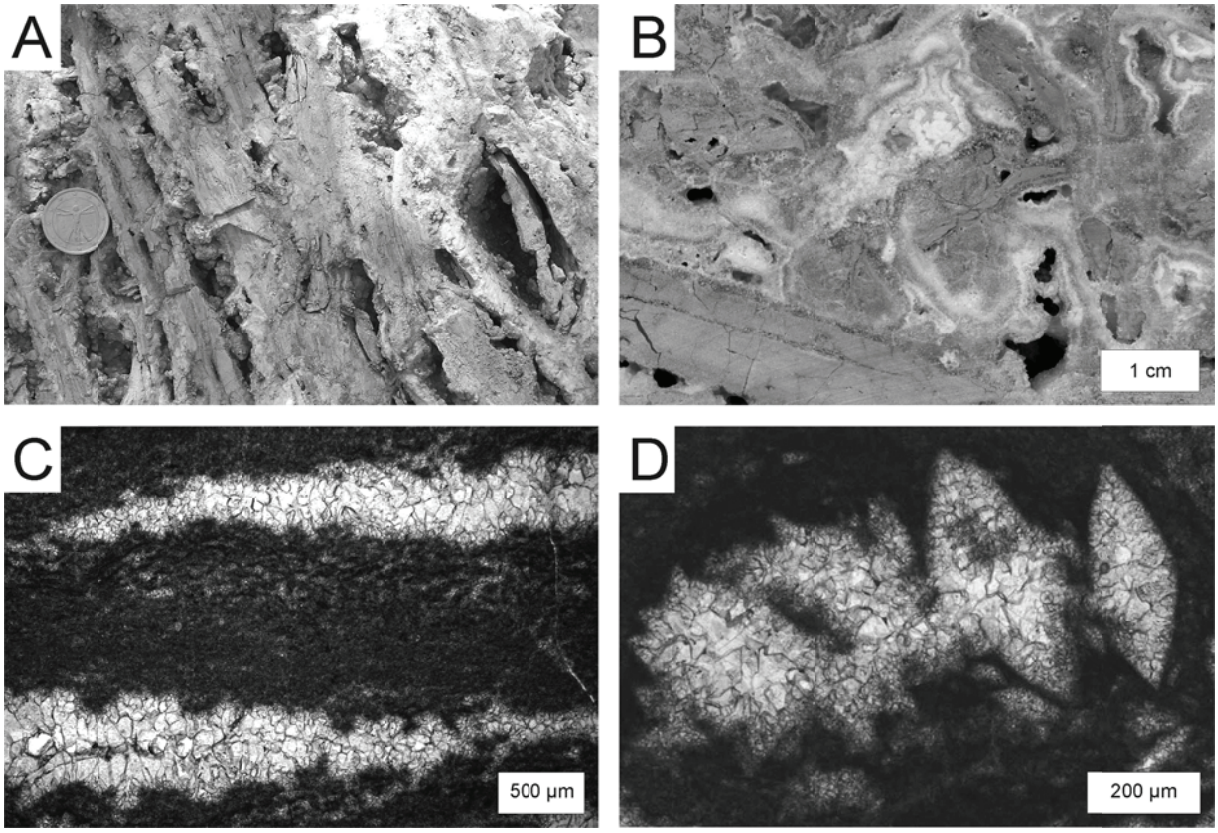

Fig. 3-7 Contrada Gaspa. (A) Limestone made of planar fragments. Coin for scale. (B) Planar fragments and chunks of micrite separated by spar cement; scanned slab. (C) Layers of micrite (dark) and spar (bright); plane-polarized light. (D) Spar-filled pseudomorphs after lenticular gypsum; plane-polarized light.

The cliff of Contrada Gaspa is formed by limestone made of planar fragments (Fig. 3-7A) that consist of low-magnesium calcite. These fragments and chunks are separated by later formed sparry calcite, fringing the micrite, and oblong cavities (Fig. 3-7B). Some of the micritic fragments are laminated. Microspar to spar separates the micrite fragments parallel to the internal lamination (Fig. 3-7C). The micrite contains calcite pseudomorphs after lenticular gypsum (Fig. 3-7D). The micrite shows high iron but low manganese contents, while the sparry calcite exhibits low contents of these elements (Table 3-1). Native sulphur has not been found in these limestones, neither during field work nor during microscopical analysis. Extraction of the limestones with organic solvents, however, yielded high amounts of sulphur. Therefore, native sulphur is apparently finely disseminated within the matrix of the limestone. The limestone also contains minor amounts of quartz, which was only

detected by XRD analysis. Even though trace amounts of celestine were identified by electron microscopy, the strontium content is rather low (Table 3-1).

3.5.1.e Monte Capodarso

From this site, limestone and anhydrite samples were analyzed. The limestone consists of small remnants of micrite, which are surrounded by a matrix of microspar to spar (Fig. 3-8A). The dense micrite is dark-brown, exhibiting only minor fluorescence. It shows elevated contents of iron and manganese (Table 3-1). Calcite pseudomorphs after lenticular gypsum (Fig. 3-8A and B) are abundant. Anhydrite is accompanied by sulphur and dolomite. It shows tabular to acicular crystal habits (Fig. 3-8C). Large anhydrite crystals project into cavities, which are filled by native sulphur. Locally, anhydrite is replaced by alabastrine gypsum (Fig. 3-8D). Occasionally, dolomite is associated

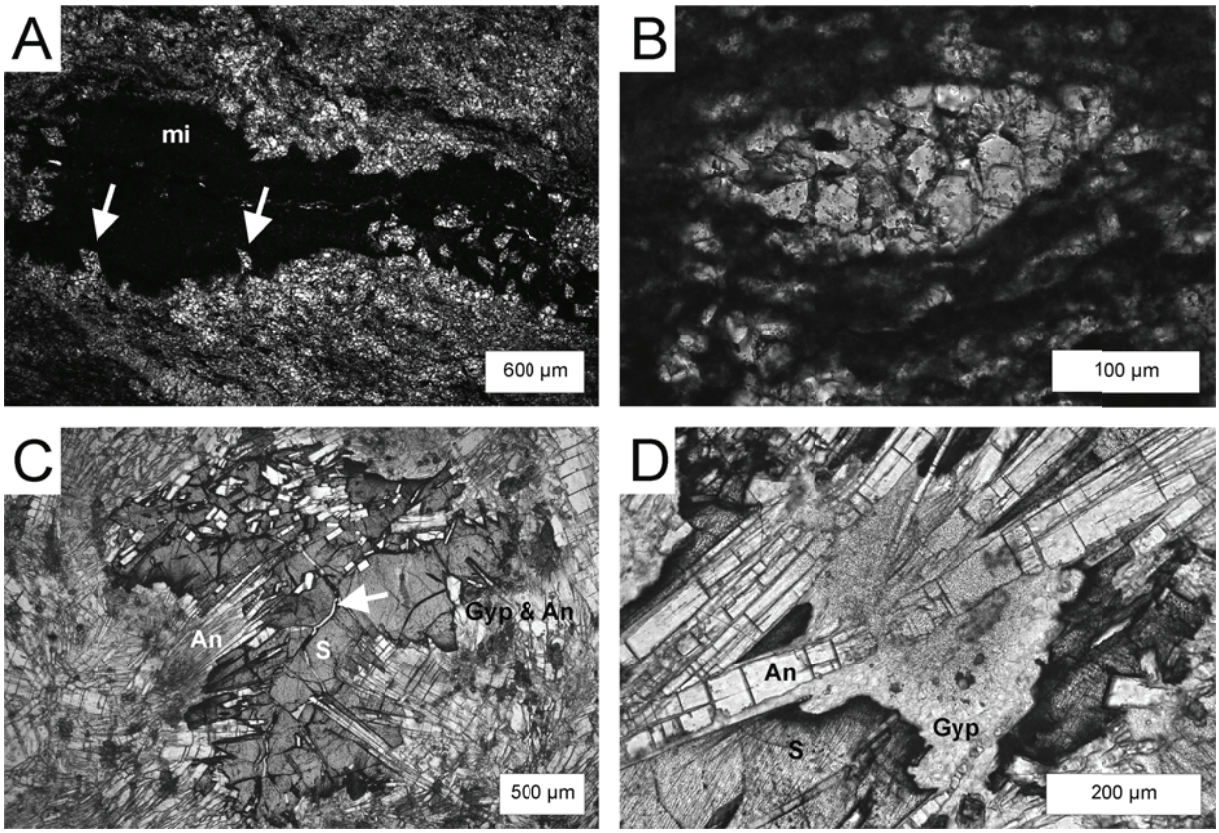

Fig. 3-8 Monte Capodarso. An = anhydrite; Gyp = gypsum; mi = micrite; S = sulphur. (A) Limestone with micritic remnants, containing spar-filled pseudomorphs after lenticular gypsum (arrows); plane-polarized light. (B) Closer view of one pseudomorph; plane-polarized light. (C) Acicular anhydrite partly recrystallized to gypsum; sulphur is filling pore-space. (D) Anhydrite partly recrystallized to alabastrine gypsum and porosity filling sulphur; plane-polarized light.

with secondary gypsum; the dolomite is rich in iron (Table 3-1) and partly accompanied by clay minerals. Dolomite also occurs, dispersed between anhydrite crystals. The magnesium content in pure anhydrite is high, while the strontium content is unusually low (Table 3-1; cf., Dworkin and Land, 1994).

3.5.2 Stable isotopes

3.5.2.a Carbon and oxygen isotopes of carbonates

Monte de Drasi carbonates show the highest $\delta^{13}C$ values ranging from −25 to −5‰ (Table 3-2; Fig. 3-9). The respective $\delta^{18}O$ values vary from −4 to +1‰. The range of the carbon isotope values of micrite and microspar from La Muculufa is rather narrow (−29 to −22‰); the corresponding $\delta^{18}O$ values range from −4 to +2‰. Cozzo Disi limestones yielded low $\delta^{13}C$ values (−50 to −29‰) and high $\delta^{18}O$ values (0 to +7‰). The dolomite sample is more enriched in ^{18}O (+9‰) than calcite as expected for the difference of oxygen isotope fractionation between the two carbonate minerals. The $\delta^{18}O_{dolomite}$ value would be +5‰, if corrected for different fractionation factors during precipitation ($\varepsilon^{18}O_{dolomite-calcite}$ = +3.2‰, Fritz and Smith, 1970; McKenzie, 1981) and for fractionation during analytical procedure ($\varepsilon^{18}O_{dolomite-calcite}$ = +0.8‰ at 25°C, Sharma and Clayton, 1965). With respect to Contrada Gaspa limestones, micrite tends to be more depleted in ^{13}C and less enriched in ^{18}O than the later spar phases (Table 3-2). These limestones yielded overall low $\delta^{13}C$ values (−46 to −41‰) and high $\delta^{18}O$ values (+3 to +5‰). Only a foraminiferal packstone revealed a somewhat different pattern ($\delta^{13}C$: −28 to −23‰, $\delta^{18}O$: +2 to +3‰; Table 3-2). Monte Capodarso limestones show the lowest $\delta^{13}C$ values (−52 to −46‰) of all limestones studied, while the $\delta^{18}O$ values are high (+4 to +5‰).

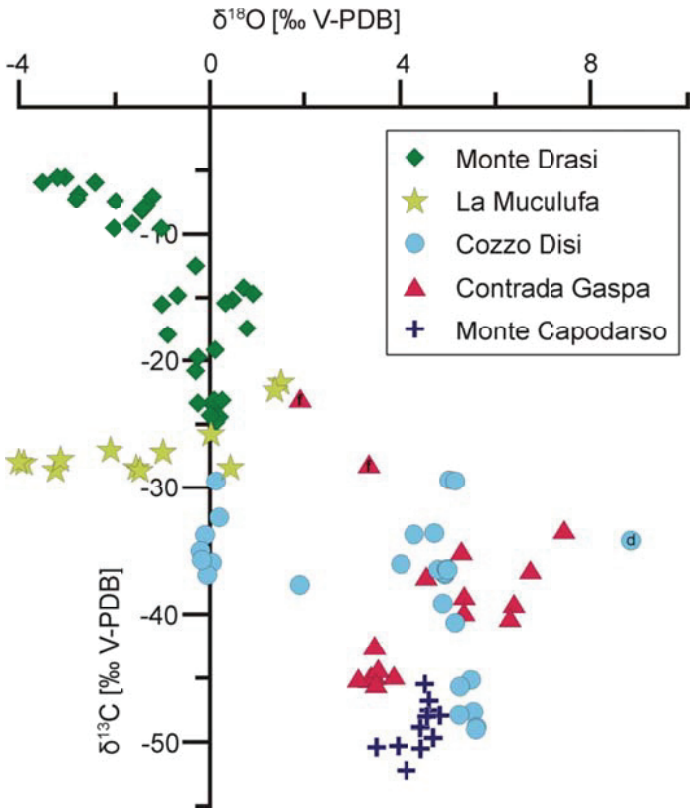

Fig. 3-9 Carbon and oxygen stable isotope compositions of individual carbonate phases. One dolomite sample from Cozzo Disi is indicated by the letter d, two samples of foraminiferal packstones are indicated by the letter f.

Table 3-2: Carbon and oxygen isotope compositions for individual carbonate phases, samples containing foraminifera are marked with *.

sample	mineralogy	crystal habit	$\delta^{13}C$	$\delta^{18}O$	sample	mineralogy	crystal habit	$\delta^{13}C$	$\delta^{18}O$
Monte de Drasi			[‰]	[‰]	**Cozzo Disi**			[‰]	[‰]
MD-1-a-I_1	calcite	microcrystalline	-23.6	0.1	CD-04_1	calcite	sparitic	-45.2	5.5
MD-1-a-I_2	calcite	microcrystalline	-24.4	0.2	CD-04_2	aragonite	prismatic	-47.7	5.5
MD-1-a-I_3	calcite	microcrystalline	-18.0	-0.9	CD-05_1	calcite	microcrystalline	-39.2	4.9
MD-1-a-I_4	calcite	sparitic	-20.8	-0.3	CD-05_2	calcite	microsparitic	-45.7	5.3
MD-1-a-I_5	calcite	sparitic	-14.8	-0.7	CD-05_3	aragonite	prismatic	-48.9	5.6
MD-1-a-I_6	calcite	microcrystalline	-23.1	0.1	CD-05_4	aragonite	prismatic	-49.0	5.6
MD-1-a-I_7	calcite	microsparitic	-24.8	0.1	CD-05_5	calcite	microsparitic	-47.9	5.2
MD-1-a-I_8	calcite	sparitic	-15.5	-1.0	CD-05_6	calcite	microcrystalline	-40.7	5.2
MD-1-a-I_9	calcite	sparitic	-23.1	0.3	CD-07_1	calcite	microspar	-36.9	4.9
MD-1-a-I_10	calcite	microcrystalline	-24.3	0.0	CD-07_2	calcite	scalenohedral	-36.7	4.9
MD-1-a-II_1	calcite	microcrystalline	-19.7	-0.2	CD-07_3	calcite	radiaxial fibrous	-33.7	4.3
MD-1-a-II_2	calcite	sparitic	-19.2	0.1	CD-08_1	calcite	microspar	-36.5	4.8
MD-1-c_1	calcite	microcrystalline	-23.3	-0.2	CD-08_2	calcite	scalenohedral	-36.4	5.0
MD-2-d-I_1	calcite	microcrystalline	-5.5	-3.0	CD-08_3	calcite	radiaxial fibrous	-36.1	4.0
MD-2-d-I_2	calcite	sparitic	-8.1	-1.4	CD-09_1	dolomite	microcrystalline	-34.2	8.8
MD-2-d-I_3	calcite	microcrystalline	-5.5	-3.2	CD-09_2	calcite	microsparitic	-29.4	5.0
MD-2-d-I_4	calcite	microcrystalline	-6.8	-2.8	CD-09_3	calcite	radiaxial fibrous	-29.5	5.2
MD-2-d-I_5	calcite	microcrystalline	-7.1	-1.2	CD-10_1	calcite	microsparitic	-33.6	4.7
MD-2-d-I_6	calcite	sparitic	-9.5	-1.0	CD-10_2	aragonite	prismatic	-36.5	5.0
MD-2-d-I_7	calcite	microcrystalline	-17.5	0.8	CD-13_1	calcite	microsparitic	-29.5	0.1
MD-2-d-I_8	calcite	microcryst.	-7.2	-2.8	CD-14_2	calcite	sparitic	-37.7	1.9
MD-2-d-I_9	calcite	microcrystalline	-5.9	-3.5	CD-14_3	calcite	sparitic	-32.4	0.2
MD-2-d-I_10	calcite	microcrystalline	-14.2	0.7	CD-16_1	calcite	microsparitic	-35.9	0.0
MD-2-d-I_11	calcite	microcrystalline	-7.7	-1.3	CD-18_1	calcite	microcrystalline*	-33.8	-0.1
MD-2-d-I_12	calcite	microcrystalline	-15.2	0.5	CD-18_2	calcite	sparitic*	-35.0	-0.2
MD-2-d-I_13	calcite	microsparitic	-9.6	-2.0	CD-20_1	calcite	sparitic	-36.9	-0.1
MD-2-d-II_1	calcite	microcrystalline	-5.9	-2.4	CD-20_2	calcite	microsparitic	-35.7	-0.2
MD-2-d-II_2	calcite	microcrystalline	-9.2	-1.6					
MD-2-d-II_3	calcite	microsparitic	-14.7	0.9	**Contrada Gaspa**				
MD-2-d-II_4	calcite	microcrystalline	-8.0	-1.4	GA-2-f_1	calcite	microcrystalline	-45.0	3.5
MD-2-d-II_5	calcite	microcrystalline	-15.4	0.3	GA-2-f_2	calcite	microcrystalline	-45.0	3.4
MD-2-d-II_6	calcite	microcrystalline	-12.5	-0.3	GA-2-f_3	calcite	microcrystalline	-45.2	3.3
MD-2-d-II_7	calcite	microcrystalline	-7.4	-2.0	GA-2-f_4	calcite	microsparitic	-45.1	3.6
					GA-2-f_5	calcite	microcrystalline	-42.6	3.5
La Muculufa					GA-2-f_6	calcite	sparitic	-38.6	5.3
LM-d_1	calcite	sparitic	-28.7	-3.2	GA-2-f_7	calcite	microsparitic	-45.1	3.1
LM-d_2	calcite	sparitic	-27.8	-3.1	GA-2-f_8	calcite	sparitic	-36.6	6.7
LM-d_3	calcite	sparitic	-27.2	-1.0	GA-2-f_9	calcite	microcrystalline	-33.5	7.5
LM-d_4	calcite	sparitic	-28.1	-3.9	GA-2-i_1	calcite	sparitic	-44.4	3.5
LM-d_5	calcite	microcrystalline	-28.4	-1.5	GA-2-i_2	calcite	microsparitic	-45.6	3.5
LM-d_6	calcite	sparitic	-28.6	-1.5	GA-2-i_3	calcite	sparitic	-39.3	6.4
LM-f_1	calcite	microcrystalline	-21.7	1.5	GA-2-i_4	calcite	sparitic	-40.4	6.3
LM-f_2	calcite	microcrystalline	-22.3	1.4	GA-2-i_5	calcite	sparitic	-39.9	5.3
LM-f_3	calcite	sparitic	-28.0	-4.0	GA-2-k_1	calcite	packstone*	-28.2	3.3
LM-f_4	calcite	micrite	-25.8	0.0	GA-2-k_2	calcite	packstone*	-23.1	1.9
LM-f_5	calcite	sparitic	-27.1	-2.1	GA-2-n_1	calcite	mudstone*	-37.1	4.6
LM-f_6	calcite	sparitic	-28.4	0.4	GA-2-n_2	calcite	mudstone*	-35.1	5.3

Table 3-2: continued

sample	mineralogy	crystal habit	$\delta^{13}C$	$\delta^{18}O$
Monte Capodarso			[‰]	[‰]
MC-c_1	calcite	sparitic	-47.6	4.6
MC-c_2	calcite	microcrystalline	-45.5	4.5
MC-c_3	calcite	microcrystalline	-48.9	4.4
MC-c_4	calcite	sparitic	-46.8	4.6
MC-c_5	calcite	sparitic	-50.3	4.0
MC-c_6	calcite	sparitic	-50.5	4.4
MC-c_7	calcite	sparitic	-52.2	4.1
MC-c_8	calcite	microcrystalline	-49.7	4.7
MC-c_9	calcite	sparitic	-48.0	4.8
MC-c_10	calcite	sparitic	-48.1	4.6
MC-c_11	calcite	sparitic	-50.4	3.5

3.5.2.b Sulphur isotopes and oxygen isotopes of sulphate

The sulphur isotope compositions of native sulphur from Monte de Drasi, celestine and native sulphur from La Muculufa, gypsum, carbonate-associated sulphate, and sulphur from Cozzo Disi, carbonate-associated sulphate and sulphur from Gaspa, and sulphur and anhydrite from Monte Capodarso have been determined (Table 3-3; Fig. 3-10). The $\delta^{34}S$ values of Monte de Drasi sulphur vary between +3 and +14‰. La Muculufa celestine is strongly enriched in ^{34}S (+44 to +48‰) compared to native sulphur (−2 to +1‰). Sulphur isotope compositions of Cozzo Disi samples display a complex diagenetic history. While some selenitic gypsum reveals high $\delta^{34}S$ values (+36 to +45‰), later secondary gypsum forming a felted mass of needles (+7 to +10‰) as well as sulphur (+4 to +10‰) show lower values (Fig. 3-10). Some native sulphur exhibits $\delta^{34}S$ values as high as +22‰ and carbonate-associated sulphate from the same sample has values as high as +61‰ (Fig. 3-10).

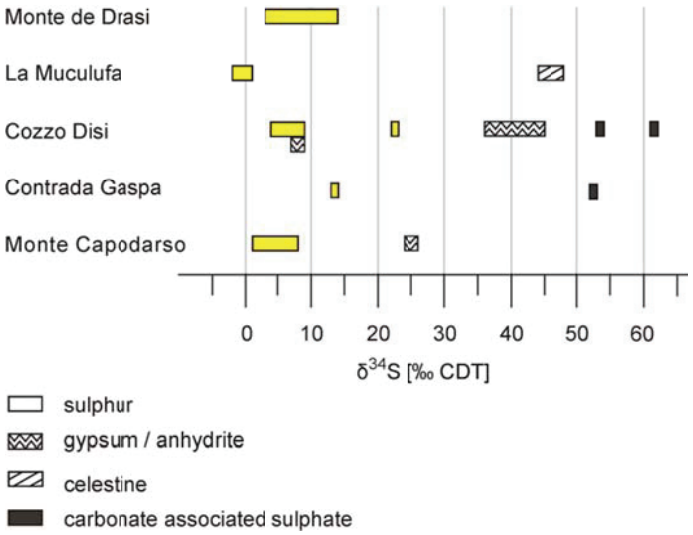

Fig. 3-10 Sulphur isotope compositions.

Finely disseminated native sulphur, which was gained by solvent extraction of the Contrada Gaspa limestone, yielded a $\delta^{34}S$ value of +13‰. Carbonate-associated sulphate recovered from Contrada Gaspa limestones is enriched in ^{34}S (+52‰). The $\delta^{34}S$ values of Monte Capodarso anhydrite range from +26 to +27‰, while native sulphur shows lower values (+1 to +8‰).

Corresponding oxygen and sulphur isotopes were measured on celestine from La Muculufa, gypsum and carbonate-associated sulphate from Cozzo Disi, carbonate-associated sulphate from Gaspa, and anhydrite from Monte Capodarso (Table 3-3; Fig. 3-11). The data show a positive relation between $\delta^{34}S$ and $\delta^{18}O$ values. In general, sulphate samples are enriched in both ^{34}S and ^{18}O compared to Messinian seawater sulphate as well as Messinian gypsum (Fig. 3-11). Only secondary sulphate from Cozzo Disi is depleted in ^{34}S and ^{18}O relative to marine gypsum.

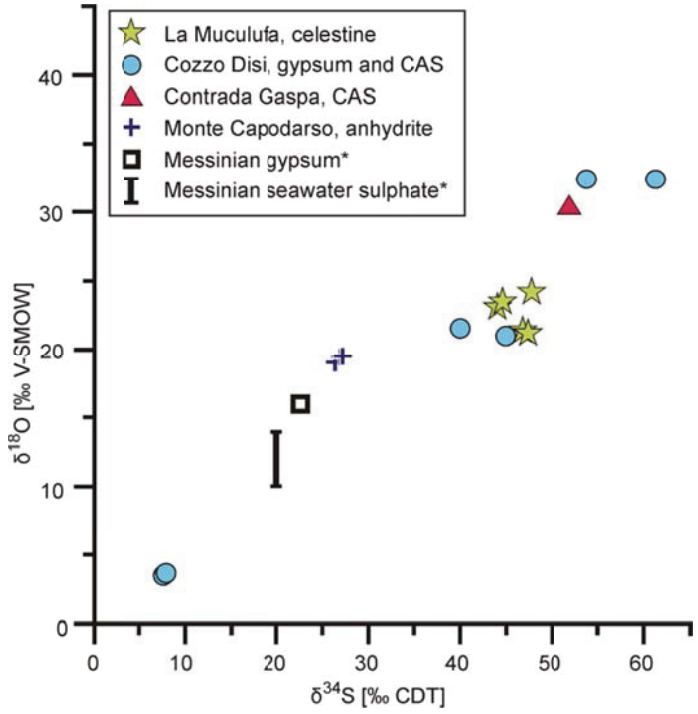

Fig. 3-11 Sulphur and oxygen isotope compositions of sulphates compared with literature data (marked with *). Messinian gypsum from the Mediterranean: $\delta^{34}S$: +22‰, $\delta^{18}O$: +16‰ (Stenni and Longinelli, 1990). Messinian seawater sulphate calculated after Messinian gypsum from the Mediterranean (see above) with fractionation effects for sulphur of 1.6‰ (Thode and Monster, 1973) and oxygen of 2 to 6‰ Lloyd (1967, 1968).

Table 3-3: Sulphur isotope compositions of native sulphur and sulphur and oxygen isotope compositions of celestine, gypsum, anhydrite, and carbonate-associated sulphate (CAS).

Sample	Mineralogy	$\delta^{34}S$ [‰ CDT]	$\delta^{18}O$ [‰ V-SMOW]	Sample	Mineralogy	$\delta^{34}S$ [‰ CDT]	$\delta^{18}O$ [‰ V-SMOW]
Monte de Drasi				**Cozzo Disi**			
MD-1_S1a	sulphur	7.3		CD-04_CAS	CAS	61.2	32.4
MD-1_S1b	sulphur	7.5		CD-04_S	sulphur	22.9	
MD-1_S2a	sulphur	14.1		CD-05_CAS	CAS	53.8	32.4
MD-1_S2b	sulphur	14.1		CD-05_S	sulphur	22.2	
MD-1_S3a	sulphur	13.1		CD-08_S-1	sulphur	4.5	
MD-1_S3b	sulphur	14.0		CD-08_S-2	sulphur	4.3	
MD-1_S4a	sulphur	12.7		CD-13_G	gypsum	40.0	21.6
MD-1_S4b	sulphur	11.6		CD-13_G-1	gypsum	8.9	
MD-1_S5a	sulphur	11.5		CD-13_G-2	gypsum	38.4	
MD-2_S1a	sulphur	4.7		CD-13_S	sulphur	5.9	
MD-2_S2a	sulphur	3.2		CD-15_G	gypsum	6.8	
MD-2_S2b	sulphur	3.8		CD-15_G-1	gypsum	7.6	3.5
MD-2_S3b	sulphur	2.8		CD-15_G-2	gypsum	7.8	3.6
MD-2_S4a	sulphur	4.5		CD-15_S-a	sulphur	6.9	
MD-2_S4b	sulphur	5.5		CD-15_S-b	sulphur	6.9	
La Muculufa				CD-20_G	gypsum	44.9	21.0
LM-i_C1	celestine	46.7	21.5	CD-20_G	gypsum	35.6	
LM-i_C2	celestine	47.3	21.3	CD-20_S	sulphur	7.7	
LM-f_C1	celestine	43.9	23.2	**Contrada**			
LM-f_C2	celestine	44.5	23.6	GA-2-J-CAS	CAS	52.0	
LM-f_C3	celestine	47.6	24.3	GA-2-J-S	sulphur	13.2	
LM-f_S1b	sulphur	1.2		**Monte**			
LM-f_S3a	sulphur	0.7		MC-a_S1b	sulphur	4.8	
LM-f_S3b	sulphur	-1.8		MC-a_S2b	sulphur	7.7	
LM-d_S1a	sulphur	-1.9		MC-a_S3a	sulphur	1.3	
LM-d_S1b	sulphur	-0.4		MC-a_S3b	sulphur	0.8	
LM-g-S1	sulphur	0.2		MC-a_S4a	sulphur	4.7	
LM-g-S2	sulphur	0.3		MC-a_A1	anhydrite	26.4	19.0
				MC-a_A2	anhydrite	27.0	19.4
				MC-a_A3	anhydrite	27.0	19.5

3.6 Discussion

3.6.1 Isotope composition of sulphur species – implications on the genesis of native sulphur

The sulphur and oxygen isotope composition of sulphur species can be used to trace redox processes (e.g., Pierre, 1985; van Stempvoort and Krouse, 1994; Böttcher et al., 1998; Brunner et al., 2005), including the identification of microbial sulphate reduction that strongly discriminates against ^{34}S (Kaplan and Rittenberg, 1964). The isotopic composition of Messinian gypsum from the Mediterranean was approximately +22‰ for sulphur and +16‰ for oxygen (Stenni and Longinelli, 1990). Only a small isotope fractionation effect of 1.6‰ for sulphur (Thode and Monster, 1973) and 2 to 6‰ for oxygen (Lloyd, 1967; 1968) is observed during the crystallization of gypsum from marine sulphate. Therefore the isotopic composition for Mediterranean seawater sulphate in the Messinian was approximately +20‰ for sulphur and +10 to +14‰ for oxygen (Fig. 3-11). As no other than Messinian evaporites are known in Sicily, Messinian seawater sulphate and gypsum are the likely sources of sulphate for sulphate reduction processes that lead to the secondary mineral formation in the Messinian strata of Sicily.

Carbonate-associated sulphate is trapped in carbonates as they form, thus it records the sulphur isotope composition of sulphate from the fluid in which precipitation took place (Burdett et al., 1989; Lyons et al., 2004; Newton et al., 2004), and is only negligibly compromised by diagenetic alteration (Gill et al., 2008). Because it is usually assumed that secondary carbonate precipitation in lithologies rich in sulphate minerals is induced by microbial sulphate reduction (e.g., Pierre and Rouchy, 1988), the isotope composition of carbonate-associated sulphate can be used as a proxy for the isotope composition of sulphate during ongoing sulphate reduction. Celestine may form upon transformation reactions in the carbonate system and fixes the isotopic composition of dissolved interstitial water sulphate (Böttcher and Parafiniuk, 1998). Due to its low solubility in sulphate-rich environments, celestine has a high preservation potential. Compared to Messinian gypsum, carbonate-associated sulphate (Contrada Gaspa, Cozzo Disi) is enriched by 30 to 39‰ in ^{34}S. Celestine found at La Muculufa is enriched by 22 to 26‰ in ^{34}S compared to Messinian gypsum. The enrichment of ^{34}S in both sulphate phases reflects the isotopic composition of residual sulphate after intense sulphate reduction (cf., Böttcher and Parafiniuk, 1998; Taberner et al., 2002).

Native sulphur likely formed by oxidation of sulphide (e.g., Machel, 1992). Since there is little sulphur isotope fractionation for oxidative processes (Fry et al., 1986) and there is rapid sulphur isotope exchange between native sulphur and sulphide (Fossing, 1995) with a small sulphur isotope equilibrium fractionation (Ohmoto and Rye, 1979), the sulphur isotope composition of native sulphur reflects the sulphur isotope composition of sulphide produced by sulphate reduction. With one exception, native sulphur from the investigated sites in Sicily is depleted by approximately 5 to 25‰ compared to Messinian sulphates (Fig. 3-10).

Using Messinian gypsum as a proxy for the isotope composition of the source of sulphate, carbonate-associated sulphate and celestine as proxies for residual sulphate affected by intense sulphate reduction, and native sulphur as proxy for produced sulphide, we infer that the sulphur isotope fractionation during sulphate reduction ranged from 5 to 60‰. This is within the range of sulphur isotope fractionations observed in pure and natural mixed cultures (Kaplan and Rittenberg, 1964; Habicht and Canfield, 1997; Bolliger et al., 2001). This observation corroborates that the investigated native sulphur deposits in Sicily resulted from intense microbial sulphate reduction. The prominence of sulphate reduction is also demonstrated by the coupled sulphur and oxygen isotope enrichment trends (Figure 11; Mizutani and Rafter, 1973; Fritz et al., 1989; Böttcher et al., 1998; Brunner et al., 2005) for celestine, as well as carbonate-associated sulphate and gypsum. The highest oxygen isotope value of carbonate associated sulphate is 32.4‰ (Table 3-3), whereas the corresponding oxygen isotope composition of the carbonate is approximately 5.5‰ (Table 3-2). Using the oxygen isotope composition of this carbonate as a proxy for the oxygen isotope

composition of water at the time the carbonate formed, it can be concluded that this heavy sulphate isotope composition was close to the apparent oxygen isotope equilibrium between sulphate and water (Fritz et al., 1989).

A late phase of gypsum in some Cozzo Disi samples, represented by small needles forming a felted mass (Fig. 3-6F), most likely derived from the oxidation of sulphide or native sulphur. The sulphur isotope composition of this secondary gypsum (+8‰) is similar to that of native sulphur from the same samples, in accord with only minor sulphur isotope fractionation during oxidation of sulphur (Kaplan and Rittenberg, 1964; Nakai and Jensen, 1964; Mizutani and Rafter, 1973). The oxygen isotope composition of sulphate produced during the oxidation of sulphur compounds is likely to be slightly enriched in ^{18}O compared to ambient water (e.g., Lloyd, 1967; Balci et al., 2007; Brunner et al., 2008), which agrees well with the $\delta^{18}O$ value of secondary gypsum of approximately +4‰.

3.6.2 Carbon sources of secondary microbial carbonates

Microorganisms are known to induce carbonate precipitation through respiration processes by increasing carbonate alkalinity (Knorre and Krumbein, 2000; Castanier et al., 2000; Wright and Oren, 2005). Among different respiration processes, microbial sulphate reduction is often considered to be a crucial factor for the formation of secondary carbonates in a variety of environments (Van Lith et al., 2003; Dupraz et al., 2004; Peckmann and Thiel, 2004; Aloisi et al., 2006). Organic matter, crude oil, and methane are known to act as reducing agents for microbial sulphate reduction (e.g., Rueter et al., 1994; Boetius et al., 2000; Rabus, 2005). These carbon sources are typified by distinct carbon isotopic compositions. Methane is extremely depleted in ^{13}C (−110 to −50‰ for biogenic methane and −50 to −20‰ for thermogenic methane; Whiticar, 1999). Crude oil is less depleted with $\delta^{13}C$ values of −35 to −25‰ (Roberts and Aharon, 1994). Marine organic matter tends to have relatively higher $\delta^{13}C$ values of approximately –25 to –20‰ (Hofmann et al., 2000). Because microorganisms preferentially take up compounds depleted in ^{13}C during the degradation of organic matter, the products of these processes are even more ^{13}C-depleted than the source. But because carbonate ions derived from the oxidation of organic matter are usually added to a pool of dissolved inorganic carbon, the carbon isotopic composition of the resultant mixture will fall on a mixing line between the isotopic compositions of the different sources. While carbonates resulting from the oxidation of crude oil are less depleted in ^{13}C, methane-derived carbonates forming at marine seeps show $\delta^{13}C$ values as low as −76‰ (Campbell, 2006). Limestones associated with stratabound sulphur deposits like those from the Carpathian foredeep ($\delta^{13}C$ values as low as −54‰; Böttcher and Parafiniuk, 1998; Gasiewicz, 2000) or the Limestone Buttes in Texas ($\delta^{13}C$ values as low as −39‰; Kirkland and Evans, 1976), but also salt-dome cap rock carbonates from the Gulf of Mexico area ($\delta^{13}C$ values as low as

−55‰; Thode et al., 1954; Feely and Kulp, 1957) show similarly low $\delta^{13}C$ values, pointing to methane as the predominant carbon source.

Carbon isotope compositions of the Sicilian limestones vary widely (−52 to −5‰). Limestones with carbonate phases most depleted in ^{13}C were sampled at Contrada Gaspa, Monte Capodarso, and Cozzo Disi. Decima et al. (1988) described the sulphureous limestones with low $\delta^{13}C$ and high $\delta^{18}O$ values as diagenetic concomitants of bacterial sulphate reduction. Non-sulphureous limestones with similar isotopic composition, however, were interpreted as the result of the conversion of aragonite to calcite in the presence of ^{13}C-depleted and ^{18}O-enriched waters, which were thought to originate from underlying organic-rich diatomites (Decima et al., 1988). We consider it unlikely that pore waters are able to change the carbon isotope composition of carbonates to such a degree. Although small celestine crystals embedded within the non-sulphureous limestones from Contrada Gaspa agree with a conversion of aragonite to calcite, it is more likely that all ^{13}C-depleted carbonates are secondary minerals that precipitated in the course of microbial alteration processes that affected the host lithologies. The lowest $\delta^{13}C$ values observed (Cozzo Disi, Gaspa, Monte Capodarso) reveal that a large fraction of the carbonate was derived from the oxidation of biogenic methane, probably in addition to other less depleted carbon sources including marine sourced bicarbonate.

La Muculufa carbonates are less depleted in ^{13}C than the carbonates of the three before-mentioned sites. This either reflects (1) oxidation of methane with a higher proportion of marine bicarbonate, (2) oxidation of fresh organic matter with virtually no admixture of other carbon sources, or (3) the oxidation of crude oil. Oxidation of methane seems unlikely, as significant admixture of marine bicarbonate is likely to result in a wider spread of $\delta^{13}C_{carbonate}$ values (Fig. 3-9). Oxidation of fresh organic matter is also not likely, as the lowest $\delta^{13}C_{carbonate}$ values (−29‰) are probably too low to be explained by this process (cf., Hofmann et al., 2000). Remineralisation of pristine organic matter also usually occurs during early diagenesis, which necessarily leads to the admixture of marine bicarbonate, resulting in a wider spread of $\delta^{13}C_{carbonate}$ values and also higher values than those of the organic source. Consequently, oxidation of crude oil during late diagenesis is most likely, as the $\delta^{13}C$ values show less variability than would be expected if mixing processes were significant and match the isotopic composition of crude oil (cf., Roberts and Aharon, 1994). The $\delta^{18}O$ values of the secondary carbonates and the dominance of later sparite over early micrite agree with a late diagenetic formation under the influence of meteoric waters. Therefore, these observations indicate that La Muculufa carbonates resulted from the oxidation of crude oil with little input from other sources. Monte de Drasi limestones mostly consist of marine carbonates with different degrees of admixture of secondary carbonates ($\delta^{13}C$: −25 to −5‰), reflecting a contribution from an unknown source of organic carbon.

3.6.3 Epi- versus syngenetic pathways

Epigenetic deposits are characterized by replacement of sulphate minerals (anhydrite or gypsum) by secondary sulphur and carbonates as a result of dissolution by meteoric waters and the action of sulphate-reducing prokaryotes subsequent to early diagenesis and compaction of the sedimentary rock. Syngenetic deposits form by similar, if not the same processes, but either during sedimentation or early diagenesis. In this case, sulphate reduction may occur in sulphate- and organic-rich sediments in evaporative settings such as lagoons. According to Wessel (1994), syngenetic sulphur deposition occurs only in modern spatially confined marine to lacustrine sedimentary environments and is not considered to be economically significant. However, Dessau et al. (1962) suggested that the economically significant Sicilian deposits are mainly, if not completely of syngenetic origin.

The secondary carbonate phases in the limestones from Contrada Gaspa and Monte Capodarso as well as some of the limestones from Cozzo Disi have in common that they all formed in an evaporitic environment where methane oxidation was apparently coupled to sulphate reduction. Evaporation is not only indicated by high $\delta^{18}O_{carbonate}$ values (as high as +8‰), but also by abundant pseudomorphs after lenticular gypsum. Some of these limestones, mostly consisting of organic-rich micrite, still exhibit a primary lamination, agreeing with syngenetic formation.

The suite of samples from Cozzo Disi provides evidence for several stages of gypsum, native sulphur, and carbonate formation. Cozzo Disi secondary carbonate phases can be divided into two groups by their oxygen isotope composition: The first group was affected by evaporation. During syngenetic mineral formation in evaporitic environments, the system varied between closed and more open conditions. Closed conditions are characterized by (a) nearly complete reduction of sulphate, resulting in high $\delta^{34}S$ values of the carbonate-associated sulphate (+54 to +61‰) and native sulphur with sulphur isotope composition corresponding to Messinian gypsum ($\delta^{34}S_{sulphur}$: approximately +22‰), (b) intense evaporation indicated by $\delta^{18}O_{carbonate}$ values higher than +5‰, and (c) intense methane oxidation reflected by low $\delta^{13}C$ values (−49 to −40‰). More open conditions are characterized by (a) the lowest $\delta^{34}S_{sulphur}$ values (+4‰), (b) less pronounced evaporation ($\delta^{18}O_{carbonate}$: <+5‰), and (c) apparently reduced methane oxidation or stronger admixture of carbonate from other sources ($\delta^{13}C_{carbonate}$: −37 to −30‰). The second group of secondary carbonate phases of Cozzo Disi formed later during epigenesis. These carbonates, with $\delta^{18}O$ values of around 0‰, reflect an increasing influence of meteoric waters. The carbonates partly replace gypsum (Fig. 3-6B) that is typified by high $\delta^{34}S$ values (+40 to +45‰). Apparently, this gypsum precipitated in an early stage from a sulphate pool affected by sulphate reduction. The native sulphur in these samples formed late in the paragenetic sequence. Its relatively low $\delta^{34}S$ values (+6 to +8‰) may thus indicate a change towards more open conditions.

The Monte de Drasi samples represent mostly primary limestones, resembling primary Calcare di Base (cf., Decima et al., 1988), as revealed by numerous peloidal to filamentous structures. Similar structures in Messinian limestones have been interpreted to represent faecal pellets (Guido et al., 2007) or microbial filaments (Oliveri et al., 2010). Hypersaline conditions during deposition of the Monte de Drasi limestones are reflected by pseudomorphs after halite and gypsum. The dissolution of evaporite minerals occurred during meteoric diagenesis, as revealed by low $\delta^{18}O_{carbonate}$ values. During diagenesis, aragonite was almost completely recrystallized to calcite, likely delivering the strontium for the precipitation of celestine (see Fig. 3-4C). Native sulphur is not associated with any of the early diagenetic phases, but only occurs in veins, which crosscut the limestone. The paragenetic sequence along with the isotope patterns reveal that the Monte de Drasi sulphur formed epigenetically.

The local source of strontium of celestine present in samples from La Muculufa is most likely the dissolution of calcium sulphate minerals (anhydrite or gypsum; see Sanz-Montero et al., 2009), as no evidence for abundant recrystallization of aragonite to calcite was found. Based on isotope patterns, anhydrite or gypsum were dissolved by meteoric waters carrying crude oil, favouring epigenetic sulphur and carbonate formation in a restricted, probably subterranean setting. Likewise, the narrow range of $\delta^{13}C$ values elucidates that the secondary carbonates precipitated mostly from one carbon source (i.e., crude oil) with very little admixture of carbon from other sources.

While the epigenetic processes that led to secondary mineral formation at La Muculufa were apparently fuelled by crude oil, syngenetic mineral authigenesis at the sites Cozzo Disi, Contrada Gaspa, and Monte Capodarso was fuelled by methane. The methane source was either the organic-rich diatomite of the Tripoli Formation as proposed by Decima et al. (1988) or contemporaneous biogenic methanogenesis, taking place in the underlying sediments.

3.7 Conclusions

Abundant secondary carbonate minerals and native sulphur enclosed in Messinian sedimentary rocks from Central Sicily formed as a consequence of microbial sulphate reduction. In contrast to previous studies, this study reveals that different Sicilian sulphur and carbonate deposits formed along both syngenetic (i.e., during early diagenesis prior to compaction) and epigenetic (i.e., during late diagenesis subsequent to compaction) pathways. This study re-establishes that syngenetic formation and not only epigenetic formation can yield economically significant amounts of sulphur.

During the evaporation of the Mediterranean Sea several small sub-basins developed in the study area. In some of these basins sulphate-reducing microorganisms flourished to such an extent

that carbonate minerals and sulphur formed as a consequence of microbial metabolism. Microbial respiration processes were fuelled by biogenic methane, which may have been produced by methanogenic microorganisms within the underlying sediments, but a deeper source of methane cannot be excluded. Carbonate minerals that formed along this syngenetic pathway are characterized by very low $\delta^{13}C$ values (−52 to −30‰), reflecting oxidation of methane, and high $\delta^{18}O$ values (+3 to +9‰), reflecting evaporation.

Epigenetic sulphur and carbonate authigenesis took place after deposition of gypsum and compaction. Epigenesis was controlled by dissolution of sulphate minerals providing sulphate for sulphate-reducing microorganisms and the presence of crude-oil laden meteoric waters. Carbonate minerals that formed along the epigenetic pathway are characterized by low $\delta^{13}C$ values (−29 to −5‰), reflecting oxidation of crude oil and possibly minor methane and by low $\delta^{18}O$ values (−4 to +1‰), reflecting meteoric conditions.

Acknowledgements

We thank W. Koot and B. Lacet (VU Amsterdam), Ralf Bätzel, as well as Sebastian Flotow (both Bremen) for thin section preparation, Christoph Voigt (Bremen) for XRD measurements, Till Heinrichs (Göttingen) for help with FE-SEM and EDX analysis, Silvana Pape and Karsten Enneking (both Bremen) for geochemical measurements, Monika Segl (Bremen) for carbon and oxygen isotope analysis, Thomas Max (Max Planck Institute for Marine Microbiology, Bremen) and Oliver Kracht (Thermo, Bremen) for mass spectrometric support, Marie-Madeleine Blanc Valleron (Paris) for helpful discussions, as well as Gail Lee Arnold (Bremen) and the journal reviewers Stefano Lugli (Modena) and an anonymous referee for their comments. This project was supported by the DFG through the international graduate college EUROPROX, the DFG Research Center “The Ocean in the Earth System”, the Max Planck Society, and the Leibniz IOW.

4 - SECOND MANUSCRIPT

Anaerobic oxidation of methane in hypersaline Messinian environments revealed by ^{13}C-depleted molecular fossils

S. B. Ziegenbalg[1], D. Birgel[2], L. Hoffmann-Sell[1], C. Pierre[3], J. M. Rouchy[4], and J. Peckmann[2]

[1] MARUM, Universität Bremen, 28359 Bremen, Germany

[2]Department für Geodynamik und Sedimentologie, Erdwissenschaftliches Zentrum, Universität Wien, Althanstraße, 1090 Wien, Austria

[3] CNRS-UMR 7159, LOCEAN, Univ. P. and M. Curie, 75252 Paris Cedex 05, France

[4] Dept. Earth History, Muséum National d'Histoire Naturelle, 75005 Paris, France

Corresponding author: Jörn Peckmann (joern.peckmann@univie.ac.at)

Abstract

The Messinian sequence of evaporitic deposits in Italy includes authigenic carbonates that have been suggested to derive from the microbial degradation of organic compounds, but the biogeochemical mechanisms that led to their formation remained unknown. To unravel these mechanisms, ^{13}C-depleted carbonate rocks including native sulphur-bearing limestone (Calcare Solfifero) from two locations in Sicily and bedded limestone from the northern Apennines have been studied. Their δ^{13}C values as low as –48‰ reflect incorporation of carbon derived from the oxidation of methane, which was previously suggested to have been linked to bacterial sulphate reduction. Molecular fossils extracted from the limestones reveal that methane was indeed oxidized in an anaerobic process by archaea and sulphate-reducing bacteria. The observed biomarker patterns resemble those of methane-seep carbonates, which form as a consequence of the anaerobic oxidation of methane (AOM). AOM-specific, ^{13}C-depleted biomarkers including archaeal lipids such as PMI (−92 to −75‰) and *sn*2-hydroxyarchaeol (−94‰) as well as compounds derived from sulphate-reducing bacteria (*iso*- and *anteiso*-fatty acids; δ^{13}C as low as −85‰) were identified in the Messinian carbonates. Although the biomarker results clearly point to AOM, the compound inventory also revealed distinct differences to patterns found at marine methane-seeps. For example, *sn*3-hydroxyarchaeol is in some samples the only hydroxyarchaeol present, something usually not found at seeps. Archaeol revealed intermediate δ^{13}C values at most sites (−55 to −30‰), pointing to other archaea than those involved in AOM. The presence of pseudomorphs after lenticular gypsum, high

$\delta^{18}O$ values, and the biomarkers extended hydroxyarchaeol, tetrahymanol, and possibly phytanylglycerol monoethers as well as non-isoprenoidal macrocyclic glycerol diethers confirms that carbonate formation took place under evaporitic conditions. AOM has previously been shown to be inhibited in some brine pools on the modern seafloor. Our observations, however, demonstrate that AOM functions in hypersaline environments as well.

4.1 Introduction

Sulphur-bearing carbonates with low $\delta^{13}C$ values were described from several regions worldwide including the Carpathian foredeep ($\delta^{13}C$ values as low as −54‰ vs. V-PDB; Böttcher and Parafiniuk, 1998; Gasiewicz, 2000), the Limestone Buttes in Texas (as low as −39‰; Kirkland and Evans, 1976), and the 'Calcare Solfifero' in Sicily (as low as −52‰; Decima et al., 1988; Ziegenbalg et al., 2010). These carbonates were interpreted to result from bacterial reduction of sulphate coupled to oxidation of methane. The rationale of this suggestion is that only the incorporation of carbon derived from the oxidation of methane, which is usually very depleted in ^{13}C, can result in such low $\delta^{13}C_{carbonate}$ values (see Peckmann and Thiel, 2004 for a review). This interpretation, however, has not been further validated by other analytical approaches.

The Sicilian sulphur-bearing limestones (Calcare Solfifero) are associated with abundant gypsum, which precipitated in the course of one of the greatest evaporitic events in Earth history, the Messinian salinity crisis (Decima and Wezel, 1973). A sea level drop caused by the cut off of the Mediterranean Sea from the Atlantic Ocean resulted in restricted conditions and the deposition of an evaporitic series, including evaporitic carbonate, sulphate, halite, and bittern salts between 5.96 and 5.33 million years ago (e.g., Hsü et al., 1973a, b; Krijgsman et al., 1999; Duggen et al., 2003). A previous study on the petrography and stable isotope composition of the 'Calcare Solfifero' confirmed that sulphur precipitation resulted from bacterial sulphate reduction, as revealed by low sulphur isotope values of native sulphur and high sulphur isotope values of the accompanying sulphate minerals ($\delta^{34}S$ values as low as −2‰ and as high as +61‰ vs. V-CDT, respectively; Ziegenbalg et al., 2010). Sulphur-bearing carbonates formed either along an (i) epigenetic pathway or a (ii) syngenetic pathway. Epigenetic carbonates are characterized by low $\delta^{13}C$ values (as low as −29‰ vs. V-PDB) due to microbial oxidation of organic compounds (e.g., crude oil) by sulphate reduction in the presence of meteoric waters (as indicated by $\delta^{18}O$ values as low as −4‰ vs. V-PDB). Syngenetic carbonates are characterized by ^{18}O-enrichment (values as high as +9‰), reflecting evaporitic conditions during precipitation. This interpretation is supported by pseudomorphs after lenticular gypsum, which grew in the unconsolidated sediment. The low $\delta^{13}C$ values of syngenetic

carbonates (as low as −52‰) have been interpreted to reflect the oxidation of methane (Decima et al., 1988; Ziegenbalg et al., 2010).

One way to test this hypothesis is the analysis of molecular fossils (i.e., lipid biomarkers). To date, only epigenetic carbonates associated with native sulphur enclosed in Zechstein carbonates of the Harz Mountains, Germany, have been analyzed for their biomarker content. The secondary aragonite ($\delta^{13}C$: −10‰), which formed in recent times, was found to contain pristine biomarkers of sulphate-reducing bacteria (Peckmann et al., 1999a). Here, we subjected syngenetic carbonates of the 'Calcare Solfifero' from Sicily to a biomarker study in order to investigate the inventory of microorganisms that prevailed in the evaporitic setting. For comparison a Messinian carbonate layer from below the base of the gypsum in the northern Apennines was analyzed. We also determined compound-specific carbon isotope compositions to identify the dominant carbon sources of the Messinian microbial community.

4.2 Geological context, rock samples, and methods

Carbonates of the Messinian 'Gessoso solfifera' Formation in Sicily from the localities of Cozzo Disi (CD) and Contrada Gaspa (GA) as well as of the northern Apennines from the Monticino locality (MO) were studied. Petrography as well as stable carbon, oxygen, and sulphur isotope data of carbonates, sulphates, and sulphur from CD and GA were presented by Ziegenbalg et al. (2010). The former sulphur mine of CD is situated southeast of Casteltermini. The CD samples studied here comprise micritic to sparitic limestone with some accessory sulphate minerals and contain large aggregates of native sulphur. The limestone encloses calcite pseudomorphs after lenticular gypsum and exhibits $\delta^{18}O$ values as high as +6‰. The corresponding $\delta^{13}C$ values range from −48 to −45‰. The abandoned sulphur mine of GA is situated close to the street S 230 from Enna to Alimena, between Casa Realmesi and Casa Bastione. The GA micrite, sampled from a limestone cliff, contains calcite pseudomorphs after lenticular gypsum. It is enriched in ^{18}O ($\delta^{18}O$: +3 to +8‰) and depleted in ^{13}C ($\delta^{13}C$: −46 to −34‰). Native sulphur is finely disseminated within the limestone (Ziegenbalg et al., 2010). The MO carbonate, sampled from the Monticino Sanctuary near Brisighella (northern Apennines, Italy; Roveri et al., 2006, p. 45 f), is homogenous and consists of fine-grained dolomite. It is less ^{13}C-depleted than the Sicilian carbonates, but also enriched in ^{18}O ($\delta^{13}C$: −27 to −23‰; $\delta^{18}O$: +7‰; unpublished results). No native sulphur was detected in the studied sample.

Sample preparation, dissolution, extraction, and analyses were performed according to methods reported by Birgel et al. (2006b). Briefly, limestones were carefully cleaned with acetone and HCl. Afterwards the carbonate was dissolved in HCl. The remaining sediment was saponified and extracted with a microwave extraction system (CEM MARS X) at 80°C and 300 W with CH_2Cl_2:MeOH

(3:1). The resulting extract was separated into four fractions of increasing polarity by column chromatography (hydrocarbons, ketones/esters, alcohols, fatty acids). In the following we discuss the hydrocarbon, alcohol, and fatty acid fractions. Compounds were examined by coupled gas chromatography-mass spectrometry (GC-MS) with a Thermo Electron Trace GC-MS. Molecules were identified based on retention times and in comparison with published mass spectra. Contents are given in ng/g dry weight of the non-decalcified sample. Compound specific carbon isotope analysis (irm-GC/MS) was performed with a Thermo Electron GC-combustion-III-interface linked to a Thermo Electron Delta-plus XP mass spectrometer. Carbon isotope values are given in the δ-notation relative to the Vienna-Peedee-Belemnite (V-PDB) standard. Several pulses of CO_2 gas of known isotopic composition at the beginning and the end of the runs were used for calibration.

4.3 Results

4.3.1 Hydrocarbon fraction

The sample GA-j shows much higher contents of total hydrocarbons (1046 ng/g; Table 4-1) than samples CD and GA-b (260 and 284 ng/g, respectively). In the Sicilian samples, *n*-alkanes are the prevalent compound class in the hydrocarbon fraction, ranging from *n*-C_{17} to *n*-C_{33}. They represent more than 50 weight% of all hydrocarbons. Short-chain hydrocarbons are predominant in the CD sample, peaking at *n*-C_{20}, which accounts for 12% of the hydrocarbons. Long-chain hydrocarbons dominate in the GA-j sample, with *n*-C_{31} as predominant compound (13%). GA-b displays a bimodal pattern, peaking at *n*-C_{20} and *n*-C_{31} (8 and 9%, respectively).

Table 4-1: Contents and stable isotope compositions of molecular fossils. Data in brackets give the percentage of the component with respect to the particular fraction; cont.: contaminated; n.a.: not analyzed; n.d.: not detected; tr.: traces. a) Hydrocarbon fraction. The hydrocarbon fraction of GA-p could not be quantified, due to contamination of the used standard. The hydrocarbon fraction of MO got lost during sample preparation.

Hydrocarbon fraction	**CD**		**GA-b**		**GA-j**		**GA-p**		**MO**
	ng/g (%)	‰	ng/g (%)	‰	ng/g (%)	‰	ng/g	‰	ng/g (%)
n-C_{20}	32.5 (12)	-29	22.8 (8)	-27	10.9 (1)	tr.			
n-C_{31}	4.2 (2)	tr.	24.5 (9)	-33	136.8 (13)	-29			
n-alkanes (sum)	*182.0 (70)*	*-29*	*159.7 (56)*	*-27*	*646.5 (62)*	*-28*	*cont.*		
PMI	13.6 (5)	-75	21.7 (8)	-92	60.4 (6)	-92		-101	
Squalane (tail to tail)	17.2 (6)	-57	n.d.		53.6 (5)	tr.		-24	n.a.
Squalane (head to tail)	n.d.		n.d.		44.8 (4)	tr.	n.d.		
Biphytane	n.d.		n.d.		17.4 (2)	tr		-95	
Pristane	n.d.		n.d.		8.9 (1)	tr.	n.d.		
Phytane	18.7 (7)	-29	tr.	tr.	9.4 (1)	-33	cont.		
Sum hydrocarbons	*260.4*		*284.4*		*1045.9*				

Tail-to-tail linked pentamethylicosane (PMI; Table 4-1) is one of the main isoprenoidal compounds in the hydrocarbon fractions of CD and GA limestones, accounting for 5 to 8%. Except for

GA-b, it is accompanied by the tail-to-tail linked C_{30} isoprenoid squalane. An accessory compound in GA-j is head-to-tail linked squalane. The head-to-tail linked C_{20} isoprenoid phytane is the main isoprenoidal compound in the hydrocarbon fraction of the CD sample, accounting for 7% of the hydrocarbons. It is also present in lower proportions in the GA-j sample and in traces in the GA-b sample. Moreover, the GA-j limestone shows minor amounts of the head-to-tail C_{19} isoprenoid pristane. In the GA-j and -p samples the head-to-head linked acyclic C_{40}-isoprenoid biphytane is present.

Table 4-1: continued. b) Alcohol fraction.

Alcohol fraction	**CD**		**GA-b**		**GA-j**		**GA-p**		**MO**	
	ng/g (%)	‰	ng/g (%)	‰	ng/g (%)	‰	ng/g (%)	‰	ng/g (%)	‰
n-C_{16}	34.3 (19)	-49	22.8 (3)	-44	98.1 (5)	-39	18.7 (4)	tr.	4.0 (6)	tr.
n-C_{18}	21.9 (12)	-28	18.3 (3)	-32	77.5 (4)	-30	21.2 (5)	-33	4.2 (7)	tr.
n-C_{24}	4.5 (3)	tr.	115.7 (17)	-17	268.3 (15)	-18	103.3 (24)	-18	2.7 (4)	tr.
n-alcohols (sum)	*105.0(60)*	*-35*	*453.4 (66)*	*-23*	*1123.6 (61)*	*-24*	*305.9 (70)*	*-22*	*21.9 (35)*	
Phytanol	9.9 (6)	-32	52.1 (8)	-36	135.7 (7)	-27	62.3 (14)	-20	2.0 (3)	tr.
Archaeol	19.3 (11)	-34	80.3 (12)	-55	254.1 (14)	-52	25.6 (6)	-30	13.4 (21)	-89
*sn*2-OH-archaeol	4.9 (3)	-94	9.8 (1)	tr.	n.d.		n.d.		n.d.	
*sn*3-OH-archaeol	n.d.		tr.	tr.	26.7 (1)	-79	n.d.		25.6 (41)	-95
Extended archaeol	n.d.		tr.	tr.	n.d.		n.d.		n.d.	
*sn*2-phytanylglycerol monoether	3.3 (2)	tr.	14.3 (2)	-29	36.7 (2)	-21	8.6 (2)	tr.	n.d.	
*sn*3-phytanylglycerol monoether	1.8 (1)	tr.	10.6 (2)	tr.	18.4 (1)	-20	2.8 (1)	tr.	n.d.	
MAGE $_{16:0}$	7.1 (4)	tr.	2.4 (<1)	tr.	9.7 (1)	tr.	n.d.		n.d.	
MAGE $_{17:0}$	1.8 (1)	tr.	n.d.		n.d.		n.d.		n.d.	
C_{30}-DAGE	n.d.		15.0 (2)	tr.	n.d.		n.d.		n.d.	
C_{31}-DAGE	6.4 (4)	tr.	n.d.		35.0 (2)	-89	n.d.		n.d.	
C_{32}-macrocyclic glycerol	5.2 (3)	tr.	4.9 (1)	tr.	5.0 (<1)	tr.	n.d.		n.d.	
C_{33}-macrocyclic glycerol	6.0 (3)	tr.	7.2 (1)	tr.	16.6 (1)	tr.	n.d.		n.d.	
C_{34}-macrocyclic glycerol	5.3 (3)	tr.	6.1 (1)	tr.	15.7 (1)	tr.	n.d.		n.d.	
Tetrahymanol	n.d.		28.0 (4)	-19	105.7 (6)	-28	24.5 (6)	-21	n.d.	
Cholesterol	3.6 (2)	tr.	7.4 (1)	tr.	66.2 (4)	-29	5.0 (1)	tr.	n.d.	
Sum alcohols	*179.3*		*691.1*		*1848.9*		*434.7*		*62.9*	

4.3.2 Alcohol fraction

The *n*-alcohols range from *n*-C_{12} to *n*-C_{32} with an even over odd predominance. Except for the MO sample, they represent 60 to 70% of the alcohol fraction (Table 4-1). Short chain *n*-alcohols from *n*-C_{14} to *n*-C_{20} are predominant in the CD limestone, with *n*-C_{16} as main compound accounting for 19% of all compounds in the alcohol fraction. In GA samples, the mid- and long-chain *n*-alcohols are prominent, peaking at *n*-C_{24} (15 to 24% of all alcohol compounds; Fig. 4-1a).

The alcohol fraction of the MO limestone contains less lipids (63 ng/g) than the Sicilian samples (179 to 1849 ng/g). The isoprenoidal compounds archaeol and *sn*3-hydroxyarchaeol are by far the most abundant compounds in the alcohol fraction of the MO sample, accounting for 21 and 41%,

respectively. The *sn*3-hydroxyarchaeol content even doubles that of archaeol, while other compounds like *n*-alcohols and phytanol are present in much lower amounts (2 to 4 ng/g).

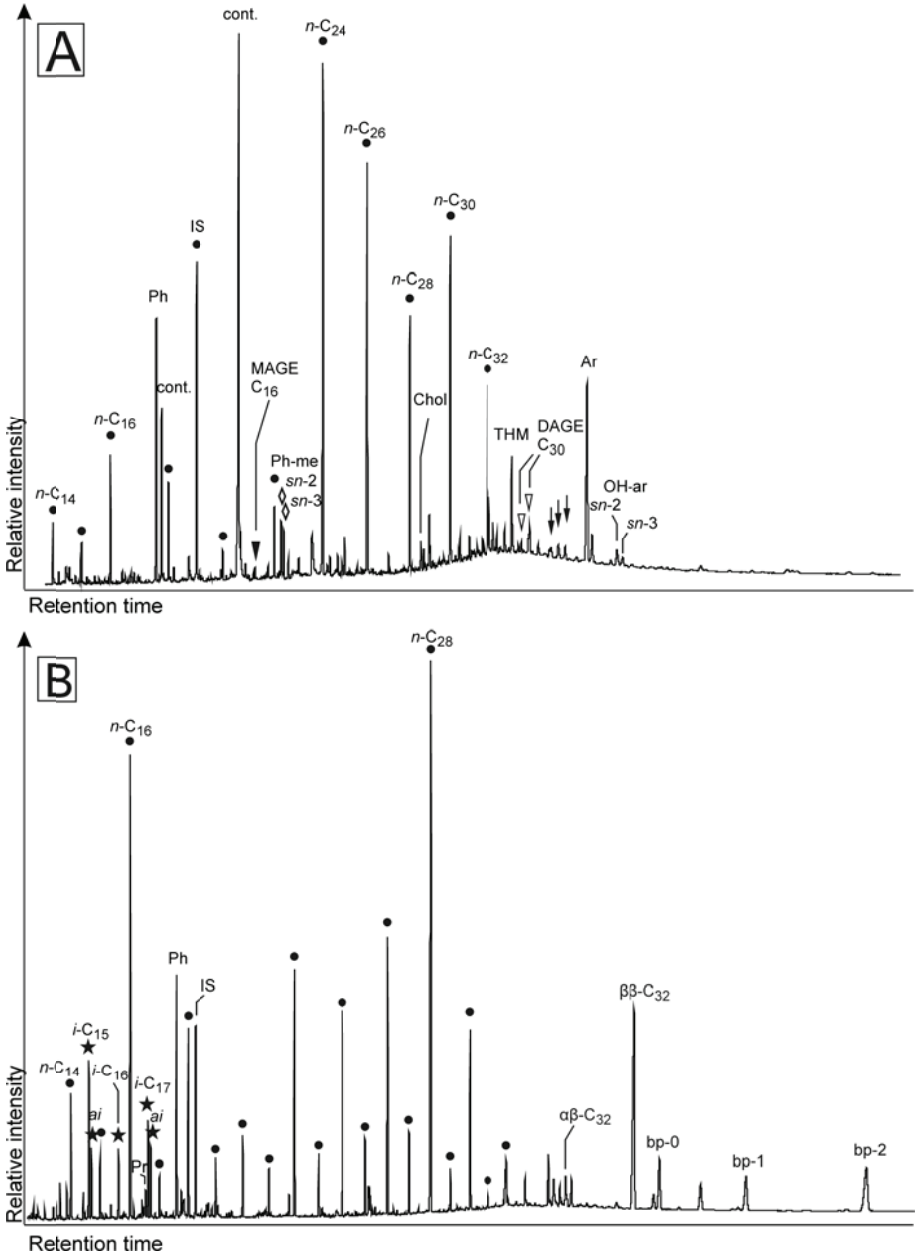

Figure 4-1 Gas chromatograms of sample GA-b. a) Alcohol fraction, black dots: saturated *n*-alcohols; black arrow-head: monoalkyl glycerolether (MAGE); white arrow-heads: dialkyl glycerolethers (DAGEs); white diamonds: phytanylglycerol monoethers (Ph-me); black arrows: macrocyclic glycerol diethers; Ar: archaeol; Chol: cholesterol; cont.: contaminant; IS: internal standard; OH-ar: hydroxyarchaeol; Ph: phytanol; THM: tetrahymanol. B) Carboxylic acid fraction; black dots: saturated *n*-fatty acids; black stars: *iso*- and *anteiso*- fatty acids; αβ-C_{32}: 17α(H), 21β(H)-C_{32}-hopanoic acid; ββ-C_{32}: 17β(H), 21β(H)-C_{32}-hopanoic acid; Bp-0, Bp-1, Bp-2: biphytanic diacids with 0, 1 or 2 cyclopentane rings; IS: internal standard; Ph: phytanic acid; Pr: pristanic acid.

In the Sicilian samples, archaeol is present in substantial amounts, representing 6 to 14% of all compounds of the alcohol fraction. It is accompanied by minor amounts of the *sn*2-hydroxyarchaeol in the CD sample, *sn*3-hydroxyarchaeol in the GA-j sample and by both compounds in the GA-b

sample. The GA-b limestone contains traces of *O*-phytanyl-*O*-sesterterpanyl glycerolether (extended archaeol). Phytanol accounts for 6 to 14%. In the GA-p limestone, its content exceeds that of archaeol. Phytanol is accompanied by smaller amounts of *sn*2- and *sn*3-phytanylglycerol monoethers in the CD and GA samples. Monoalkyl glycerolethers (MAGEs) and dialkyl glycerolethers (DAGEs) are present in the CD limestone, where they account for 1 to 4%. In the same sample, non-isoprenoidal C_{32}, C_{33}, and C_{34} macrocyclic glycerol diethers (cf., Blumenberg et al., 2007) represent 3% of all compounds in the alcohol fraction. MAGEs, DAGEs, and macrocyclic glycerol diethers are also present in minor amounts in the Gaspa-b and -j samples. The most abundant pentacyclic terpenoid in the GA samples is tetrahymanol. This compound was not detected in the CD and MO limestones. Cholesterol was the only tetracyclic terpenoid present, but its contents are only minor.

Table 4-1: continued. Carboxylic acid fraction; Bp-0, Bp-1, Bp-2: biphytanic diacids with 0, 1 or 2 cyclopentane rings.

Carboxylic acids	**CD**		**GA-b**		**GA-j**		**GA-p**		**MO**	
	ng/g (%)	‰	ng/g (%)	‰	ng/g (%)	‰	ng/g (%)	‰	ng/g (%)	‰
n-$C_{15:0}$	26.8 (3)	-31	24.4 (1)	-41	112.5 (2)	-36	56.6 (3)	-30	7.8 (3)	-37
n-$C_{16:0}$	245.2 (26)	-34	186.1 (10)	-36	775.7 (15)	-34	516.8 (23)	-30	46.3 (19)	-28
n-$C_{17:0}$	8.4 (1)	-31	16.7 (1)	-33	83.3 (2)	-30	28.1 (1)	-27	5.1 (2)	-24
n-$C_{18:0}$	62.7 (7)	-27	74.0 (4)	-28	357.3 (7)	-29	186.6 (8)	-28	23.8 (10)	-25
n-$C_{22:0}$	225.6 (24)	-24	97.6 (5)	-18	360.5 (7)	-22	195.0 (9)	-20	22.6 (9)	-20
n-$C_{28:0}$	51.7 (6)	-14	291.4 (15)	-21	392.5 (8)	-22	214.1 (9)	-21	5.8 (2)	-29
n-carboxylic acids (sum)	*719.2 (76)*	*-25*	*1205.3 (62)*	*-24*	*3516.3 (69)*	*-25*	*1856.2 (81)*	*-23*	*198.9 (81)*	*-26*
iso-$C_{15:0}$	20.9 (2)	-83	58.5 (3)	-80	136.2 (3)	-81	39.7 (2)	tr.	4.2 (2)	-33
anteiso-$C_{15:0}$	11.6 (1)	-53	24.9 (1)	-68	69.4 (1)	-70	27.1 (1)	tr.	3.5 (1)	-27
iso-$C_{16:0}$	15.0 (2)	-85	28.3 (2)	-70	71.3 (1)	-68	20.2 (1)	tr.	3.1 (1)	-26
iso-$C_{17:0}$	17.4 2)	-84	39.1 (2)	-55	92.8 (2)	-55	22.2 (1)	tr.	2.8 (1)	-34
anteiso-$C_{17:0}$	tr.	tr.	28.3 (1)	-70	58.0 (1)	-61	13.6 (1)	tr.	1.5 (1)	-31
10Me-$C_{16:0}$	48.4 (5)	-90	n.d.		28.4 (1)	tr.	n.d.		2.7 (1)	-69
αβ-C_{32}-hopanoic acid	n.d.		20.7 (1)	-52	tr.	tr.	n.d.		n.d.	
ββ-C_{32}-hopanoic acid	46.0 (5)	-87	238.0 (12)	-77	648.3 (13)	-76	100.4 (4)	-65	11.5 (5)	-31
Bp-0	tr.	tr.	59.4 (3)	-97	n.a.	n.a.	17.9 (1)	-78	7.3 (3)	-73
Bp-1	tr.	tr.	53.3 (3)	-104	n.a.	n.a.	9.5 (<1)	-100	5.5 (2)	-93
Bp-2	tr.	tr.	95.0 (5)	-105	n.a.	n.a.	14.0 (1)	-103	3.9 (2)	-99
Phytanic acid	25.7 (3)	-97	99.2 (5)	-42	227.5 (5)	-32	157.1 (7)	-21	n.d.	
Pristanic acid	tr.	tr.	n.d.		32.0 (1)	tr.	19.1 (1)	tr.	n.d.	
Sum carboxylic acids	*946.8*		*1950.1*		*5070.1*		*2297.0*		*245.0*	

4.3.3 Carboxylic acid fraction

This fraction revealed the highest contents of compounds for all sites. The GA-j sample shows the highest total contents (5070 ng/g; Table 4-1). Saturated *n*-fatty acids are the predominant components, accounting for 62 to 81%. They range from *n*-C_{12} to *n*-C_{30} with an even over odd predominance, peaking either at *n*-C_{16} (CD, GA-j and -p, MO), or at *n*-C_{28} (GA-b; Fig. 4-1b). The

terminally-branched *iso*- and *anteiso*-$C_{15:0}$ and $C_{17:0}$ fatty acids, as well as *iso*-$C_{16:0}$ fatty acid are present in all samples, representing 1 to 3%. The ratio of *anteiso*-$C_{15:0}$ relative to *iso*-$C_{15:0}$ is between 0.4 and 0.8. The contents of the branched fatty acids even partly exceeds the saturated unbranched homologues (*iso*-$C_{15:0}$> *n*-$C_{15:0}$ and *iso*-$C_{17:0}$> *n*-$C_{17:0}$ in GA-b and -j). A mid-chain methyl branched $C_{16:0}$ fatty acid, namely 10Me-$C_{16:0}$, is present in substantial amounts in the CD limestone, accounting for 5% of all compounds in the carboxylic acid fraction (Table 4-1). This compound is present in lower amounts in the GA-j and MO limestones. 17β(H),21β(H)-C_{32} hopanoic acid is found in all samples. It accounts for 4 to 5% of the carboxylic acids in the CD, GA-p, and MO samples. In the GA-b and -j limestones it is among the major compounds, representing 12 to 13% (Table 4-1). In the GA-b limestone, the ββ isomer is accompanied by minor amounts of the αβ isomer. Sparse pristanic (CD, GA-j and-p) and more abundant phytanic acid (all samples except MO) were detected. Biphytanic diacids with 0, 1, or 2 cyclopentane rings are present in almost all samples (not detected in the GA-j sample). They account for up to 5% in the GA-b limestone.

4.3.4 Compound specific stable carbon isotope data

The *n*-alkanes, *n*-alcohols, and *n*-fatty acids display $\delta^{13}C$ values from −49‰ to −20‰ (Table 4-1; Fig. 4-2). The branched fatty acids from the CD and GA limestone, show low $\delta^{13}C$ values (−90 to −53‰). Similar $\delta^{13}C$ values were obtained for the 17β(H),21β(H)-C_{32}-hopanoic acid for the CD and GA samples (−87 to −65‰). In the MO sample, the $\delta^{13}C$ values of the terminally-branched fatty acids as well as the 17β(H),21β(H)-C_{32}-hopanoic acid are in the same range as the *n*-fatty acids.

Among the isoprenoids, biphytanic diacids (−105 to −73‰) and PMI (−101 to −75‰) are the most ^{13}C-depleted compounds in all samples. Interestingly, biphytanic diacids show a decrease in their $\delta^{13}C$ value with increasing number of rings. Biphytane (−95‰) and *sn*2- and *sn*3-hydroxyarchaeol (−94 to −79‰) belong to the group of ^{13}C-depleted compounds. The isotopic composition of archaeol varies significantly among the various samples. Intermediate $\delta^{13}C_{archaeol}$ values were obtained for the GA-b and -j samples (−55 and −52‰, respectively), while higher values were measured for the CD and GA-p samples (−34 and −30‰, respectively). Only in the MO limestone, archaeol exhibits a strong ^{13}C-depletion (−89‰). Values of irregular squalane vary between −57‰ (CD) and −24‰ (GA-p). The two isoprenoids *sn*2- and *sn*3-phytanylglycerol monoethers ($\delta^{13}C$: −29 to −20‰) as well as the pentacyclic terpenoid tetrahymanol ($\delta^{13}C$: −28 to −19‰) revealed $\delta^{13}C$ values typical for marine lipids.

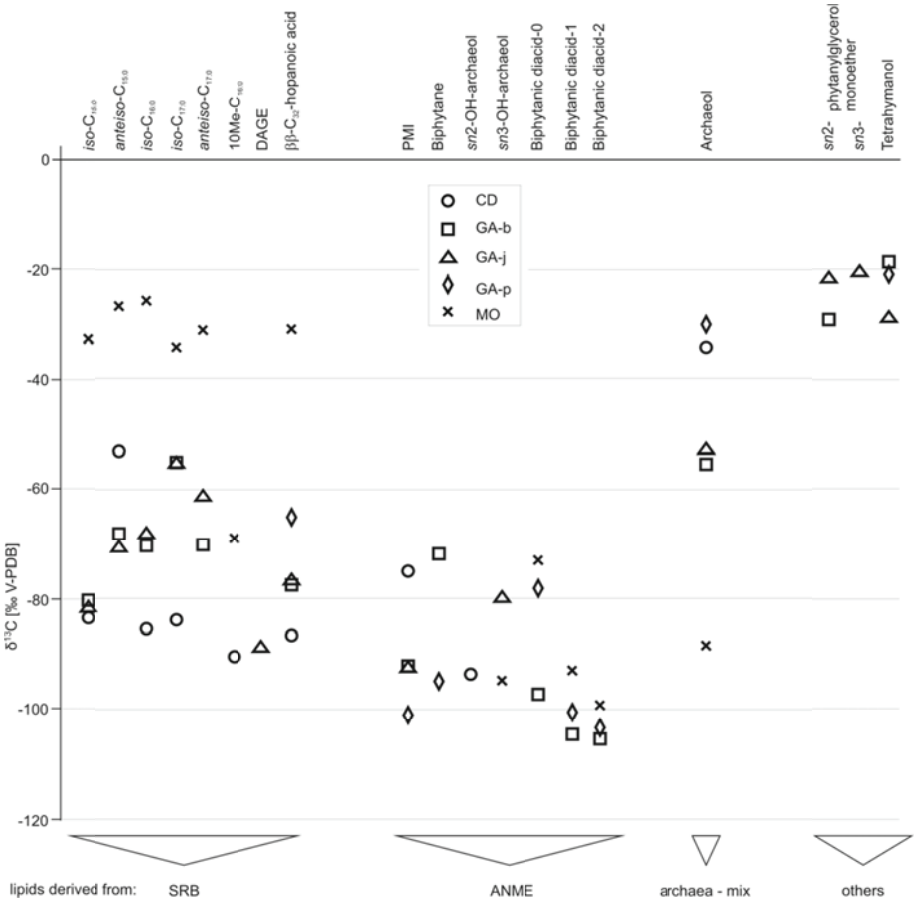

Figure 4-2 Carbon isotopic composition of selected molecular fossils, illustrating a shift towards slightly higher $\delta^{13}C$ values from markers of anaerobic methanotrophic archaea (ANME) to markers of sulphate reducing bacteria (SRB) and the wide span of $\delta^{13}C$ values reflecting a mixture from ANME-sourced archaeol and archaeol derived from other, non-methanotrophic archaea carrying the isotopic signature of organic matter from the water column (archaea – mix). Note that SRB lipids from Monticino cluster at higher $\delta^{13}C$ values (black crosses).

4.4 Discussion

4.4.1 Molecular fossils of Messinian authigenic carbonates resemble those of methane-seep carbonates

Sulphate-dependent anaerobic oxidation of methane (AOM) is performed by a consortium of anaerobic methane-oxidizing archaea (ANME) and sulphate-reducing bacteria (SRB; Boetius et al., 2000; Hinrichs et al., 2000; Orphan et al., 2001a; Thiel et al., 2001; Michaelis et al., 2002; Knittel et al., 2003). PMI with extremely low $\delta^{13}C$ values is among the most persistent molecular fossils of ANME in methane-seeps deposits (e.g., Peckmann et al., 1999b, 2009; Thiel et al. 1999; Birgel et al., 2008b). The presence of ^{13}C-depleted PMI ($\delta^{13}C$ values as low as −101‰) in all Sicilian samples reveals that ANME were present in the sediment during carbonate formation, confirming that methane was oxidized anaerobically in the Messinian hypersaline environment. When found in seep settings, ^{13}C-depleted archaeol has been attributed to ANME related to the order *Methanosarcinales* (Hinrichs et al., 1999). The strongly ^{13}C-depleted archaeol in the MO sample was most likely sourced

exclusively or predominantly by ANME. In contrast, in all Sicilian samples archaeol shows a significant variation in $\delta^{13}C$ values compared to PMI (Fig. 4-2). Since archaeol is a common membrane lipid in many euryarchaea including methanogens and halophiles (Tornabene and Langworthy, 1979; De Rosa and Gambacorta, 1988; Kates, 1993; Koga et al., 1993, 1998), this compound apparently derived from various archaeal sources, causing the wide scatter of its isotopic composition. In contrast to archaeol, the diethers *sn*2- and *sn*3-hydroxyarchaeol yielded $\delta^{13}C$ values in the same range as PMI, pointing to ANME as exclusive source organisms. Whereas *sn2*-hydroxyarchaeol is commonly observed especially in ANME-2 (e.g., Hinrichs et al., 1999, 2000; Pancost et al., 2000; Blumenberg et al., 2004; Niemann and Elvert, 2008), *sn*3-hydroxyarchaeol is not common in seep-dwelling ANME; if present, it is accompanied by *sn*2-hydroxyarchaeol (Pancost et al., 2001b; Elvert et al., 2005). Like in GA-j and MO limestones, *sn*3-hydroxyarchaeol was found as the sole hydroxyarchaeol only in methane-seep carbonates from the Sorokin Trough (Black Sea) and Eocene carbonate-cemented tubular sandstones, agreeing with its origin from yet unknown ANME in these settings (Stadnitskaia et al., 2005; De Boever et al., 2009). Stadnitskaia et al. (2005) proposed that its source organisms are closely related to ANME-1. The absence of crocetane in the Messinian samples, a molecular fossil indicative of ANME-2 (Blumenberg et al., 2004), also suggests that the Messinian methane-oxidizing archaea were related to ANME-1 rather than to ANME-2 archaea. Furthermore, ^{13}C-depleted biphytanic diacids with no to two cyclopentane rings were found in almost all samples (Fig. 4-2). Although the source of biphytanic diacids is yet to be determined, they have been regularly found in ancient seep limestones (Birgel et al., 2008a), including the Eocene carbonate-cemented tubular sandstones that also yielded *sn3*-hydroxyarchaeol as the sole hydroxyarchaeol homologue (De Boever et al., 2009). This pattern indicates that the ^{13}C-depleted biphytanic diacids derived exclusively from methanotrophic euryarchaea, making them excellent candidates to trace the endmember isotopic composition of lipids derived from methane-oxidizing archaea (cf., Birgel et al., 2008a).

SRB of the genera *Desulfosarcina/Desulfococcus (DSS)* are the syntrophic partners of ANME-1 and -2 (e.g., Orphan et al., 2001a; Knittel et al., 2003). Biomarkers of *DSS*, including the relative persistent terminally-branched fatty acids *iso*- and *anteiso*-$C_{15:0}$ (Birgel et al., 2006a), have been identified in various methane-seep environments (Niemann and Elvert, 2008). As all Sicilian samples yielded ^{13}C-depleted terminally-branched fatty acids (Table 4-1), SRB were apparently involved in the oxidation of methane in the Messinian sediments. Likewise, the observation that the SRB markers are about 10 to 30‰ less depleted in ^{13}C than the archaeal markers indicates that methane was oxidized in a similar fashion like at methane-seeps (Fig. 4-2; cf., Hinrichs et al., 2000; Orphan et al., 2001a).

Although the biomarker pattern of the Messinian limestones revealed remarkable similarities with that of methane-seep deposits, there are also distinct differences. A preponderance of *anteiso*-$C_{15:0}$ over *iso*-$C_{15:0}$ fatty acid has commonly been observed in seep deposits (e.g., Hinrichs et al. 2000; Elvert et al. 2003; Pape et al. 2005; Niemann and Elvert, 2008). This pattern was also recognized in cultures of *Desulfosarcina* and *Desulfococcus* (Rütters et al., 2001, 2002), genera representing the syntrophic partners of ANME (Boetius et al., 2000; Orphan et al., 2001a, b, 2002; Knittel et al., 2003). In contrast to this, the *anteiso*-$C_{15:0}$ to *iso*-$C_{15:0}$ ratios vary from 0.4 (GA-b) to 0.8 (MO) in the Messinian limestones. Such ratios have been reported from cultured sulphate-reducing bacteria, which are not commonly associated to ANME, as for example *Desulfobacter* and *Desulfovibrio* (Taylor and Parkes, 1983; Edlund et al., 1985; Dowling et al., 1986; Londry et al., 2004). Similar and even lower ratios were found in reef-microbialites from off Tahiti, where SRB have been suggested to drive carbonate precipitation (Heindel et al., 2010).

Apart from *iso*- and *anteiso*-$C_{15:0}$ fatty acids of *iso*- and *anteiso*-$C_{17:0}$ fatty acids were found in all GA samples. Contents of terminally-branched $C_{15:0}$ and $C_{17:0}$ fatty acids mostly exceed those of the corresponding *n*-C fatty acids in the GA samples. Although *iso*- and *anteiso*-$C_{17:0}$ fatty acids occur in *DSS,* they are not as prominent in these bacteria as in other sulphate-reducing bacteria like *Desulfobacter* and *Desulfovibrio* (Taylor and Parkes, 1983; Rütters et al., 2001; Könneke and Widdel, 2003). Furthermore, 10Me-$C_{16:0}$ fatty acid, one of the most abundant and most ^{13}C-depleted fatty acids in the CD limestone, is a very prominent compound in the genus *Desulfobacter* (Taylor and Parkes, 1983; Dowling et al., 1986; Coleman et al., 1993; Könneke and Widdel, 2003; Londry et al., 2004), but it has not been reported to be synthesized by *DSS*. Like the terminally-branched fatty acids, it has been detected at modern methane-seeps and was suggested to be derived from yet unknown sulphate reducers involved in AOM based on its ^{13}C-depletion (e.g., Hinrichs et al. 2000; Elvert et al. 2003). The non-isoprenoidal mono- and dialkyl glycerolethers (MAGEs and DAGEs) detected in the Messinian limestones have commonly been interpreted as molecular fossils of sulphate-reducing bacteria involved in AOM when found at seeps (cf., Hinrichs et al., 2000; Orphan et al., 2001a; Pancost et al., 2001a; Werne et al., 2002). Even so the contents of MAGEs and DAGEs are low, and only one $\delta^{13}C$ value of −89‰ was obtained for DAGE-C_{31} (GA-j), their presence in the CD, GA-b, and GA-j samples contributes to the line of evidence that sulphate-reducing bacteria were involved in methane oxidation in the Messinian evaporitic settings.

The ββ-bishomohopanoic acid is present in all Sicilian samples in substantial amounts, especially in the GA samples. Its low $\delta^{13}C$ values demonstrate the incorporation of methane-derived carbon. Pancost et al. (2000) interpreted ^{13}C-depleted hopanoids accompanying other ^{13}C-depleted bacterial markers as lipids derived from sulphate-reducing bacteria involved in AOM. Similarly, hopanoic acids

found in microbial mats from the Black Sea have been interpreted to be derived from anaerobic bacteria (Thiel et al., 2003). Blumenberg et al. (2006), studying enrichment cultures from the Black Sea mats, confirmed that *Desulfovibrio* strains are able to produce bacteriohopanepolyols. To date, *Desulfovibrio* are the only SRB known to synthesize hopanoids. The $\delta^{13}C$ values of the ββ-bishomohopanoic acids in the Sicilian samples fall in the range of SRB-derived branched fatty acids (Table 4-1), which would agree with an assignment of this compound to SRB, but another bacterial source including aerobic bacteria cannot be excluded.

In the sample from the northern Apennines, the lipids derived from sulphate-reducing bacteria (terminally-branched fatty acids, possibly ββ-bishomohopanoic acid) are not strongly ^{13}C-depleted, in contrast to the archaeal markers (Fig. 4-2). The majority of sulphate-reducing bacteria, which were present in that ecosystem, were apparently not involved in AOM. Deduced from FISH-SIMS data, Orphan et al. (2002) stated that ANME-1 appear not to be as dependent on their SRB partners as ANME-2. Accordingly, some methanotrophic archaea seem to be able to run sulphate-dependent AOM completely autonomous as reported from a subzero hypersaline methane-seep (Niederberger et al., 2010). The lack of ^{13}C-depleted bacterial lipids in the sample from the northern Apennines may consequently indicate that AOM was performed by archaea alone, as a preservational bias seem unlikely, given that AOM-lipids tend to be very well preserved in methane-derived carbonates (Birgel et al., 2008b).

4.4.2 The Messinian microbial ecosystem characterized by molecular fossils

In a previous study on the Messinian limestones, including the GA and CD samples, very low $\delta^{13}C_{carbonate}$ values were interpreted to reflect methane oxidation coupled to the reduction of sulphate (Ziegenbalg et al., 2010). The new biomarkers now show that carbonate precipitation was induced by the activity of an AOM consortium similar to that at methane-seeps. But in contrast to seep carbonates, high $\delta^{18}O$ values and pseudomorphs after gypsum in the CD and GA samples reflect hypersaline conditions (Ziegenbalg et al., 2010). Although sulphate-dependant AOM has been suggested to occur in hypersaline environments (Pancost et al., 2000, 2001b; Daffonchio et al., 2006; Huguen et al., 2009; Omoregie et al., 2009; Wankel et al., 2010), Joye et al. (2009b) argued that high chloride concentrations suppress the activity of methane-oxidizing archaea.

Additional evidence for the presence of hypersaline conditions during the formation of the Messinian carbonates stems from some of the observed molecular fossils. Although the pentacyclic terpenoid tetrahymanol, which is present in all GA samples, was detected in various organisms including ferns (Zander et al., 1969), rumen fungus (Kemp et al., 1984), bacteriovorous ciliates (Harvey and McManus, 1991), and in anoxygenic phototrophic bacteria (Kleemann et al., 1990;

Rashby et al., 2007), this compound or its putative diagenetic product gammacerane is particularly abundant in hypersaline environments (ten Haven et al., 1988, 1989). Extended archaeol is among the most specific molecular fossils of halophilic archaea (Teixidor et al., 1993). This compound is present in GA-b. Other than extended archaeol, *sn2*- and *sn3*-hydroxyarchaeol are ubiquitously distributed in methanogenic, methanotrophic, and facultative halophilic archaea of the orders *Methanosarcinales* and *Methanococcales* (Sprott, 1992; Sprott et al., 1990, 1993; Koga et al., 1993). Since *sn2*- and *sn3*-hydroxyarchaeol revealed significant ^{13}C-depletion, a methanotrophic source organism seems likely. Only in sample GA-j *sn3*-hydroxyarchaeol is about 10‰ less depleted in ^{13}C than PMI, possibly suggesting an additional contribution from non-methanotrophic archaea.

Although PMI is now commonly used as a biomarker for methanogenic or methanotrophic archaea, PMI was originally accounted as marker for hypersaline conditions (Waples et al., 1974). This reasoning was based on the ability of halophilic methanogenic archaea to synthesize this compound (Holzer et al., 1979; Tornabene et al., 1979). However, based on the low δ^{13}C values of PMI in the analyzed samples, a significant contribution from methanogenic archaea is unlikely. In contrast to PMI and the hydroxyarchaeols, archaeol revealed a wide range of δ^{13}C values. In all Sicilian samples it is less depleted than the AOM lipids (Table 4-1, Fig. 4-2), pointing to additional sources to methanotrophic archaea.

The phytanylglycerol monoethers identified in all Sicilian samples have been suggested to represent hydrolysis-products of hydroxyarchaeol based on lab cultures (Koga et al., 1993; Oba et al., 2006). The only report from environmental samples stems from modern seeps, where a highly ^{13}C-depleted *sn*1-phytanylglycerol monoether (equivalent to our *sn*3-phytanylglycerol monoether) was suggested to derive from diethers of methanotrophic archaea (Hinrichs et al., 2000). With respect to the Sicilian samples the strong difference of δ^{13}C values between the phytanylglycerol monoethers (δ^{13}C: −29 to −20‰) and the two hydroxyarchaeols (δ^{13}C: −95 and −79‰) disagrees with a common source of these compounds. Instead, phytanylglycerol monoethers derived from non-methanotrophic archaea, possibly halophiles.

The non-isoprenoidal macrocyclic glycerol diethers found in the CD and GA-b and -j samples (Table 4-1) were described from hydrothermal systems (Pancost et al., 2006; Blumenberg et al., 2007), but were never extracted from cultured bacteria. Recently, Baudrand et al. (2010) described these compounds from a hypersaline, non-hydrothermal setting from the Messinian of Egypt and Spain. Although evaporitic settings may be hot, there is no indication that the rocks analyzed here or those analyzed by Baudrand et al. (2010) formed under hydrothermal conditions. It seems, therefore, most likely that these compounds derived from unknown halophilic bacteria (cf., Baudrand et al., 2010).

4.5 Conclusions

^{13}C-depleted molecular fossils of anaerobic methane-oxidizing archaea and sulphate-reducing bacteria are present in authigenic carbonates, which occur in sediments deposited during the Messinian salinity crisis in Sicily and the northern Apennines. The carbonates precipitated during evaporitic and hypersaline conditions as confirmed by high δ^{18}O values, pseudomorphs after lenticular gypsum, and biomarkers indicating hypersaline conditions including extended archaeol, tetrahymanol, phytanylglycerol monoethers, and non-isoprenoidal macrocyclic glycerol diethers . These results confirm that sulphate-dependent anaerobic oxidation of methane functions under hypersaline conditions as well. The observed biomarker pattern shows that the microbial consortium that mediated anaerobic oxidation of methane (AOM) was similar but not identical to AOM consortia at methane-seeps. Some ^{13}C-depleted lipids like PMI, *sn*2-hydroxyarchaeol, *iso*- and *anteiso*-$C_{15:0}$ fatty acid, MAGEs and DAGEs point to the presence of ANME and their syntrophic partners *DSS*, typically inhabiting methane-seeps. Other lipids including *sn*3-hydroxyarchaeol, and 10Me-$C_{16:0}$ fatty acid as well as the ratio between the *iso*- and *anteiso*- fatty acids suggest that different methanotrophic archaea and sulphate-reducing bacteria were involved in methane oxidation in the Messinian hypersaline environment.

Acknowledgements

We thank Sebastian Flotow (Bremen) for sample preparation, Sarah Janoschek and Karsten Hellwig (both Bremen) for analytical support, as well as Adrian Immenhauser (Bochum), Marie-Madeleine Blanc-Valleron (Paris), Antonio Caruso (Paris), Beno Brunner (Bremen), and Patrick Meister (Bremen) for help collecting the samples. This project was supported by the Deutsche Forschungs Gemeinschaft through the international graduate college EUROPROX and the DFG-Excellence Cluster MARUM, Bremen.

5 - THIRD MANUSCRIPT

Gypsum whiskers in Messinian evaporites identified by µ-XRD²

S.B. Ziegenbalg[1], C. Berthold[2], A. Kappler[3], J. Peckmann[4]

[1] University of Bremen, MARUM – Center for Marine Environmental Sciences, 28359 Bremen, Germany

[2] Eberhard-Karls-University Tübingen, Institute for Geoscience, AB Mineralogy & Geodynamics, Applied Mineralogy, 72074 Tübingen, Germany

[3] Eberhard-Karls-University Tübingen, Center for Applied Geoscience, Geomicrobiology, 72076 Tübingen, Germany

[4] Department of Geodynamics and Sedimentology, Center for Earth Sciences, University of Vienna, Althanstrasse 14, 1090 Vienna, Austria

Corresponding author: Jörn Peckmann (joern.peckmann@univie.ac.at)

Keywords: Gypsum whisker; Anhydrite; Native sulphur; Gypsum efflorescence; Micro XRD

Abstract

The gypsum mineralogy of hair-like, so-called whisker crystals was determined by micro X-ray diffractometry equipped with a focussing X-ray optic and a 2-dimensional detector (µ-XRD²). Gypsum whiskers typically form by efflorescence on surfaces that are in contact with water. The delicate whiskers studied here formed within a Messinian evaporite mostly consisting of anhydrite. They project from alabastrine gypsum into former cavities. The gypsum resulted from hydration of anhydrite. Whiskers were finally engulfed by biogenic, native sulphur, which filled the cavities in the course of microbial alteration of the host lithology. The sulphur protected the delicate whisker crystals from destruction, including a period of exposure to weathering on a dumping site of a former mine where the rocks have been sampled. To the best of our knowledge, this is the first report of gypsum whiskers in evaporites. More significantly, this study reveals that µ-XRD² has great potential for sedimentary petrology, allowing the in situ identification of minute mineral phases that cannot be identified with conventional techniques.

5.1 Introduction

Gypsum crystals exhibit various growth forms including tabular, prismatic, and acicular habits, but also granular and fibrous masses have been described (Nesse 2004). Fibres or filaments, usually composed of gypsum, have been recognised as speleothems forming cave hair, cave cotton, and other delicate crystal forms (Hill and Forti 1997). Hair-like crystals are commonly referred to as whiskers, which are defined as filamentary single crystals with a length to diameter ratio of at least five and a diameter between 20 nm and 100 µm (Evans 1972). Gypsum whiskers have been found to grow from aqueous solution (Strickland-Constable 1968; Hünger and Henning 1988), particularly from solutions with low supersaturation ($\alpha \leq 2$; Hünger and Henning 1988) where growth is inhibited in two dimensions (Strickland-Constable 1968).

Within Messinian evaporitic rocks from Sicily, we recognised similar peculiar hair-like, fibrous crystals, closely resembling gypsum whiskers. The whisker-like crystals are associated with anhydrite and alabastrine gypsum and are surrounded by native sulphur. Because such whiskers have not been previously recognised in evaporites (pers. comm. C. Pierre, J.M. Rouchy, and B.C. Schreiber), we tried to determine their mineralogy, applying optical and electron microscopy, conventional X-ray diffractometry (XRD), as well as energy-dispersive X-ray spectrometry (EDX) for qualitative element analysis. Unfortunately, none of these techniques was successful due to the size of crystals and their entombment in native sulphur. Because of these difficulties, we used a micro-X-ray diffractometer equipped with a focussing X-ray-polycapillary microlense, which provided the opportunity to analyze mineral phases with a local resolution in the hundred µm range (cf., Berthold et al. 2009). This new technique allowed the identification of the whiskers as gypsum crystals.

5.2 Geological context and materials

Loose blocks of sulphur-bearing anhydrite were sampled from a dumping site of the former sulphur mine at Monte Capodarso, north-east of the town of Caltanissetta, Sicily. The evaporites belong to the sulphate-bearing strata of Sicily, which formed during the Late Miocene (Messinian) salinity crisis (Colalongo and Pasini 1997 and references therein). A sea-level drop caused by the cut off of the Mediterranean Sea from the Atlantic Ocean resulted in the apparent desiccation of the Mediterranean Sea between 5.96 and 5.33 million years ago (Hsü et al. 1973b; Krijgsman et al. 1999; Duggen et al. 2003). The development of restricted conditions led to the deposition of evaporitic series including evaporitic carbonate, sulphate, halite, and bittern salts in deeper Messinian basins (Hsü et al. 1973a) as well as in Sicily (Decima and Wezel 1973). Besides primary evaporitic carbonate, a second type of carbonate rock is present in the Messinian sequence of Sicily. Apart from carbonate minerals, rocks of this type contain variable amounts of sulphate minerals and in some places, native

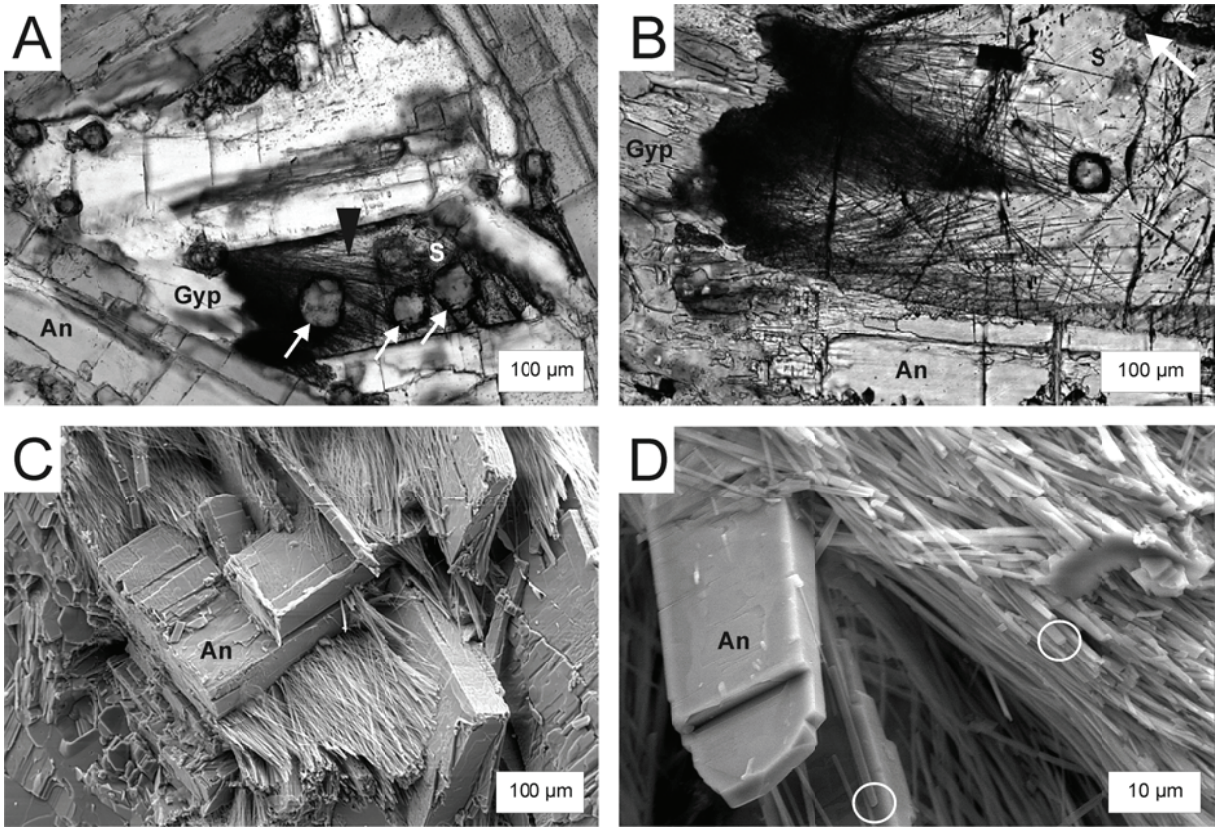

Fig. 5-1 Photomicrographs of gypsum whiskers and associated phases. An anhydrite; Gyp gypsum, S sulphur. (A) Gypsum whiskers (black arrowhead) associated with dolomite (white arrows) within a sulphur filled cavity surrounded by gypsum and anhydrite; plane polarized light. (B) Gypsum whiskers (black) originating on gypsum and projecting into a former cavity now filled by native sulphur and minor dolomite (white arrow); plane-polarized light. (C) Gypsum whiskers between anhydrite; FE-scanning electron micrograph. (D) Gypsum whiskers show an angular profile. Circles mark two angular crystal terminations with high width to height ratios; FE-scanning electron micrograph

sulphur. Such parageneses have been described in evaporitic strata worldwide and are linked to the former presence of crude oil or methane. The carbonate minerals and native sulphur have been found to result from microbial sulphate reduction using locally-derived sulphate ions and organic compounds that infiltrated the host lithology (Thode et al. 1954; Feely and Kulp 1957; Davis and Kirkland 1970; Pierre and Rouchy 1988; Böttcher and Parafiniuk 1998; Peckmann et al. 1999). Such secondary carbonates and native sulphur are particularly abundant in Messinian strata at different sites in Sicily (Dessau et al. 1962; Ziegenbalg et al. 2010). With respect to the location Monte Capodarso, microbial sulphate reduction was found to have been coupled to oxidation of methane during sedimentation and early diagenesis, resulting in secondary carbonates with $\delta^{13}C$ values as low as −52‰ V-PDB (Ziegenbalg et al. 2010). The accompanying native sulphur yielded rather low $\delta^{34}S$ values (as low as +1‰ V-CDT), corroborating that it formed as a consequence of microbial sulphate reduction (Ziegenbalg et al. 2010).

5.3 Methods

Thin-sections were studied with transmitted light and fluorescence microscopy using a Zeiss Axioskop 40 optical microscope (lamp: HBO 50, filters: BP 365/12 FT 395 LP 397 and BP 450-490 FT 510 LP 515). Standard X-ray diffraction (XRD) was performed on powdered samples with a Philips X'Pert Pro MD. A LEO 1530 Gemini and an attached energy-dispersive X-ray spectrometer (EDX) Oxford Inca 400 were used for field-emission scanning-electron microscopy (FE-SEM) and qualitative element identification. The micro-scale phase determination of the whisker crystals was performed directly on uncovered thin sections by micro X-ray diffraction. In order to make the crystals accessible for the analysis, the sulphur entombing the whiskers was dissolved beforehand with hexane. We used the Bruker D8 DISCOVER GADDS XRD^2-micro diffractometer at the IFG-Tübingen equipped with a focussing polycapillary microlens and 2-dimensional HI-STAR detector (cf., Berthold et al. 2009). The spotsize of the used microlens was approximately 50 µm. Due to the fixed incident angle of 10° and sample rotation, the analyzed area on the thin section had a diameter of approximately 400 µm.

5.4 Results

Tabular to acicular anhydrite crystals represent the dominant phase in the studied rocks. Anhydrite is partly altered to alabastrine gypsum (Fig. 5-1A and B). Bundles of fluorescent, thin fibrous crystals project from the alabastrine gypsum into former cavities, which are now filled by native sulphur and minor spheroidal dolomite. Electron microscopy indicates that the thin fibrous crystals are also directly associated with anhydrite (Fig. 5-1C). The crystal fibres are apparently single crystals, which are several hundred µm long (Fig. 5-1B), flat shaped with a width of approximately 1 µm and a height in the nm scale (Fig. 5-1C and D). They are consequently characterized by a length to width ratio considerably higher than hundred and are therefore referred to as whisker crystals.

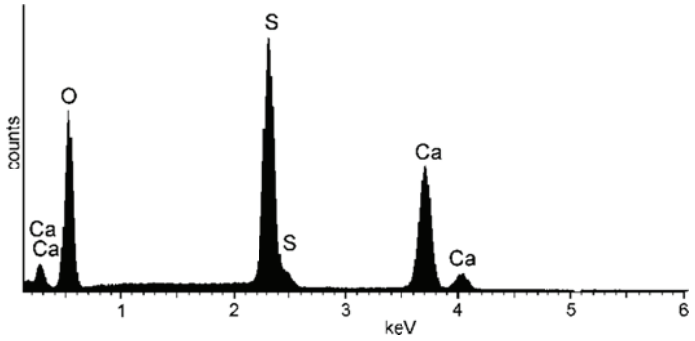

Fig. 5-2 EDX spectrum of gypsum whiskers

Bulk XRD measurements of powdered samples revealed the presence of anhydrite, gypsum, and sulphur (data not shown). EDX analyses showed that whiskers contain calcium, oxygen, and sulphur (Fig. 5-2). For micro X-ray analysis, the X-ray spot was focussed on crotches between anhydrite crystals (Fig. 5-3A), where whiskers are particularly abundant, forming bundles of fibres. Anhydrite as well as gypsum were detected (Fig. 5-3B), but no other minerals. These two minerals showed distinctly different diffraction patterns on the 2-dimensional HI-STAR detector. The anhydrite generated only few intense spots on the corresponding peak positions (Fig. 5-3C), typical for large single crystals. In contrast to this, the gypsum showed a pattern with typical diffraction rings of a powder for each (hkl)-reflection (Fig. 5-3C), caused by the random orientation of many small whisker crystals.

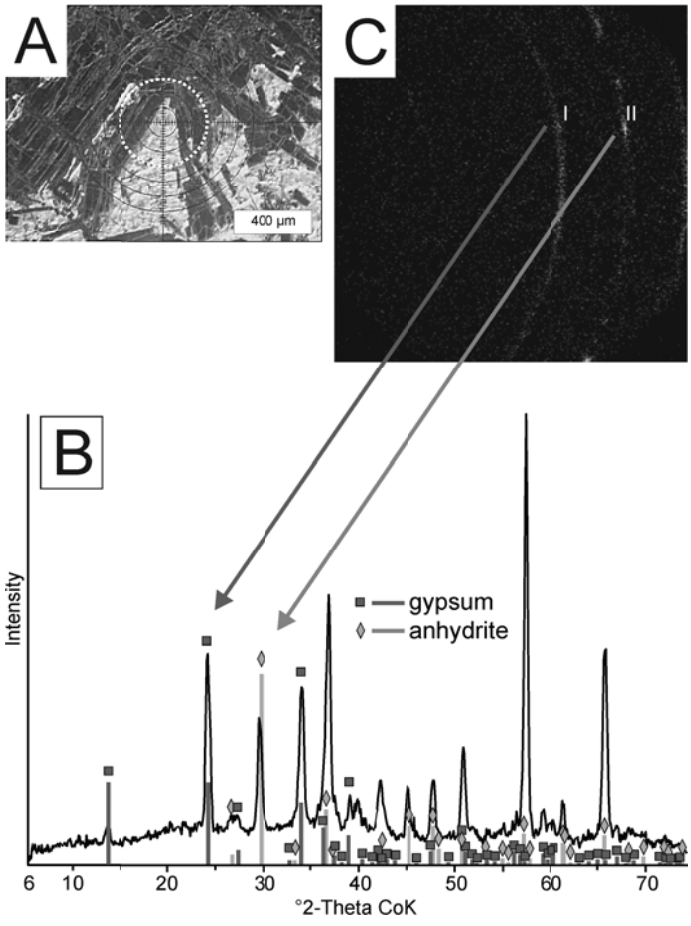

Fig. 5-3 (A) Position of the X-ray spot on the thin-section. (B) Diffraction pattern of the spot shown in A with peaks of gypsum whiskers and anhydrite. (C) Diffraction image from the 2-dimensional HI-STAR detector with a spotty diffraction of anhydrite (II) and evenly filled diffraction rings of gypsum whiskers (I) in the cone section

5.5 Discussion

Conventional techniques including optical microscopy, electron microscopy coupled with EDX, and standard XRD failed to identify the mineralogy of whisker crystals enclosed in Messinian evaporites from Sicily. Optical microscopy did not allow the mineralogy to be determined due to limited crystal diameter and the entombment of crystals in native sulphur. Although EDX measurements revealed that the whiskers are comprised of calcium, oxygen, and sulphur, this did not unequivocally constrain mineralogy. Based on the paragenetic sequence and EDX results, different mineralogies still appeared feasible, including anhydrite, bassanite (calcium sulphate hemihydrate; cf., Allen and Kramer 1953; Bundy 1956; Peckmann et al. 2003), and gypsum. Under these circumstances, conventional XRD-techniques require either sufficient amounts of fine-ground material of the respective mineral phase or separation of single crystals. Because the whiskers were only recognised in limited amounts in few thin sections, neither bulk analyses nor their separation were feasible.

With the advent of μ-XRD^2 equipped with focussing microlenses it is now possible to identify even small amounts of mineral phases in situ on uncovered thin sections (Berthold et al. 2009). A problem that needed to be overcome with respect to the whiskers in the Sicilian samples was their entombment in native sulphur. Surficial dissolution of sulphur by hexane caused the surface of the thin section to become uneven, with the whiskers now being exposed, but situated within a depression. This situation was not ideal for μ-XRD^2, which benefits from even and polished surfaces, but no relevant negative effect was observed by this surface topology, confirming the great potential of this technique.

To the best of our knowledge, this study is the first report of gypsum whiskers in evaporitic lithologies. Similar hair-like structures, however, have been recognised in gypsum and halite deposits of modern and Permian acid saline lakes (Benison et al. 2008). These structures were found to be a composite of gypsum and carbon, prompting Benison et al. (2008) to interpret them as remains of acidophilic microorganisms. No carbon was found to be associated with the Sicilian whiskers. Despite their distinct fluorescence, which appears to be caused by crystal boundaries, a microbial origin seems unlikely. Gypsum whiskers are typically formed by efflorescence on moist porous surfaces (Evans 1972) or as speleothems (Vidal Romani and Rodriguez 2007). In the Sicilian evaporites, the gypsum whiskers formed predominantly on alabastrine gypsum, growing into cavity spaces. The gypsum obviously originated from the hydration of anhydrite (Fig. 5-1). Water consequently penetrated into the pore space of the Messinian evaporites and this water most likely contained significant amounts of dissolved sulphate. As part of the water was consumed in the gypsification of the anhydrite, the sulphate concentration of the solution necessarily increased. As the formation of

gypsum whiskers starts even at very low rates of supersaturation (cf., Strickland-Constable 1968; Hünger and Henning 1988), gypsification of anhydrite may have been sufficient to induce crystal growth. Whisker precipitation apparently preceded sulphur emplacement, as indicated by the paragenetic sequence with sulphur filling the residual pore space after whisker growth. Because sulphur formation was syngenetic at the studied location, occurring during early diagenesis (Ziegenbalg et al. 2010), the whiskers would have to be of Neogene age. A later formation of whiskers, however, cannot be excluded. If the sulphur was remobilized at some point, the whiskers may have formed epigenetically, possibly even in the course of mining activities or afterwards. Independent on the time of whisker formation, the entombment by hydrophobic sulphur efficiently protected the delicate gypsum crystals from dissolution during the exposure of the evaporites on the dumping site.

5.6 Conclusions

Because micron-sized mineral phases are often difficult to analyse and identify with conventional techniques, the use of micro X-ray diffractometry with focussing microlenses and a 2-dimensional detector promises a substantial advancement for sediment petrology. We applied μ-XRD^2 to uncovered thin sections of Messinian evaporites from Sicily that contain peculiar delicate hair-like crystals, revealing their gypsum mineralogy. With a length to width ratio considerably higher than hundred, these crystals can be referred to as gypsum whiskers. The whiskers formed by efflorescence from alabastrine gypsum, which resulted from the hydration of anhydrite. The entombment by biogenic sulphur finally enabled the preservation of the delicate whisker crystals.

Acknowledgements

We thank Sebastian Flotow (Bremen) for thin section preparation, Christoph Voigt (Bremen) for standard XRD measurements, Till Heinrichs (Göttingen) for help with the FE-SEM and EDX analyses, as well as B. Charlotte Schreiber (Seattle) and an anonymous referee for comments on the manuscript. Daniel Birgel (Bremen), Marie-Madeleine Blanc-Valleron (Paris), Antonio Caruso (Palermo), Adrian Immenhauser (Bochum), Catherine Pierre (Paris), and Jean Marie Rouchy (Paris) participated in the field trip during which the studied rocks have been sampled. This project was supported by the Deutsche Forschungsgemeinschaft through the international graduate college EUROPROX and the Research Center “The Ocean in the Earth System”.

.

6 - FOURTH MANUSCRIPT

Authigenesis of native sulphur and dolomite in a lacustrine evaporitic setting (Hellín basin, Late Miocene, SE Spain)

J. Lindtke[1], S.B. Ziegenbalg[1], B. Brunner[2], J.M. Rouchy[3], C. Pierre[4] and J. Peckmann[5]

[1] MARUM, Universität Bremen, 28359 Bremen, Germany

[2] Max-Planck-Institut für Marine Mikrobiologie, 28359 Bremen, Germany

[3] Département Histoire de la Terre, Muséum National d'Histoire Naturelle, 75005 Paris, France

[4] CNRS-UMR 7159, LOCEAN, Univ. P. and M. Curie, 75252 Paris Cedex 05, France

[5] Department für Geodynamik und Sedimentologie, Erdwissenschaftliches Zentrum, Universität Wien, Althanstraße 14, 1090 Wien, Austria

Corresponding author: Jörn Peckmann (joern.peckmann@univie.ac.at)

Keywords: native sulphur, authigenic dolomite, bacterial sulphate reduction, lacustrine setting

Abstract

Abundant sulphur is present in the Late Miocene evaporitic sequence of the lacustrine Hellín basin in SE Spain. Weathering of Triassic evaporites controlled the chemical composition of the Miocene lake. The lacustrine deposits comprise gypsum, marlstones, diatomites, and carbonate beds. Sulphur-bearing carbonate deposits predominantly consist of early diagenetic dolomite. Abundant dolomite crystals with a spheroidal habit are in accordance with an early formation and point to a microbial origin. The carbon isotopic composition of the dolomite ($\delta^{13}C$ values between −11 to −4‰) indicates mixing of lake water carbonate and carbonate derived from the remineralisation of organic matter by heterotrophic bacteria. Dolomite precipitated syngenetically under evaporitic conditions as indicated by high oxygen isotope values ($\delta^{18}O$ between +6 and +11‰). Nodules of native sulphur are found in gypsum, carbonate beds, and marlstone layers. Sulphur formed in the course of microbial sulphate reduction, as reflected by its strong depletion in ^{34}S ($\delta^{34}S$ values as low as −17‰). Near to the surface many of the sulphur nodules were in part or completely substituted by secondary gypsum, which still reflects the sulphur isotopic composition of native sulphur (−18 to −11‰). This study exemplifies the role of bacterial sulphate reduction in the formation of dolomite and native sulphur in a semi-enclosed lacustrine basin during the Late Miocene.

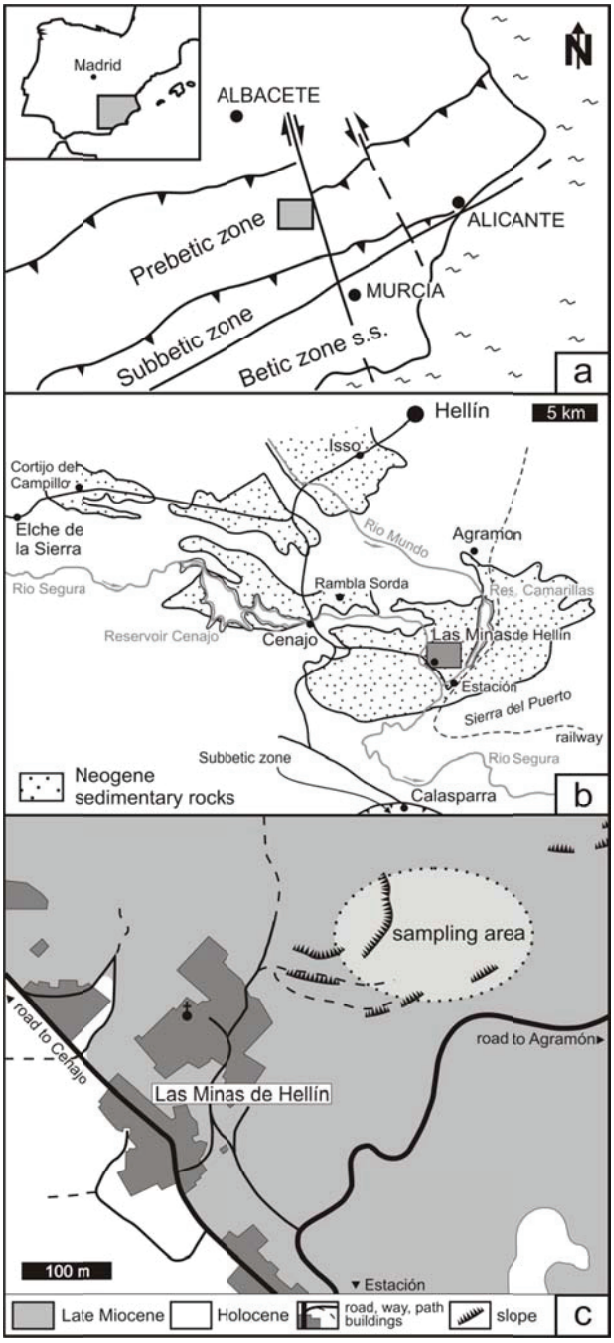

Fig. 6-1 Working area. (a) Location of the Hellín basin in tectonic context of the Betic Chain; modified after Calvo and Elizaga (1989). (b) Sub-basins of the Hellín basin with Neogene sediments; modified after Calvo and Elizaga (1989). (c) Location of the sampling area in the former sulphur mine of Las Minas.

6.1 Introduction

Native sulphur occurrences are commonly closely associated with evaporites and authigenic carbonates (e.g. Dessau et al., 1962; Davis and Kirkland, 1979; Pierre and Rouchy, 1988; Youssef, 1989). Examples of this paragenesis are found in cap rocks of salt diapirs (Ruckmick et al., 1979) and strata-bound deposits like those of northern Iraq (Jassim et al., 1999), the Delaware basin (Hentz and Henry, 1989), the Carpathian foredeep (Böttcher and Parafiniuk, 1998), and the Mediterranean area

(Dessau et al., 1962; Anadón et al., 1992; Rouchy et al., 1998; Ortí et al., 2003; Ziegenbalg et al., 2010). Both native sulphur and associated authigenic carbonate minerals are commonly considered as products of bacterial sulphate reduction (Feely and Kulp, 1957; Dessau et al., 1962; Davis and Kirkland, 1979; Peckmann et al., 1999; Ziegenbalg et al., 2010). In this process, the heterotrophic bacteria oxidize locally abundant crude oil, methane, or more pristine organic matter and produce sulphide ions, facilitating subsequent biological or abiological sulphide oxidation to native sulphur (Machel, 1992). Another common consequence of bacterial sulphate reduction is an increase of alkalinity, which results in the precipitation of carbonate minerals (Castanier et al., 1999).

Depending on the time of formation of authigenic minerals, Ruckmick et al., (1979) distinguished between syngenetic and epigenetic processes. Syngenesis takes place during sedimentation and early diagenesis. Notably, precipitation of carbonate minerals induced by sulphate-reducing bacteria has been described in modern hypersaline environments as well as in laboratory experiments (Lalou, 1957; Vasconcelos and McKenzie, 1997; van Lith et al., 2003; Wright and Wacey, 2005). Epigenesis, on the other hand, takes place after deposition during late diagenesis. In the case of epigenetic mineral formation, sulphate, the electron acceptor for the involved heterotrophic bacteria, is delivered by dissolution of sulphate minerals by meteoric waters.

Because bacterial sulphate reduction is dependent on a high supply of sulphate ions, it is favoured in marine rather than in lacustrine environments. In lacustrine settings, methanogenesis tends to act as the main process of organic matter remineralisation (Cerling et al., 1988; Talbot and Kelts, 1990). Nevertheless, some examples of carbonate mineral formation induced by sulphate reduction in lacustrine deposits are known, including lakes in SW Australia (Wright, 1999) and the eastern USA (Riccioni et al., 1996). Sulphur-bearing authigenic carbonates have been reported from the lacustrine Teruel basin in Spain (Anadón et al., 1992), where weathering of Triassic marine evaporites provided the sulphate for bacterial sulphate reduction (Utrilla et al., 1992). A similar occurrence of native sulphur and associated authigenic carbonates is known from the Late Miocene Hellín basin in SE Spain (Servant-Vildary et al., 1990). This restricted basin was typified by lacustrine conditions with only episodic inflow of marine waters (Servant-Vildary et al., 1990). Although dolomite and native sulphur have been suggested to derive from bacterial sulphate reduction using sulphate that originated from the dissolution of Triassic gypsum (Servant-Vildary et al., 1990), these authigenic minerals have not been studied in detail to date. Here we present a petrographic and isotopic study on the evaporitic sedimentary sequence of the Hellín basin, focussing on authigenic carbonates and native sulphur. Our study confirms that sulphate-reducing bacteria can be major players in the early diagenesis of lacustrine settings as well, provided that sufficient sulphate ions are available.

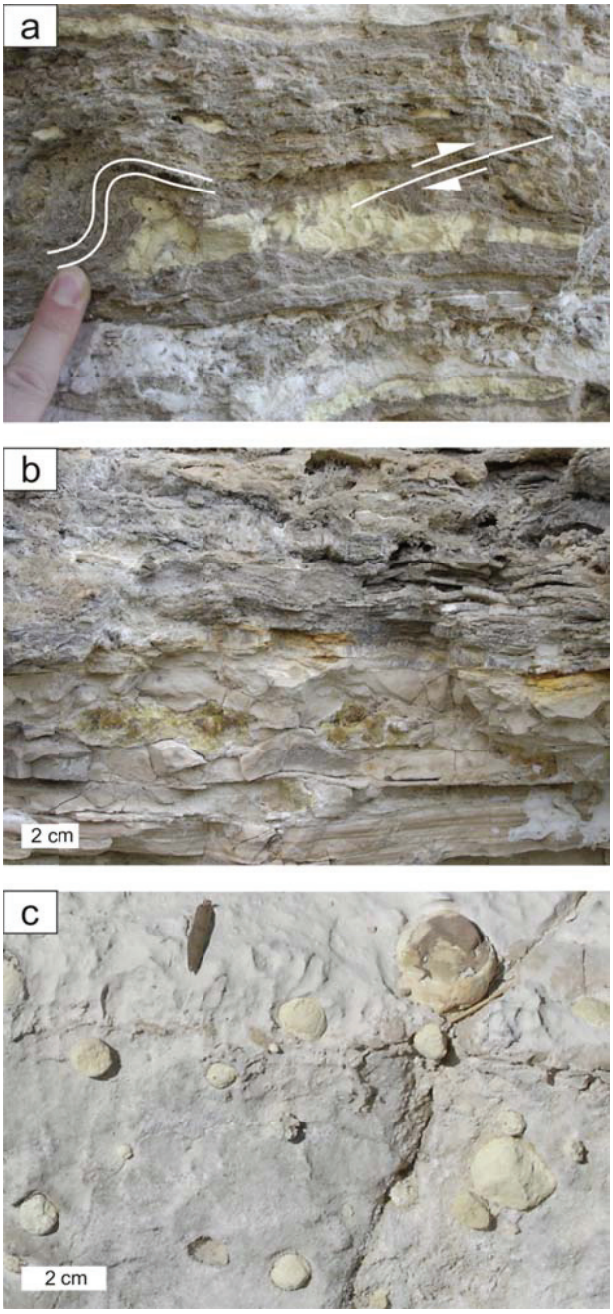

Fig. 6-2 Native sulphur. (a) Sulphur enclosed in secondary gypsum; overlying laminar gypsum beds are bent and faulted (see indication), Las Minas. (b) Sulphur enclosed in carbonate deposits, Las Minas. (c) Sulphur nodules embedded in a carbonate bed, Cenajo.

6.2 Geological setting and material

The Hellín basin of SE Spain is an intramontane basin in the external part of the Betic chain (Fig 6-1a). Cretaceous limestones and Triassic evaporites represent the basement of the basin (Servant-Vildary et al., 1990). Basin development is attributed to subsidence related to a system of transform faults of an extensional regime, which was active during the Neogene; subsidence terminated in the Late Tortonian (Giese et al., 1982; Sanz de Galdeano, 1990; Krijgsman et al., 2000; Jolivet et al.,

2006). Initially the basin was filled by marine sediments dominated by marls and marly carbonate beds. The last marine sedimentation occurred in the Middle Tortonian (Calvo et al., 1978). A late phase of north-south oriented compression started in the Tortonian and led to regional uplift of the crust (Rouchy et al., 1998; Jolivet et al., 2006). Subsequently, folding of Mesozoic to Cainozoic rocks ended in the development of several local swells that divided the Hellín basin into several sub-basins (Fig. 6-1b). Formation of a swell to the south close to Calasparra led to the successive isolation of the Hellín basin from the marine environment (Calvo and Elizaga, 1989; Servant-Vildary et al., 1990). The change to lacustrine conditions resulted in the accumulation of evaporites and carbonate deposits of the Las Minas de Hellín formation, which are overlain by carbonate deposits, marls, and diatomite (Servant-Vildary et al., 1990). The evaporites, mainly represented by gypsum, derived from the dissolution of Triassic evaporites; continued dissolution of gypsum of the Triassic basement (Garcia Domingo et al. 1980) is reflected by karst phenomena in the Hellín basin (Navarro Hervás and Rodríguez Estrella, 1985). In the sub-basins of Cenajo and Las Minas, the Las Minas de Hellín formation contains native sulphur, which was mined until 1960.

For this study, carbonate and gypsum rocks containing native sulphur were collected from the mining area north-east of the small miner's village Las Minas (Fig. 6-1c). Sections of evaporites and carbonates are well exposed, but strongly weathered; the samples studied here derived from the upper part of the stratigraphic interval described by Servant-Vildary et al., (1990). Strata-bound nodules of native sulphur are predominantly embedded in laminated gypsum beds (Fig. 6-2a) and to a lesser degree in carbonate beds (Fig. 6-2b). A similar sedimentary sequence is found in the Las Minas de Hellín formation of the Cenajo sub-basin. The aggregates of native sulphur in the Cenajo sequence resemble those of the Las Minas sequence, although ball-shaped nodules of sulphur have only been recognized in carbonate deposits from Cenajo (Fig. 6-2c).

6.3 Methods

Thin sections were studied with transmitted light and fluorescence microscopy on a Zeiss Axioskop 40 A Pol, equipped with an Axio-Cam MRc digital camera (lamp: HBO 50, filter: BP 365 FT 395 LP 397 and BP 450-490 FT 510 LP 515). Thin sections were partly stained with combined potassium ferricyanide and alizarin red solution (Füchtbauer, 1988). Scanning-electron microscopy with qualitative element recognition was performed with a Zeiss Supra 40 REM equipped with an Oxford EDX-detector (Inca Penta FETx3). Mineralogy was determined with a PANalytical X'Pert Pro diffractometer using a Ni-filtered Cu-anode, equipped with a multichannel detector (X'cellerator). Mineral content was estimated semi-quantitatively using the peak areas. Proportions of magnesium

to calcium in dolomite were calculated after Lumsden (1979) by quartz-corrected d-values. A LECO CS 200 was used for determination of contents of total organic carbon.

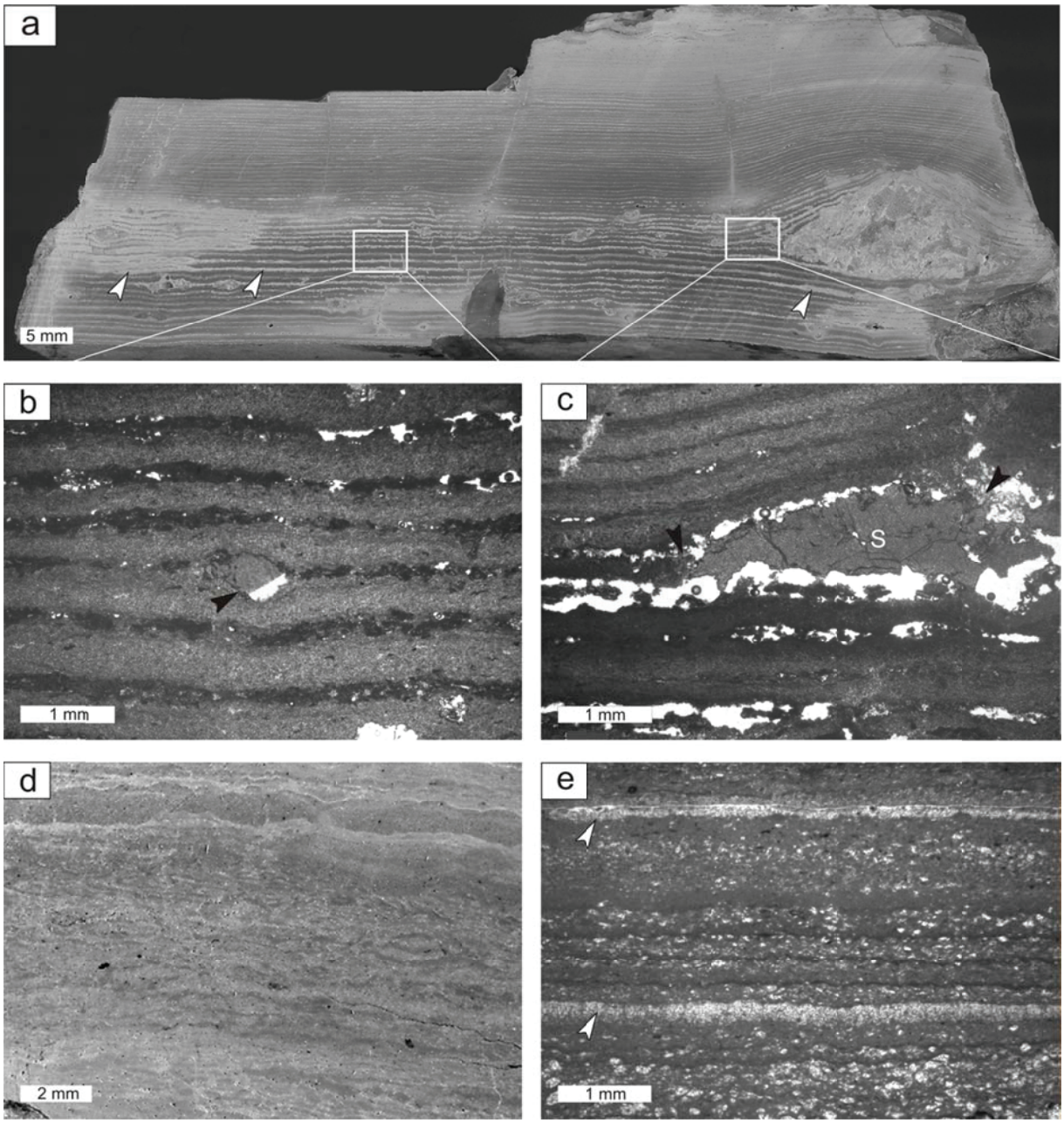

Fig. 6-3 Laminated carbonate bed. (a) Carbonate bed with varved lamination, which is bent around a sulphur nodule; arrowheads indicate laminae of secondary gypsum; scanned slab. (b) Detail of (a), carbonate laminae and small sulphur nodule (arrowhead); plane-polarized light. (c) Detail of (a), bent lamination around a sulphur nodule (S), which is partly dissolved and replaced by diagenetic gypsum (arrowheads); plane-polarized light. (d) Mat-like lamination; plane-polarized light. (e) Irregular lamination with two chert laminae (arrowheads); plane-polarized light.

For stable isotope analyses mineral phases were drilled from the surface of slabs with a hand-held micro drill. Measurements of carbon and oxygen isotopes (sample weight: 0.02 to 0.10 mg) were performed with a Finnigan MAT 251 mass spectrometer using the Kiel carbonate device type "Bremen" against natural CO_2 from Burgbohl/Rheinland. A Solenhofen limestone was used as

internal standard, which was calibrated against the international standard NBS 19. Values are reported in the δ-notation relative to Vienna Pee Dee Belemnite (VPDB) standard. Long time standard deviation (1σ) for this measurement was ±0.05‰ for $\delta^{13}C$ and ±0.07‰ for $\delta^{18}O$ values. Oxygen isotope values of dolomite were not corrected for its different fractionation compared to calcite during precipitation (McKenzie, 1981) or during the analytical procedure (Sharma and Clayton, 1965) because of an undetermined admixture of minor calcite.

For oxygen isotope analysis of sulphate, gypsum was dissolved with sodium chloride solution. After acidification of the solution, sulphate was precipitated as barium sulphate by addition of barium chloride. Sulphur isotopes of gypsum were measured either on gypsum without pre-treatment or on barium sulphate precipitated as above. Samples of sulphur received no pre-treatment for sulphur isotope measurements. Sulphur and oxygen isotope measurements were performed with a Thermo Finnigan mass spectrometer Delta V in a continuous flow setup. For sulphur isotope analysis 0.3 mg of barium sulphate, 0.4 mg of calcium sulphate, or 0.05 mg of native sulphur (with 1 mg of V_5O_5 as catalyst, respectively) were weighted into tin capsules and combusted in an Euro EA Elemental Analyzer (EuroVector, Milan, Italy). The sulphur isotope measurements were calibrated with reference materials NBS 127 and IAEA-SO-6. The sulphur isotopic composition is reported in the δ-notation relative to Vienna Cañon Diablo Troilite (VCDT) standard. The standard errors (1σ) were less than ±0.2‰ for $\delta^{34}S$ values. For oxygen isotope analysis 0.16 mg of barium sulphate was weighted into silver capsules. Under presence of graphite and glassy carbon oxygen from sulphate was transferred to carbon monoxide within an elemental analyzer (TC/EA, Thermo Fisher Scientific). NBS 127, IAEA-SO-5, and IAEA-SO-6 were used as references for calibration. The oxygen isotopic composition is reported in the δ-notation relative to Vienna Standard Mean Ocean Water (VSMOW). The standard errors (1σ) were less than ±0.3‰ for $\delta^{18}O$ values.

6.4 Results

6.4.1 Petrography

6.4.1.a Carbonate lithology

Sampled carbonate beds consist predominantly of dolomite with varying amounts of gypsum, calcite, and accessory minerals, including clay minerals, feldspars, and quartz. Only few carbonate beds contain more calcite than dolomite. The $MgCO_3$ content of dolomite is generally high (47 to 50%). The total organic carbon content of carbonate deposits is low to moderate (0.2 to 0.7%). Most of the carbonate deposits exhibit a distinct lamination, which can be grouped into three types (Fig. 6-3). (1) A very regular, varve-like rhythmic lamination is characterized by thin laminae, approximately

0.5 mm in thickness that consist of light-coloured dolomitic microspar and dark organic-rich dolomicrite, respectively (Fig. 6-3a, b). Where sulphur nodules occur, the lamination is bent and occasionally faulted (Figs 6-2a, 6-3a-c). The dolomicrite is partly dissolved or replaced by gypsum, especially in the surroundings of sulphur nodules. Less commonly dolomitic microspar is replaced by gypsum. (2) A second type of lamination is less regular, resembling lamination in microbial mats (Fig. 6-3d). The carbonate laminae, which differ in thickness, show an uneven surface, and wedge out laterally. They are interbedded with discontinuous clay layers. The predominant mineral is dolomite.

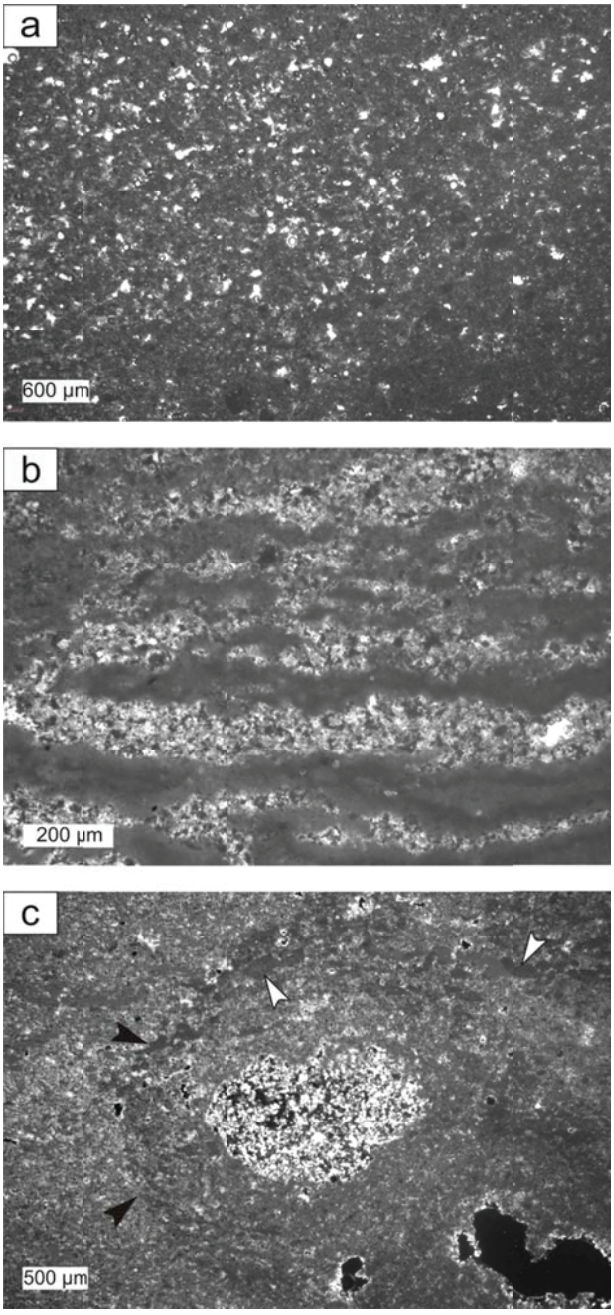

Fig. 6-4 Carbonate deposits; plane-polarized light. (a) Clotted dolomicrite to microspar. (b) Irregular alternation of dolomicrite and microspar. (c) Peloidal carbonate with a former sulphur nodule substituted by gypsum surrounded by a dark rim (black arrowheads). White arrowheads point to large peloids; crossed nichols.

(3) A third type of lamination comprises dolomite and gypsum laminae of irregular thickness, ranging from a few to 300 µm, accompanied by late diagenetic calcite and chert laminae (Fig. 6-3e). Plant fragments are common in this lithology.

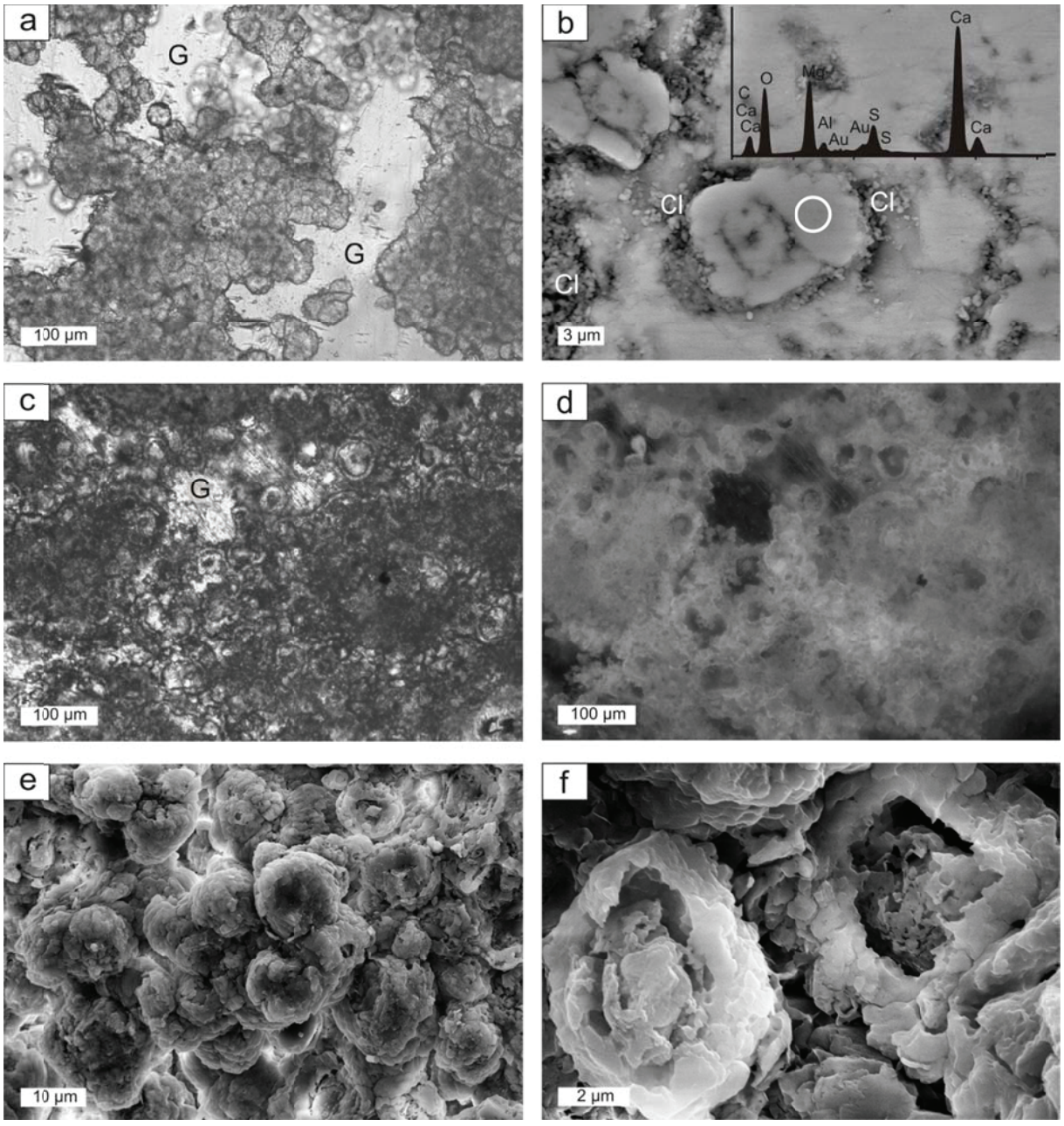

Fig. 6-5 Spheroidal dolomite. G = gypsum, (a) Spheroidal dolomite with gypsum; plane-polarized light. (b) Spheroidal dolomite and associated clay minerals (Cl); SEM micrograph of thin section; circle displays area of EDX-measurement, spectrum with counts from 0 to 5 keV, gold peak from coating. (c) Spheroidal dolomite with gypsum, plane-polarized light. (d) Same detail as (c); note autofluorescence of spheroids; fluorescence image. (e) Aggregate of spheroidal dolomite; SEM micrograph. (f) Close-up view of two spheroids; SEM micrograph.

Beside laminated carbonate beds, dense beds of dolomicrite occur, which are up to a few centimetres in thickness. These beds commonly reveal a clotted (Fig. 6-4a) or peloidal microfabric. Former cavities, now filled by authigenic minerals, are abundant in this lithology (Fig. 6-4a). In places the dolomicrite is alternating with dolomitic spar (Fig. 6-4b). Dolomicritic peloids are up to 30 µm in diameter and are partly recrystallized to microspar along their margins. Peloids tend to form dense fringes around sulphur nodules, which are commonly partly or completely replaced by gypsum (Fig. 6-4c). Blocky calcite spar with crystals up to 200 µm in diameter is an accessory phase in this lithology. In different types of dolomitic beds spheroidal dolomite is observed in rock-forming quantities. The pore space left by spheroids is filled by gypsum (Fig. 6-5a). In some of the vugs, interlayers, and surroundings of spheroids submicroscopic aggregates of clay minerals are present (Fig. 6-5b). The fluorescent spheroids reveal a dark core of unknown composition surrounded by concentric rings of dolomite (Fig. 6-5c, d). Spheroids vary between 5 and 10 µm in diameter and are composed of irregularly arranged crystals (Fig. 6-5e, f).

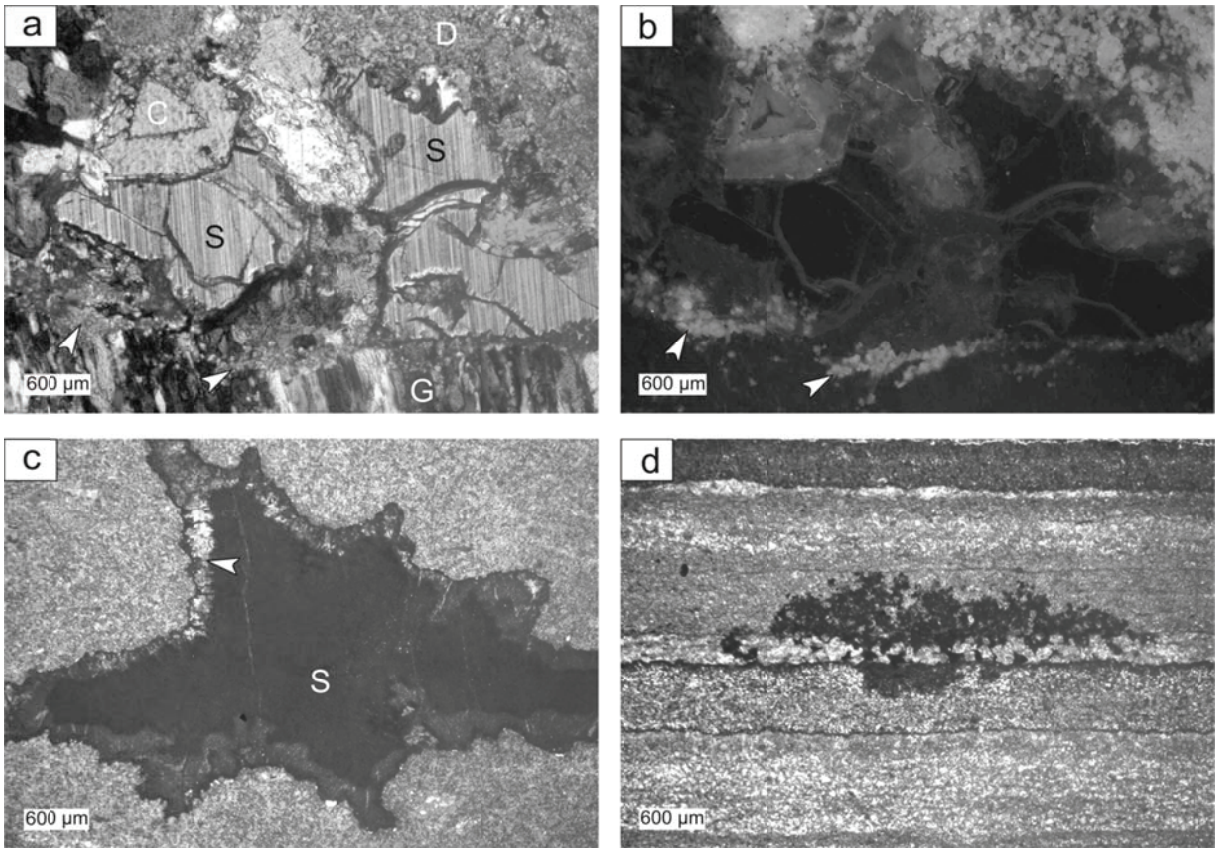

Fig. 6-6 Native sulphur. C = carbonate; D = dolomite; G = gypsum; S = native sulphur. (a) Well-preserved sulphur surrounded by spheroidal dolomite (arrowheads); gypsum-filled fissure in the lower part of the photomicrograph; plane-polarized light. (b) Same detail as (a), note fluorescence of spheroidal dolomite (arrowheads); fluorescence image. (c) Slightly weathered aggregate of sulphur with a rim of gypsum (arrowhead); plane-polarized light. (d) Minor accumulation of sulphur in a laminated carbonate bed; plane-polarized light.

6.4.1.b Native sulphur

Native sulphur occurs as large bright orange to yellow crystals with sharp crystal boundaries (Fig. 6-6a, b); the crystals are translucent in transmitted light. Sulphur is commonly closely associated with spheroidal dolomite and vugs or fissures filled by secondary gypsum (Fig. 6-6a, b). Weathered sulphur is bright yellow to whitish in colour (Fig. 6-2 a), shows a powdery consistency, is blurry in transmitted light, and is abundantly surrounded by secondary gypsum (Fig. 6-6c). In carbonate beds with a varve-like lamination, sulphur aggregates tend to be particular round (Fig. 6-3a-c). In carbonate beds of the types 2 and 3 described above, lamination is partly interrupted by sulphur nodules. Native sulphur also appears as ameboidal aggregates (Fig. 6-6c), possibly filling former cavities and as tiny accumulations finely dispersed in the host rock (Fig. 6-6d). Very regular, fluorescent globules with a diameter of approximately 20 µm were recognized in one sample of well-preserved sulphur (Fig. 6-7).

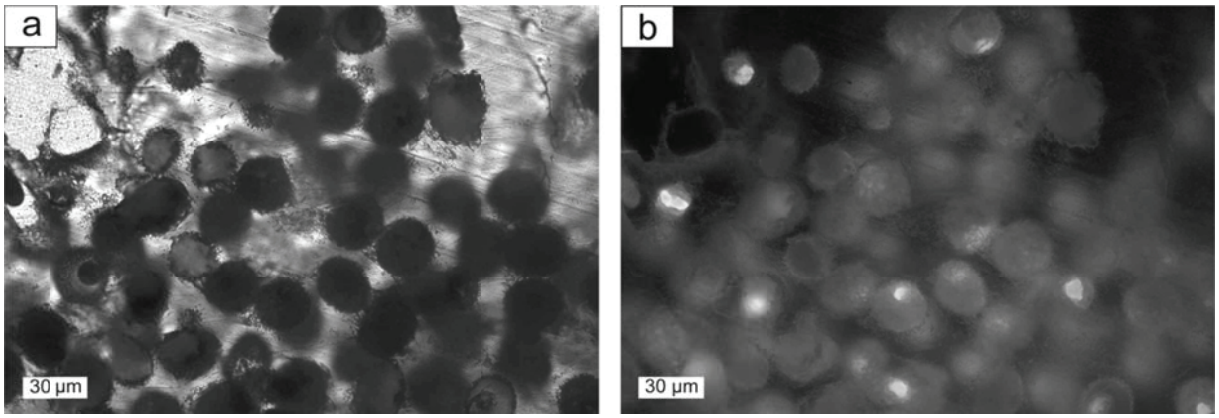

Fig. 6-7 (a) Putative fossilized bacteria enclosed in sulphur; plane-polarized light. (b) Same detail as (a); fluorescence image.

6.4.1.c Gypsum

Gypsum is ubiquitous in the studied sedimentary rocks. In some carbonate beds, gypsum is finely dispersed in the rock matrix. Elsewhere, it represents a secondary mineral, growing as large crystals perpendicular to bedding. Secondary gypsum, which has been described in detail by Servant-Vildary et al., (1990), is commonly replacing sulphur (Figs 6-3c, 6-4c, 6-6c) and dolomitic microspar. It also fills fissures and vugs in carbonate deposits (Fig. 6-8). Growth of palisade-like gypsum commonly disturbed the primary lamination. The secondary gypsum of the Las Minas de Hellín sequence closely resembles diagenetic gypsum from the Miocene lacustrine sequence of the Teruel basin in NE Spain (cf., Ortí et al., 2010).

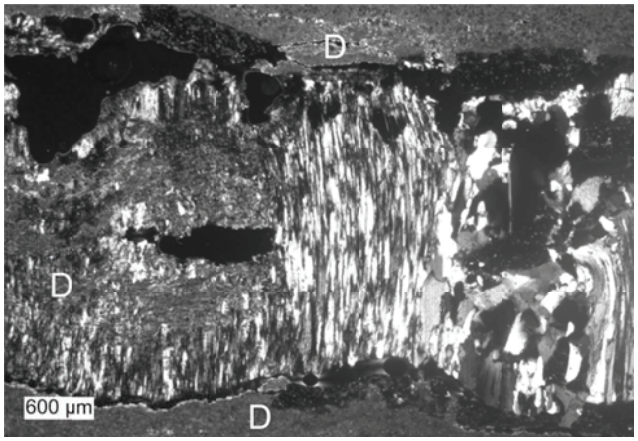

Fig. 6-8 Fissure filled with fibrous gypsum (centre), blocky gypsum (right), and minor dolomite (D) derived from the rock matrix.

6.4.2 Stable isotopes

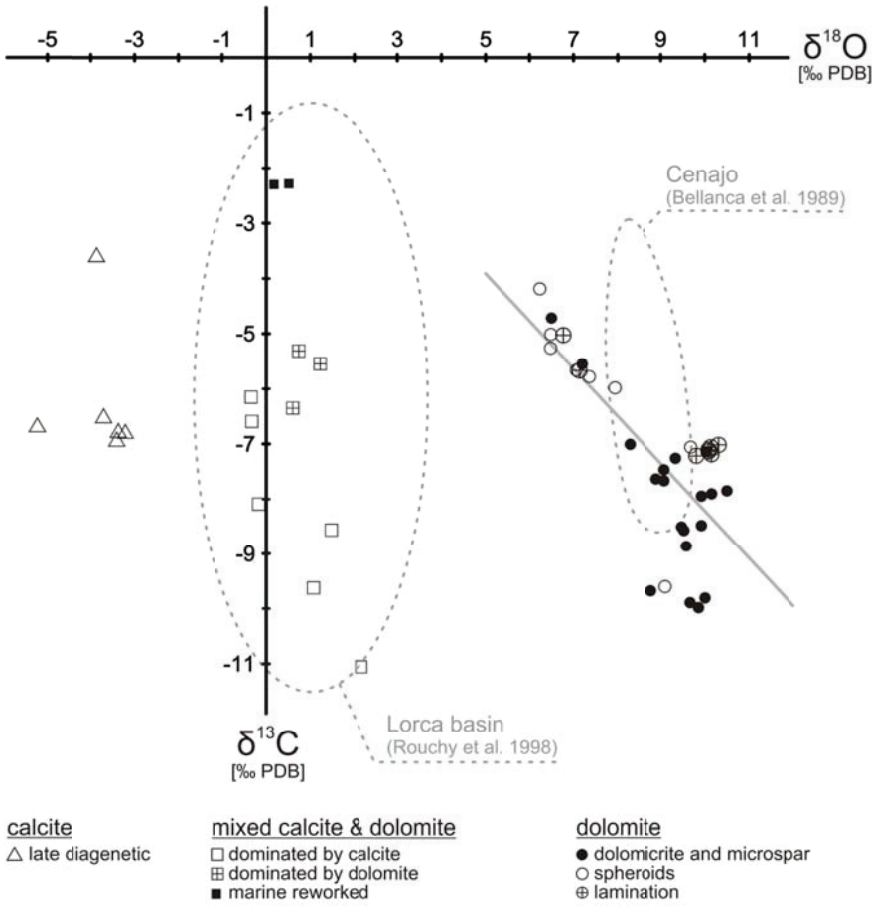

Fig. 6-9 Stable carbon and oxygen isotope values of carbonate deposits of Las Minas de Hellín. Trend line indicates linear regression of dolomite values. Fields defined by dotted lines indicate composition of carbonates from the Lorca and Cenajo basin.

Table 6-1: Stable isotopes of carbon ($\delta^{13}C$) and oxygen ($\delta^{18}O$) in carbonate deposits and stable isotopes of sulphur ($\delta^{34}S$) in native sulphur and stable isotopes of sulphur ($\delta^{34}S$) and oxygen ($\delta^{18}O$) in secondary gypsum of Las Minas de Hellín and one sample of Triassic gypsum from near Cenajo.

	Carbonate			sulphate & sulphur		
sample	$\delta^{13}C$ [‰	$\delta^{18}O$ [‰	texture/mineralogy	$\delta^{34}S$ [‰	$\delta^{18}O$ [‰	texture/mineralogy
H 1	-7.9	10.2	peloidal dolomite	-14.4	4.7	gypsum filled fissure
H 1	-7.9	9.9	peloidal dolomite			
H 1	-7.8	10.5	peloidal dolomite			
H 1	-7.1	10.0	peloidal dolomite			
H 1	-7.1	9.7	spheroidal dolomite			
H 3				-13.0	8.1	gypsum, substituted sulphur
H 3				-17.1		gypsum, substituted sulphur
H 5A	-7.0	10.3	laminated dolomite	-3.7		native sulphur
H 5A	-7.1	10.1	laminated dolomite	-7.0		native sulphur
H 5A	-7.2	9.8	laminated dolomite			
H 5B	-7.1	10.1	laminated dolomite	-4.3		native sulphur
H 5B	-7.2	10.1	laminated dolomite	-3.7		native sulphur
H 5B	-7.1	10.1	laminated dolomite			
H 6A	-5.0	6.8	microsparitic dolomite	-11.1	6.0	gypsum filled fissure
H 6A	-5.7	7.1	microsparitic dolomite	-12.8	6.3	gypsum filled fissure
H 6A	-6.0	7.9	spheroidal dolomite			
H 6A	-5.8	7.4	spheroidal dolomite			
H 6B	-5.3	6.5	spheroidal dolomite	-18.2		gypsum, rim around native
H 6B	-5.0	6.5	spheroidal dolomite	-6.7		native sulphur
H 6B				-6.3		native sulphur
H 7	-8.6	9.5	micritic dolomite			
H 7	-8.9	9.6	micritic dolomite			
H 8	-8.5	9.9	microsparitic dolomite			
H 8	-8.5	9.5	microsparitic dolomite			
H 8	-7.3	9.3	clotted dolomite			
H 8	-7.5	9.1	clotted dolomite			
H 8	-7.6	8.9	microsparitic/clotted			
H 8	-7.7	9.1	microsparitic/clotted			
H 9A	-6.6	-0.3	matrix calcite & dolomite	-13.5		native sulphur
H 9A	-6.2	-0.3	matrix calcite & dolomite	-12.3		gypsum, rim around native
H 9A	-6.4	0.6	peloidal dolomite			
H 9A	-5.3	0.7	clotted dolomite			
H 9A	-5.5	1.2	clotted dolomite			
H 9B				-7.8		native sulphur
H 9B				-15.0		native sulphur
H 12	-6.5	8.3	peloidal dolomite	-15.3		gypsum, inside chert layer
H 12	-4.2	6.2	microsparitic dolomite	-14.3	7.6	gypsum filled fissure
H 12				-15.0	7.6	gypsum filled fissure
H 13A	-5.6	7.2	clotted dolomite	-9.5		gypsum filled cavity
H 13A	-4.7	6.5	clotted dolomite			
H 13B				-7.0		native sulphur
H 14	-11.1	2.2	matrix calcite			
H 14	-9.6	1.1	matrix calcite			
H 14	-3.6	-3.9	microsparitic calcite			
H 15	-2.3	0.2	matrix calcite (marine			
H 15	-2.3	0.5	matrix calcite (marine			

Table 6-1: continued

	Carbonate			Sulphate & sulphur		
sample	$\delta^{13}C$	$\delta^{18}O$	texture/mineralogy	$\delta^{34}S$	$\delta^{18}O$	texture/mineralogy
H 16	-8.1	-0.2	matrix calcite & dolomite	-11.3	5.2	gypsum, inside lamination
H 16	-8.6	1.5	matrix calcite & dolomite	-12.6	6.1	gypsum, inside lamination
H 19	-6.8	-3.2	microsparitic calcite	-15.7		native sulphur
H 19	-6.9	-3.4	microsparitic calcite			
H 19	-6.5	-3.7	microsparitic calcite			
H 20.1	-9.8	10.0	microsparitic dolomite			
H 20.1	-9.9	9.7	microsparitic dolomite	-7.8		native sulphur
H 20.1	-10.0	9.9	microsparitic dolomite			
H 20.1	-9.6	9.1	microsparitic dolomite	-11.4	5.0	gypsum filled fissure
H 20.1	-6.8	-3.4	sparitic calcite	-11.9	5.2	gypsum filled fissure
H 20.1	-6.6	-5.2	sparitic calcite	-13.4		gypsum filled fissure
H 20.1	-9.7	8.8	microsparitic dolomite			
H 21				-17.1		native sulphur
H 21				-14.2		native sulphur
H 21				-11.9	7.5	gypsum, substituted lamination
H 21				-11.6	7.9	gypsum, substituted lamination
Triassic gypsum (near Cenajo)				12.0	11.7	gypsum

6.4.2.a Carbon and oxygen isotopes of carbonates

Oxygen isotope values scatter widely from −5.2 to +10.5‰ (Table 6-1; Fig. 6-9). Dolomite is more enriched in ^{18}O than calcite. Spheroidal dolomite shows slightly lower $\delta^{18}O$ values (+6.2 to +9.7‰) than other varieties of dolomite (+6.8 to +10.5‰). A group of samples with a mixed dolomite and calcite composition exhibits oxygen isotope values close to 0‰. The lowest oxygen isotope values are found for late diagenetic calcite (−5.2 to −3.2‰).

Most carbon isotope values range from −11.1 to −3.6‰. Two samples with slightly higher values (−2.3‰) probably reflect reworked marine carbonate. The $\delta^{13}C$ values of samples with a mixed calcite and dolomite composition (−5.3 to −11.1‰) as well as the $\delta^{13}C$ values of dolomite (−4.2 to −10.0‰) scatter widely. The $\delta^{13}C$ values of dolomite are negatively correlated with the $\delta^{18}O$ values, corresponding to a correlation coefficient of r = −0.75 (Fig. 6-9).

6.4.2.b Oxygen isotopes of gypsum and sulphur isotopes of gypsum and native sulphur

Oxygen isotope values of gypsum range from +4.7 to +8.1‰ (Table 6-1; Fig. 6-10). Native sulphur and secondary gypsum show much lower $\delta^{34}S$ values (−18.3 to −3.7‰, Table 6-1; Figs 6-10, 6-11) than primary gypsum of the Las Minas sequence (+13 to +19‰; Servant-Vildary et al., 1990; Fig. 6-10). Sulphur isotope values of native sulphur fall into two groups (Fig. 6-11). One group is less depleted in ^{34}S (−7.8 to −3.7‰), whereas the other group shows very low $\delta^{34}S$ values (−17.1 to −13.5‰), which are in the same range as values of secondary gypsum (−18.2 to −11.1‰). Triassic

gypsum sampled from the periphery of the Cenajo sub-basin exhibits a positive sulphur isotope value (+12.0‰), in accord with data of Claypool et al., (1980).

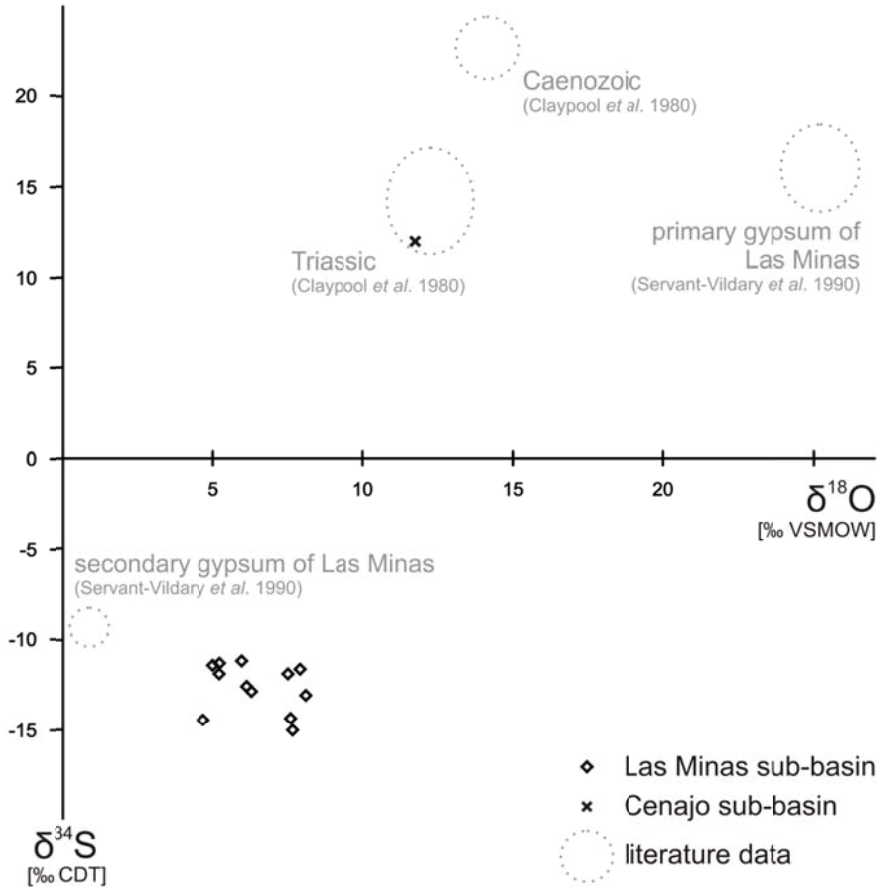

Fig. 6-10 Stable sulphur and oxygen isotope values of secondary gypsum from Las Minas de Hellín and Triassic gypsum from Cenajo. Triassic and Cainozoic marine sulphate for comparison.

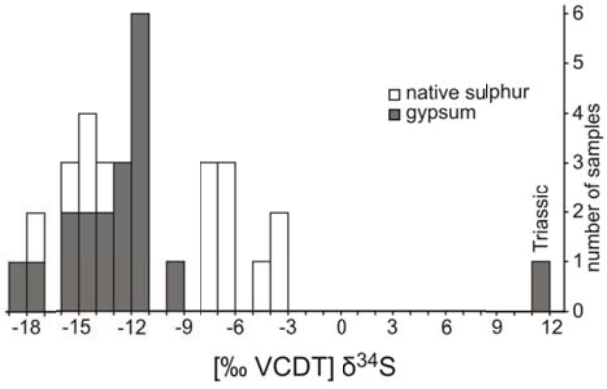

Fig. 6-11 Stable sulphur (δ34S) isotope values of Neogene secondary gypsum and native sulphur from Las Minas de Hellín and Triassic gypsum from Cenajo.

6.5 Discussion

6.5.1 Formation of authigenic carbonate minerals

In lacustrine environments, carbonate minerals can precipitate from dissolved inorganic carbon (DIC) in the upper water column and accumulate at the lake bottom (Stabel, 1986; Talbot and Kelts, 1990). The carbon isotopic composition of dissolved carbonate in a lacustrine environment is influenced by several factors including the amount and the composition of inflowing water, residence time, and lake size (Talbot and Kelts, 1990; Lee et al., 1987). Furthermore, the $\delta^{13}C$ values of DIC can shift towards higher values due to primary production inside the lake and evaporation (Talbot, 1990). In closed lakes, $\delta^{13}C$ values of primary carbonates usually range from –5 to +3‰ (McKenzie, 1985b; Talbot, 1990; Talbot and Kelts, 1990, Tenzer et al., 1997). The Miocene Hellín lake was most likely hypersaline, because Late Miocene climatic conditions favoured evaporation in the Mediterranean area (van Dam and Weltje, 1999; García-Alix et al., 2008) and abundant Miocene evaporites are present in the Hellín basin. The variable $\delta^{18}O$ values of the studied carbonates reflect the strong influence of inflow and evaporation, which is typical for hydrologically closed lakes (cf., Talbot and Kelts, 1990).

Apart from formation in the water column, early diagenesis in lacustrine sediments can induce carbonate precipitation as well. As a consequence of anaerobic remineralisation of organic matter, in particular bacterial sulphate reduction, carbonate alkalinity is commonly increasing (Abd-El-Malek and Rizk, 1963a; Abd-El-Malek and Rizk, 1963b; van Lith et al., 2003). The resulting authigenic carbonate minerals are characterized by low $\delta^{13}C$ values depending on the source of fresh organic matter or fossil hydrocarbons (Irwin et al., 1977; Peckmann and Thiel, 2004). The $\delta^{13}C$ values of higher land plants (as low as −34‰) tend to be lower than that of freshwater algae (−23‰; Smith and Epstein, 1971). Because of the preferential uptake of ^{12}C-enriched compounds during microbial remineralisation, the produced carbonate is even more depleted in ^{13}C than the source material (e.g. Lee et al., 1987). The carbon isotopic composition of the Hellín basin carbonate deposits (as low as −11.‰; Fig. 6-9), thus, reflects a combination of lake water DIC and carbonate alkalinity produced by the remineralisation of organic matter. Dolomite from the Cenajo sub-basin of the Hellín Basin and the Lorca basin reveals similar $\delta^{13}C$ values, which have been attributed to bacterial sulphate reduction (Bellanca et al., 1989; Rouchy et al., 1998).

Additional evidence for a microbial origin of the Hellín basin dolomites stems from the anticorrelation between $\delta^{13}C$ and $\delta^{18}O$ values (Fig. 6-9). During phases of enhanced evaporation the sulphate concentration in the lake water increased, allowing sulphate ions to penetrate deeper into the sediment, which consequently expanded the sulphate reduction zone (cf., Kasten and Jørgensen,

2000). When this happened, sulphate reduction overprinted carbonate beds by inducing the interstitial precipitation of ^{18}O-enriched and ^{13}C-depleted dolomite, with ^{18}O-enrichment reflecting a high degree of evaporation and ^{13}C-depletion corresponding to a high contribution of carbonate derived from bacterial sulphate reduction coupled to oxidation of organic matter, crude oil, or methane.

An anoxic milieu in the lacustrine sediments of the Hellín basin, which is required for sulphate reduction, agrees with the lack of bioturbation as revealed by the undisturbed lamination in the sulphur-bearing strata. The absence of replacive growth supports an early origin of dolomite (cf., Servant-Vildary et al., 1990). The biological origin of the studied dolomite – resulting from microbially-induced precipitation and not from dolomitisation – is evidenced by microfabrics such as mat-like lamination, aggregates of clotted or peloidal dolomicrite, and particularly spheroidal dolomite. The strong fluorescence of the spheroids indicates a high content of organic matter (cf., Dravis and Yurewicz, 1985). Notably, spheroidal dolomite has been suggested to result from the bacterial remineralisation of organic matter (Lalou, 1957; Gunatilaka, 1989; Ayllón-Quevedo et al., 2007; Sanz-Montero et al., 2009), indicating that this fabric is typical for microbial dolomite. Similar fabrics have been observed in microbial dolomite forming in modern lagoonal environments (Vasconcelos and McKenzie, 1997; Wright, 1999). The shape of spheroids is believed to reflect microenvironments of mineral precipitation, where cells and extracellular polymeric substances act as nucleation sites (Vasconcelos et al., 1995; Burns et al., 2000; van Lith et al., 2003; Ayllón-Quevedo et al., 2007; Dupraz et al., 2008).

High sulphate concentrations were found to inhibit dolomite precipitation (e.g. Baker and Kastner, 1981; for an opposing view see Sánchez-Román et al., 2009). Dolomite forms under surface conditions when bacterial sulphate reduction effectively reduces sulphate concentration (Baker and Kastner, 1981; Vasconcelos and McKenzie, 1997; Wright and Wacey, 2005). Sulphate-reducing bacteria are believed to favour dolomite formation by the liberation of magnesium ions, which are efficiently complexed by sulphate ions (Slaughter and Hill, 1991; Vasconcelos et al., 1995; Vasconcelos and McKenzie, 1997). A magnesium to calcium ratio of 5:1 to 10:1 has been found to be necessary for dolomite precipitation (e.g. Folk and Land, 1975; Warren, 2000). In lacustrine environments such high Mg:Ca ratios can be achieved (1) by consumption of calcium ions during gypsum precipitation (Folk and Land, 1975; Hardie, 1987), (2) by precipitation of calcite (Land, 1998), or (3) during early diagenesis of clay minerals with a release of magnesium ions (Kahle, 1965; Weaver and Beck, 1971). Whereas the latter process has been suggested to have played a significant role during the precipitation of dolomite spheroids in Kuwait (Khalaf, 1990), the first factor and, to a lesser degree, the second factor probably favoured dolomite formation in the Hellín basin.

Variations in lake water chemistry are a possible cause for the changes from calcite to dolomite lithologies in the sedimentary strata of the Hellín basin (cf., Servant-Vildary et al., 1990). Such a scenario has been described for the Devonian Orcadian basin and the modern Lagoa Vermelha, where dolomite formation is believed to be linked to periods of enhanced evaporation and calcite formation supposedly takes place during periods of enhanced freshwater input (Janaway and Parnell, 1989; Vasconcelos and McKenzie, 1997). High $\delta^{18}O$ values of Hellín basin dolomites (+6.2 to +10.5‰) confirm that dolomite precipitated in an environment typified by evaporation (cf., Talbot and Kelts, 1990), as the highest value for a calculated calcite would still be +7.1‰ after the correction for different fractionation factors during precipitation ($\varepsilon^{18}O_{dolomite-calcite}$ = +2.6‰, Vasconcelos et al., 2005) and for fractionation during the analytical procedure ($\varepsilon^{18}O_{dolomite-calcite}$ = +0.8‰ at 25°C, Sharma and Clayton, 1965). Carbonate deposits with a mixed composition of calcite and dolomite and $\delta^{18}O$ values close to 0‰ probably reflect periods of dilution of the lake by freshwater, whereas calcite spar with negative $\delta^{18}O$ values precipitated from meteoric waters during late diagenesis.

6.5.2 Formation of native sulphur and secondary gypsum

Microbial sulphate reduction releases hydrogen sulphide, which is further oxidized to native sulphur in some settings (e.g. Machel, 1992). Sulphate-reducing bacteria discriminate against ^{34}S, resulting in the formation of hydrogen sulphide with low $\delta^{34}S$ values (e.g. Kaplan and Rittenberg, 1964; Canfield, 2001). Similar to other basins in Spain like the Teruel basin, the Ebro basin, or basins in the eastern Betics (Anadón et al., 1992; Utrilla et al., 1992; Playà et al., 2000), Triassic evaporitic rocks with an average $\delta^{34}S$ value of +12‰ are present in the drainage area of the Hellín basin (Servant-Vildary et al., 1990). During the Miocene, the Triassic evaporites were dissolved by meteoric waters and the resultant sulphate ions were subjected to bacterial sulphate reduction in the Hellín basin. The primary gypsum of the lacustrine sedimentary sequence of the Hellín basin is slightly enriched in ^{34}S compared to Triassic gypsum (+13 to +19‰, Servant-Vildary et al., 1990), reflecting the removal of isotopically light sulphate by bacterial sulphate reduction. The oxidation of sulphide to sulphur involves only a negligible fractionation effect for sulphur isotopes (Canfield, 2001; Hoefs, 2004). Therefore, the low $\delta^{34}S$ values of native sulphur from the Hellín basin (−17.1 to −3.7‰) reflect the isotopic composition of sulphide produced by bacterial sulphate reduction. The accordant fractionation of sulphur isotopes between sulphate and sulphide (14 to 30‰) is well within the known range of bacterial sulphate reduction (Hartmann and Nielsen, 1969; Goldhaber and Kaplan, 1974, Bolliger et al., 2001; Detmers et al., 2001).

The oxidation of hydrogen sulphide to native sulphur occurs abiologically or biologically (Machel, 1992). One observation suggests that at least part of the native sulphur of the Hellín basin results from biological oxidation. The fluorescent globules enclosed in native sulphur (Fig. 6-7) probably

represent fossilized bacterial cells. They resemble the sulphide-oxidizing bacteria *Thiomargarita* sp. or *Achromatium* sp. (written comm. H. N. Schulz-Vogt, 2009). *Thiomargarita* sp. have been exclusively described from marine sediments (Schulz and Schulz, 2005). Their metabolism is based on oxidation of sulphide with oxygen or nitrate (Schulz and Jørgensen, 2001; Schulz, 2002). *Achromatium* sp., however, prefer lacustrine conditions and gain energy by the oxidation of sulphide to sulphate with native sulphur as intermediate (Gray et al., 1999). The bending of sediment layers around sulphur nodules points to a syngenetic formation of sulphur and thus, agrees with biological oxidation of hydrogen sulphide.

Most of the gypsum in the Las Minas de Hellín formation is obviously of a diagenetic origin, resembling diagenetic gypsum of the Miocene Teruel basin (cf., Ortí et al., 2010). Such an origin is revealed by the replacement of sulphur nodules or carbonate laminae and the infilling of late fissures. The oxidation of reduced sulphur species produces sulphuric acid, which causes a drop in pH leading to carbonate dissolution (Boudreau, 1991; Walter et al., 1993; Ku et al., 1999, Pirlet et al., 2010). The gypsum that tends to precipitate under these conditions replaces carbonate and native sulphur in the sedimentary sequence (Servant-Vildary et al., 1990). The fractionation effect for sulphur isotopes during the precipitation of gypsum (1.6‰) is small (Nakai and Jensen, 1964; Thode and Monster, 1973; Claypool et al., 1980). The low $\delta^{34}S$ values (–11.1 to –18.2‰) of diagenetic gypsum consequently confirm its origin from the oxidation of native sulphur. This secondary gypsum is also characterized by low $\delta^{18}O$ values, reflecting the uptake of oxygen derived from meteoric waters (cf., Taylor and Wheeler, 1984; Brunner et al., 2005).

6.6 Conclusions

The native sulphur and authigenic dolomite present in the lacustrine evaporitic sequence of the Late Miocene Las Minas de Hellín formation of the Hellín basin in SE Spain formed as a consequence of bacterial sulphate reduction. The high sulphate concentration of the Miocene lake led to the deposition of primary lacustrine gypsum and served as an electron acceptor for bacterial remineralisation of organic matter. A microbial origin of authigenic dolomite is confirmed by its $\delta^{13}C$ values as low as −11‰ and textural evidence including spheroids, clotted and peloidal fabrics, as well as mat-like lamination. Microfossils preserved in native sulphur indicate that hydrogen sulphide produced by the sulphate-reducing bacteria was at least partially oxidized biologically, resulting in sulphur formation. The putative bacterial fossils resemble the sulphide-oxidizing bacteria *Thiomargarita* and *Achromatium*. A significant amount of the native sulphur in the Las Minas de Hellín formation was later oxidized to ^{34}S-depleted secondary gypsum ($\delta^{34}S$ values as low as −18‰), still reflecting the sulphur isotope composition of the biogenic sulphur ($\delta^{34}S$ values as low as −17‰).

Acknowledgements

We thank Sebastian Flotow (Bremen) for thin section preparation, Brit Kockisch (Bremen) for TOC measurements, Thomas Max (MPI Bremen) for help with sulphur and oxygen isotope analysis, Monika Segl (Bremen) for carbon and oxygen isotope analysis, Christoph Vogt (Bremen) for XRD measurements, Petra Witte (Bremen) for help with REM analysis, and Heide Schulz-Vogt (MPI Bremen) for comments on sulphide-oxidizing bacteria. Comments by Federico Ortí (Barcelona) and an anonymous referee helped improving the manuscript. This project was supported by the DFG Research Center “The ocean in the Earth system”, the international graduate college EUROPROX, and the Max Planck Society.

7 - CONCLUDING REMARKS AND PERSPECTIVES

The main conclusions of the presented thesis are:

I) All examined deposits of native sulphur and accompanying carbonate are the result of microbial activity, with bacterial sulphate reduction as main and most important process. This is evidenced by large sulphur isotope fractionation between sulphate and reduced sulphur species (up to 60‰), best visible in the large difference between $\delta^{34}S_{CAS}$ and $\delta^{34}S_{sulphur}$. The $\delta^{34}S_{CAS}$ is regarded as good measure for the sulphur isotopic composition of sulphate contemporaneously to carbonate precipitation. The low carbon isotopic ratios of the carbonates reveals the incorporation of carbon derived from microbial processes as the degradation of organic matter or crude oil or the oxidation of methane. The presence of microfabrics like biomat-resembling lamination and spheroidal dolomite further supports the biogenicity of these deposits.

II) Although these microbial processes led to the same type of sulphur and carbonate deposits, very similar at first glance, there are two different pathways of deposition. During sedimentation or very early diagenesis, within the unconfined sediment, sulphate reducing bacteria use dissolved sulphate to oxidize mainly methane. The resulting carbonate contains pseudomorphs after lenticular gypsum and is enriched in ^{18}O, displaying evaporitic conditions during authigenesis, which is furthermore evidenced by the presence of lipid biomarkers putatively derived from halophilic organisms. So, in accordance with Dessau et al. (1962) and in opposition to other publications (Ruckmick et al., 1979; Manzi et al., 2010) the presented results show that not all but some of the Sicilian sulphur and carbonate deposits precipitated syngenetically. The same pathway is obvious for Hellín deposits, especially because of the presence of native sulphur nodules embedded in laminated carbonate. In contrast to that syngenetic pathway the epigenetic pathway occurs late-diagenetic. Sulphate minerals as gypsum or anhydrite are dissolved by meteoric waters to provide the sulphate source. The carbonates derived from that are characterized by low $\delta^{18}O$ values. Partly the replacement of gypsum by carbonate is nicely visible (see Fig. 3-6B). Overall it has to be pointed out here, that syngenetic deposits do not only account for small occurrences in modern settings as proposed by Wessel (1994) but seem to be more widespread than formerly thought.

III) Carbonates which are most depleted in ^{13}C are indeed induced by sulphate-dependent AOM, substantiated by molecular fossils and their compound-specific very low carbon isotope values. Two groups of organisms are involved in AOM. Anaerobic methanotrophic archaea are displayed by lipids as PMI, *sn*2-hydroxyarchaeol and biphytanic diacids with $\delta^{13}C$ values as low as −105‰. The sulphate

reducing bacteria are represented by e.g., ββ-bishomohopanoic acid, *iso*- and *anteiso*-$C_{15:0}$ and $C_{17:0}$ and the 10Me-$C_{16:0}$ fatty acids, all likewise substantially depleted in ^{13}C ($\delta^{13}C$ as low as −90‰). Interestingly the lipid biomarker inventory differs slightly compared to studies of consortia of ANME and SRB typically associated to methane seepage. Therefore an assignment to one of the common ANME groups was not possible. Nonetheless these results clearly demonstrate that sulphate-dependent AOM was occurring in evaporitic settings of the Messinian, despite recent studies which suggested that AOM is inhibited by high chloride concentrations (Joye et al., 2009a, b).

Some aspects are still to be discussed:

The process of sulphide oxidation to native sulphur remains rather enigmatic. Samples from the Hellín basin indicate that sulphide oxidation might have occurred biologically, as fossils preserved in the samples resemble sulphide oxidizing bacteria. Unfortunately lipids derived from these organisms are not very specific, especially in sediments where sulphate reducing bacteria are ubiquitous (Arning et al., 2008). Synproportionation should produce $\delta^{34}S_{sulphur}$ values plotting exactly between $\delta^{34}S_{sulphate}$ and $\delta^{34}S_{sulphide}$. In Sicilian samples no sulphide minerals could be obtained. As $\delta^{34}S_{sulphate}$ is as high as +60‰ and the $\delta^{34}S_{sulphur}$ is mainly about 0 to 10‰, the sulphide from which the sulphur was formed would have been as low as −50‰, resulting in a fractionation of more than 100‰, which is far out of the range of published data. Synproportionation is therefore an unlikely process for generation of native sulphur from sulphide for the Sicilian deposits. The abiological oxidation of sulphide to native sulphur with oxygen would have required alternation between reducing and oxidizing conditions. Developing methods to determine the oxidative path of sulphur deposition would be highly necessary. A recent study by Zerkle et al. (2009) for example proposed the potential of multiple sulphur isotope studies ($\delta^{33}S$ and $\delta^{34}S$) for discrimination of different oxidation pathways, as phototrophic, chemotrophic and abiological sulphide and sulphur oxidation. The investigation of modern sulphur-precipitating environments would be of great help. Butlin and Postgate (1954) described active microbial sulphur precipitation in lagoonal lakes in Cyrenaica, Libya. Similar occurrences are also present in an alpine lake called Alatsee (pers. com. Ulrich Struck). Furthermore the investigation of ancient sulphur deposits with a better constrained geological frame (e.g., salt dome cap rocks, or small lacustrine sulphur-containing basins) could be combined to the application of a box-model, which integrates the stability and dissolution of gypsum to calculate the gypsum to sulphur transformation and the accompanied precipitation of carbonates. In a closed system the distribution of sulphur isotopes between the different sulphur phases could be calculated and compared to nature. That offers conclusions about the possible pathways of sulphide to sulphur oxidation and the possibility to compare it to the less well-confined Sicilian sulphur deposits.

Although fractionation between sulphate and native sulphur is as high as 60‰, an important contribution of bacterial disproportionation is unlikely for the Sicilian deposits, first because of the large amounts of native sulphur still present and secondly because disproportionation produces protons which would have inhibited carbonate precipitation (cf., Cypionka et al., 1998; Finster et al., 1998). Nevertheless it would be interesting to investigate the influence of disproportionation in these types of settings and to evaluate the conditions which favour disproportionation. Mass dependent processes like sulphate reduction should produce a $\delta^{33}S$ that is about half the $\delta^{34}S$ value ($\delta^{33}S = 0.515*\delta^{34}S$; Farquhar et al., 2003). Recent experiments and model calculations show that although both processes are mass-dependent, bacterial sulphate reduction and disproportionation are distinguishable by means of relationship between $\delta^{34}S$ and $\delta^{33}S$ of sulphate and sulphide (Farquhar et al., 2003; Johnston et al., 2005a, b, 2007, 2008).

Böttcher and Brunner (pers. com.) suggested a very elegant method to investigate the temperature conditions during carbonate precipitation with the help of $\delta^{18}O$ values of CAS. The difference in $\delta^{18}O$ between carbonate and water in equilibrium is described by the temperature-dependent separation factor ε. The oxygen isotopic composition of water can be calculated from the $\delta^{18}O$ values of the carbonate and differs with changing temperature (Zheng, 1999). The oxygen isotopic composition of sulphate in a solution that is influenced by microbial sulphate reduction can be assumed from the oxygen isotopic composition of the water (Fritz et al., 1989) and appears to be temperature-dependent as well. The $\delta^{18}O$ value of CAS coincides with a $\delta^{18}O$ value of dissolved sulphate at a certain temperature, which represents the temperature of the solution from which the carbonate precipitated. This method provides not only information about environmental conditions during carbonate precipitation; it may also offer a way to distinguish bacterial from thermochemical sulphate reduction. Although TSR can be excluded for the Sicilian deposits and for Hellín, because a) there is no indication that the deposits were exposed to elevated temperatures, b) the sulphur isotope fractionation is substantially higher than proposed for TSR (cf., Machel et al., 1995; Worden et al., 1997) and c) the lipid biomarker data gave robust evidence for microbially mediation in the Sicilian samples, I would recommend that method for other sulphur deposits, e.g., salt dome cap rocks, where elevated temperature might have occurred.

Furthermore the study of so far purely investigated deposits of most likely biogenic native sulphur and authigenic carbonates, as for example in Romania (pers. com. Eugen Gradninaru) could provide further insides into sulphur and carbonate genesis. The molecular fossil approach should be applied also to other locations to further corroborate the importance of microorganisms in carbonate and sulphur authigenesis and to extend our understanding about the microbes that are flourishing extreme environments.

8 - REFERENCES

Abd-El-Malek Y, Rizk SG (1963a) Bacterial sulphate reduction and the development of alkalinity. I. Experiments with synthetic media. *Journal of Applied Bacteriology* **26** 7-13.

Abd-El-Malek Y, Rizk SG (1963b) Bacterial sulphate reduction and the development of alkalinity. II. Laboratory experiments with soils. *Journal of Applied Bacteriology* **26** 14-19.

Aeckersberg F, Rainey FA, Widdel F (1998) Growth and natural relationships, cellular fatty acids and metabolic adaption of sulfate-reducing bacteria that utilize long-chain alkanes under anoxic conditions. *Archives of Microbiology* **170** 361–369.

Allen RD, Kramer H (1953) Occurrence of bassanite in two desert basins in southeastern California. *The American Mineralogist* **38** 1266-1268.

Aloisi G, Gloter A, Krüger M, Wallmann K, Guyot F, Zuddas P (2006) Nucleation of calcium carbonate on bacterial nanoglobules. *Geology* **34** 1017-1020.

Anadón P, Rosell L, Talbot MR (1992) Carbonate replacement of lacustrine gypsum deposits in two Neogene continental basins, eastern Spain. *Sedimentary Geology* **78** 201-216.

Arning ET, Birgel D, Schulz-Vogt HN, Holmkvist L, Jørgensen BB, Larson A, Peckmann J (2008) Lipid biomarker patterns of phosphogenic sediments from upwelling regions. *Geomicrobiology Journal* **25** 69-82.

Ayllón-Quevedo F, Souza-Egipsy V, Sanz-Montero M E, Rodríguez-Aranda JP (2007) Fluid inclusion analysis of twinned selenite gypsum beds from the Miocene of the Madrid basin (Spain). Implication on dolomite bioformation. *Sedimentary Geology* **201** 212-230.

Baker PA, Kastner M (1981) Constraints on the formation of sedimentary dolomite. *Science* **213** 214-216.

Balci N, Shanks III WC, Mayer B, Mandernack KW (2007) Oxygen and sulfur isotope systematics of sulfate produced by bacterial and abiotic oxidation of pyrite. *Geochimica et Cosmochimica Acta* **71** 3796–3811.

Barker JM, Cochran DE, Semrad R (1979) Economic geology of the Mishraq native sulfur deposit, Northern Iraq. *Economic Geology* **74** 484-495.

Baudrand M, Grossi V, Pancost R, Aloisi G (2010) Non-isoprenoid macrocyclic glycerol diethers associated with authigenic carbonates. *Organic Geochemistry* **41** 1341-1344.

Bellanca A, Calvo JP, Censi P, Elizaga E, Neri R (1989) Evolution of lacustrine diatomite carbonate cycles of Miocene age, southeastern Spain: petrology and isotope geochemistry. *Journal of Sedimentary Petrology* **59** 45-52.

Benison KC, Jagniecki EA, Edwards TB, Mormile MR, Storrie-Lombardi MC (2008) "Hairy blobs": Microbial suspects preserved in modern and ancient extremely acid lake evaporites. *Astrobiology* **8** 807-821.

Berthold C, Bjeoumikhov A, Brügemann L (2009) Fast XRD^2 microdiffraction with focussing X-ray microlenses. *Particle & Particle Systems Characterization* **26** 107-111.

Beyerinck WM (1895) Ueber *Spirillum desulfuricans* als Ursache von Sulfatreduction. *Centralblatt für Bakteriologie und Parasitenkunde* **1** 1–9, 49–59, 104–114.

Birgel D, Elvert M, Han X, Peckmann J (2008a) ^{13}C-depleted biphytanic diacids as tracers of past anaerobic oxidation of methane. *Organic Geochemistry* **39** 152-156.

Birgel D, Himmler T, Freiwald A, Peckmann J (2008b) A new constraint on the antiquity of anaerobic oxidation of methane: Late Pennsylvanian seep limestones from southern Namibia. *Geology* **36** 543-546.

Birgel D, Peckmann J, Klautzsch S, Thiel V, Reitner J (2006a) Anaerobic and aerobic oxidation of methane at Late Cretaceous seeps in the Western Interior seaway, USA. *Geomicrobiology Journal* **23** 565-577.

Birgel D, Thiel V, Hinrichs K-U, Elvert M, Campbell KA, Reitner J, Farmer JD, Peckmann J (2006b) Lipid biomarker patterns of methane-seep microbialites from the Mesozoic convergent margin of California. *Organic Geochemistry* **37** 1289-1302.

Blumenberg M, Krüger M, Nauhaus K, Talbot HM, Oppermann BI, Seifert R, Pape T, Michaelis W (2006) Biosynthesis of hopanoids by sulfate-reducing bacteria (genus *Desulfovibrio*). *Environmental Microbiology* **8** 1220-1227.

Blumenberg M, Seifert R, Petersen S, Michaelis W (2007) Biosignatures present in a hydrothermal massive sulfide from the Mid-Atlantic Ridge. *Geobiology* **5**, 435-450.

Blumenberg M, Seifert R, Reitner J, Pape T, Michaelis W, (2004) Membrane lipid patterns typify distinct anaerobic methanotrophic consortia. *Proceedings of the National Academy of Sciences of the United States of America* **101** 11111-11116.

Boetius A, Ravenschlag K, Schubert CJ, Rickert D, Widdel F, Gieseke A, Amann R, Jørgensen BB, Witte U, Pfannkuche O (2000) A marine microbial consortium apparently mediating anaerobic oxidation of methane. *Nature* **407** 623-626.

Bolliger C, Schroth MH, Bernasconi SM, Kleikemper J, Zeyer J (2001) Sulfur isotope fractionation during microbial sulfate reduction by toluene-degrading bacteria. *Geochimica et Cosmochimica Acta* **65** 3289-3298.

Böttcher ME, Brumsack H-J, de Lange GJ (1998) Sulfate reduction and related stable isotope (^{34}S, ^{18}O) variations in interstitial waters of the eastern Mediterranean. In: Robertson AHF, Emeis K-C, Richter C, Camerlenghi A (Eds.) *Proceedings of the Ocean Drilling Program: Scientific results* **160**, pp. 365–373.

Böttcher ME, Parafiniuk J (1998) Methane-derived carbonates in a native sulfur deposit: stable isotope and trace element discriminations related to the transformation of aragonite to calcite. *Isotopes in Environmental and Health Studies* **34** 177-190.

Böttcher ME, Thamdrup B, Vennemann TW (2001) Oxygen and sulfur isotope fractionation during anaerobic bacterial disproportionation of elemental sulfur. *Geochimica et Cosmochimica Acta* **65** 1601-1609.

Boudreau BP (1991) Modelling the sulfide-oxygen reaction and associated pH gradients in porewaters. *Geochimica et Cosmochimica Acta* **55** 145-159.

Briand F (2007) Executive summary. In: Briand F (Ed.) CIESM, 2007. The Messinian Salinity Crisis from mega-deposits to microbiology — a consensus report. *CIESM Workshop Monographs* **33**, Monaco, pp. 7–28.

Brocks JJ, Buick R, Summons RE, Logan GA (2003) A reconstruction of Archean biological diversity based on molecular fossils from the 2.78 to 2.45 billion-year-old Mount Bruce Supergroup, Hamersley Basin, Western Australia. *Geochimica et Cosmochimica Acta* **67** 4321-4335.

Brunner B, Bernasconi SM (2005) A revised isotope fractionation model for dissimilatory sulfate reduction in sulfate reducing bacteria. *Geochimica et Cosmochimica Acta* **69** 4759-4771.

Brunner B, Bernasconi SM, Kleikemper JA, Schroth MH (2005) A model for oxygen and sulfur isotope fractionation in sulfate during bacterial sulfate reduction processes. *Geochimica et Cosmochimica Acta* **69** 4773–4785.

Brunner B, Yu JY, Mielke RE, MacAskill JA, Madzunkov S, McGenity TJ, Coleman M (2008) Different isotope and chemical patterns of pyrite oxidation related to lag and exponential growth phases of *Acidithiobacillus ferrooxidans* reveal a microbial growth strategy. *Earth and Planetary Science Letters* **270** 63–72.

Bundy WM (1956) Petrology of gypsum-anhydrite deposits of southwestern Indiana. *Journal of Sedimentary Petrology* **26** 240-256.

Burdett JW, Arthur MA, Richardson M (1989) A Neogene seawater sulfur isotope age curve from calcareous pelagic microfossils. *Earth and Planetary Science Letters* **94** 189-198.

Burhan RYP, Trendel JM, Adam P, Wehrung P, Albrecht P, Nissenbaum A (2002) Fossil bacterial ecosystem at methane seeps: Origin of organic matter from Be'eri sulfur deposit, Israel. *Geochimica et Cosmochimica Acta* **66** 4085-4101.

Burns SJ, McKenzie JA, Vasconcelos C (2000) Dolomite formation and biogeochemical cycles in the Phanerozoic. *Sedimentology* **47** 49-61.

Butler RWH, Lickorish WH, Grasso M, Pedley HM, Ramberti L (1995) Tectonics and sequence stratigraphy in Messinian basins, Sicily: Constraints on the initiation and termination of the Mediterranean salinity crisis. *Geological Society of America Bulletin* **107** 425-439.

Butlin KR, Postgate JR (1954) The microbiological formation of sulphur in Cyrenaican lakes. In: Cloudsley-Thompson JL (Ed.) Biology of Deserts — the Proceedings of a Symposium on the Biology of Hot and Cold Deserts Organized by the Institute of Biology. Institute of Biology, London, pp. 112–122.

Calvo JP, Elizaga E (1989) Sedimentación evaporítica en las cuencas de Cenajo y Las Minas - Camarillas (región de Hellín, Mioceno Superior del área Prebética). In: Ortí F, Salvany JM (Eds.) Formaciones evaporíticas de la Cuenca del Ebro y cadenas periféricas, y de la zona de Levante. University of Barcelona, Barcelona, pp. 246-250.

Calvo JP, Elizaga E, Lopez Martinez N, Robles F, Usera J (1978) El Mioceno superior continental del Prébetico Externo: Evolución del Estrecho Nordbético. *Boletín Geológico y Minero* **89** 407-426.

Campbell KA (2006) Hydrocarbon seep and hydrothermal vent paleoenvironments and paleontology: past developments and future research directions. *Palaeogeography, Palaeoclimatology, Palaeoecology* **232** 362–407.

Canfield DE, Raiswell R (1999) The evolution of the sulfur cycle. *American Journal of Science* **299** 697-723.

Canfield DE, Thamdrup B (1994) The production of ^{34}S-depleted sulfide during bacterial disproportionation of elemental sulfur. *Science* **266** 1973-1975.

Canfield DE (2001) Biogeochemistry of sulfur isotopes. In: Valley JW, Cole DR (Eds.) Stable Isotope Geochemistry. Mineralogical Society of America and Geochemical Society: Reviews in Mineralogy and Geochemistry. Mineralogical Society of America, Washington, DC, pp. 607-636.

Castanier S, Le Métayer-Levrel G, Perthuisot JP (1999) Ca-carbonate precipitation and limestone genesis – the microbiogeologist point of view. *Sedimentary Geology* **126** 9-23.

Castanier S, Le Métayer-Levrel G, Perthuisot J-P (2000) Bacterial roles in the precipitation of carbonate minerals. In: Riding RE, Awramik SM (Eds.) Microbial Sediments. Springer, Berlin, Heidelberg, pp. 32-39.

Cerling TE, Bowman JR, O'Neil JR (1988) An isotopic study of a fluvial-lacustrine sequence: The Plio-Pleistocene Koobi Fora sequence, East Africa. *Paleogeography, Palaeoclimatology, Palaeoecology* **63** 335-356.

Cheney ES, Jensen ML (1965) Stable carbon isotopic composition of biogenic carbonates. *Geochimica et Cosmochimica Acta* **29** 1331-1346.

Choquette PW, Trusell FC (1978) A procedure for making the Titan-yellow stain for Mg-calcite permanent. *Journal of Sedimentary Research* **48** 639–641.

Claypool GE, Holser WT, Kaplan IR, Sakai H, Zak I (1980) The age curve of sulfur and oxygen isotopes in marine sulfate and their mutual interpretation. *Chemical Geology* **28** 199-260.

Colalongo ML, Pasini G (1997) The Messinian historical stratotype and the Tortonian/Messinian boundary. In: Montanari A, Odin GS, Coccioni R (Eds.) Miocene stratigraphy: An integrated approach. *Developments in palaeontology and stratigraphy* **15** 107-123.

Coleman ML, Raiswell R (1995) Source of carbonate and origin in zonation in pyritiferous carbonate concretions: Evaluation of a dynamic model. *American Journal of Science* **295** 282-308.

Coleman ML, Hedrick DB, Lovley DR, White DC, Pye K (1993) Reduction of Fe (III) in sediments by sulphate-reducing bacteria. *Nature* **361** 436-438.

Craig H (1953) The geochemistry of the stable carbon isotopes. *Geochimica et Cosmochimica Acta* **3** 53-92.

Cypionka H, Smock AM, Böttcher ME (1998) A combined pathway of sulfur compound disproportionation in *Desulfovibrio desulfuricans*. *FEMS Microbiology Letters* **166** 181-186

Daffonchio D, Borin S, Brusa T, Brusetti L, van der Wielen PWJJ, Bolhuis H, Yakimov MM, D'Auria G, Giuliano L, Marty D, Tamburini C, McGenity TJ, Hallsworth JE, Sass AM, Timmis KN, Tselepides A, de Lange GJ, Hübner A, Thomson J, Varnavas SP, Gasparoni F, Gerber HW, Malinverno E, Corselli C and the Biodeep scientific party (2006) Stratified prokaryote network in the oxic-anoxic transition of a deep-sea halocline. *Nature* **440** 203-207.

Davis JB, Kirkland DW (1970) Native sulfur deposition in the Castile Formation, Culberson County, Texas. *Economic Geology* **65** 107-121.

Davis JB, Kirkland DW (1979) Bioepigenetic sulfur deposits. *Economic Geology and the Bulletin of the Society of Economic Geology* **74** 462-468.

Davis JB, Stanley JP, Custard HC (1970) Evidence against oxidation of hydrogen sulfide by sulfate ions to produce elemental sulfur in salt domes. *American Association of Petroleum Geologists Bulletin* **54** 2444-2447.

De Boever E, Birgel D, Thiel V, Muchez P, Peckmann J, Dimitrov L, Swennen R (2009) The formation of giant tubular concretions triggered by anaerobic oxidation of methane as revealed by archaeal molecular fossils (Lower Eocene, Varna, Bulgaria). *Palaeogeography Palaeoclimatology Palaeoecology* **280** 23-36.

De Laeter JR, Böhlke JK, De Bièvre P, Hidaka H, Peiser HS, Rosman KJR, Taylor PDP (2003) Atomic weight of the elements: Review 2000. *Pure and Applied Chemistry* **75** 683-800.

De Rosa M, Gambacorta A (1988) The lipids of archaebacteria. *Progress in Lipid Research* **27** 153-175.

Decima A, McKenzie JA, Schreiber BC (1988) The origin of "evaporative" limestones: An example from the Messinian of Sicily (Italy). *Journal of Sedimentary Petrology* **58** 256-272.

Decima A, Wezel FC (1973) Late Miocene evaporites of the central Sicilian basin, Italy. In: Ryan WBF, Hsü KJ, Dumitrica P, Lort JM, Maync W, Nesteroff WD, Pautot G, Stradner H, Wezel FC (Eds.) Initial Reports of the Deep Sea Drilling Project, Volume 13. US Government Printing Office, Washington, pp. 1234-1241.

Dessau G, Jensen ML, Nakai N (1962) Geology and isotopic studies of Sicilian sulfur deposits. *Economic Geology* **57** 410-438.

Detmers J, Brüchert V, Habicht KS, Kuever J (2001) Diversity of sulfur isotope fractionations by sulfate-reducing prokaryotes. *Applied and Environmental Microbiology* **67** 888-894.

Ding T, Valkiers S, Kipphardt H, de Bièvre P, Taylor PDP, Gonfianti R, Krouse R (2001) Calibrated sulfur isotope abundance ratios of three IAEA sulfur isotope reference materials and V-CDT with a reassessment of the atomic weight of sulfur. *Geochimica et Cosmochimica Acta* **65** 2433-2437.

Dowling NJE, Widdel F, White DC (1986) Phospholipid ester-linked fatty acid biomarkers of acetate-oxidizing sulphate-reducers and other sulphide-forming bacteria. *Journal of General Microbiology* **132** 1815-1825.

Dravis JJ, Yurewicz DA (1985) Enhanced carbonate petrography using fluorescence microscopy. *Journal of Sedimentary Petrology* **55** 795-804.

Druckmann Y, Weissbrod T, Aharon P (1994) Evidence for methane and hydrogen sulfide venting imprinted on a Quaternary eolianite from southern Israel. *Geo-Marine Letters* **14** 170-176.

Duggen S, Hoernle K, van den Bogaard P, Rüpke L, Morgan JP (2003) Deep roots of the Messinian salinity crisis. *Nature* **422** 602-606.

Dupraz C, Visscher PT, Baumgartner LK, Reid RP (2004) Microbe-mineral interactions: early carbonate precipitation in a hypersaline lake (Eleuthera Island, Bahamas). *Sedimentology* **51** 745–765.

Dupraz C, Reid RP, Braissant O, Decho AW, Norman RS, Visscher PT (2008) Processes of carbonate precipitation in modern microbial mats. *Earth-Science Reviews* **96** 141-162.

Dworkin SI, Land LS (1994). Petrographic and geochemical constraints on the formation and diagenesis of anhydrite cements, Smackover sandstones, Gulf of Mexico. *Journal of Sedimentary Research* **A64** 339–348.

Eckelmann WA, Broecker WS, Whitlock DW, Allsup JR (1962) Implications of carbon isotopic composition of total organic carbon of some recent sediments and ancient oils. *American Association of Petroleum Geologists Bulletin* **46** 699-704.

Edlund A, Nichols PD, Roffey R, White DC (1985) Extractable and lipopolysaccharide fatty acid and hydroxy acid profiles from *Desulfovibrio* species. *Journal of Lipid Research* **26**, 982-988.

Elvert M, Boetius A, Knittel K, Jørgensen BB (2003) Characterization of specific membrane fatty acids as chemotaxonomic markers for sulphate-reducing bacteria involved in anaerobic oxidation of methane. *Geomicrobiology Journal* **20** 403-419.

Elvert M, Hopmans EC, Treude T, Boetius A, Suess E (2005) Spatial variations of methanotrophic consortia at cold methane seeps: implications from a high-resolution and isotopic approach. *Geobiology* **3** 195-209.

Elvert M, Suess E, Whiticar MJ (1999) Anaerobic methane oxidation associated with marine gas hydrates: superlight C-isotopes from saturated and unsaturated C-20 and C-25 irregular isoprenoids. *Naturwissenschaften* **86** 295-300.

Evans CC (1972) Whiskers. Mills and Boon Limited, London, pp. 72.

Farquhar J, Johnston DT, Wing BA, Habicht KS, Canfield DE, Airieau S, Thiemes MH (2003) Multiple sulphur isotopic interpretations of biosynthetic pathways: implications for biological signatures in the sulphur isotope record. *Geobiology* **1** 27–36.

Feely HW, Kulp JL (1957) Origin of gulf coast salt-dome sulphur deposits. *Bulletin of the American Association of Petroleum Geologists* **41** 1802-1853.

Feigl F (1960) Tüpfelanalyse - Band 1: Anorganischer Teil. Akademische Verlagsgesellschaft m.b.H., Frankfurt am Main, 594p.

Ferdelman TG, Fossing H, Neumann K (1999) Sulfate reduction in surface sediments of the southeast Atlantic continental margin between 15°38'S and 27°57'S (Angola and Namibia). *Limnology and Oceanography* **44** 650-661.

Ferdelman TG, Lee C, Pantoja S, Harder J, Bebout BM, Fossing H (1997) Sulfate reduction and methanogenesis in a *Thioploca*-dominated sediment off the coast of Chile. *Geochimica et Cosmochimica Acta* **61** 3065-3079.

Finster K, Liesack W, Thamdrup B (1998) Elemental sulfur and thiosulfate disproportionation by *Desulfocapsa sulfoexigens* sp. nov., a new anaerobic bacterium isolated from marine surface sediments. *Applied and Environmental Microbiology* **64** 119-125.

Folk RL, Land LS (1975) Mg/Ca ratio and salinity: two controls over crystallization of dolomite. *American Association for Petroleum Geologists Bulletin* **59** 60-68.

Fossing H (1995) S-35-radiolabeling to probe biogeochemical cycling of sulfur. *American Chemical Society Symposium Series* **612** 348–364.

Fritz P, Smith DGW (1970) The isotopic composition of secondary dolomites. *Geochimica et Cosmochimica Acta* **34** 1161–1173.

Fritz P, Basharmal GM, Drimmie RJ, Ibsen J, Qureshi RM (1989) Oxygen isotope exchange between sulphate and water during bacterial reduction of sulphate. *Chemical Geology* **79** 99-105.

Fry B, Cox J, Gest H, Hayes JM (1986) Discrimination between ^{34}S and ^{32}S during bacterial metabolism of inorganic sulfur compounds. *Journal of Bacteriology* **165** 328-330.

Fry B, Jannasch HW, Molyneaux SJ, Wirsen CO, Muramoto JA, King S (1991) Stable isotope studies of the carbon, nitrogen and sulfur cycles in the Black Sea and the Cariaco Trench. *Deep-Sea Research* **38** (suppl. 2) S1003-S1019.

Füchtbauer H (1988) Sedimente und Sedimentgesteine. Schweizerbart‘sche Verlagsbuchhandlung, Stuttgart, 1141p.

Garcia Domingo A, Lopez Olmedo F, Jerez Mir L, Gallego Coiduras I (1980) Mapa Geológico de España, hoja 868 Isso, Escala 1:50.000, Instituto Geológico y Minero de España.

García-Alix A, Minwer-Barakat R, Suárez EM, Freudenthal M, Martín JM (2008) Late Miocene–Early Pliocene climatic evolution of the Granada Basin (southern Spain) deduced from the paleoecology of the micromammal associations. *Paleogeography, Palaeoclimatology, Palaeoecology* **265** 214-225.

Gasiewicz A (2000) Comparative study of major element geochemistry of gypsum-ghost limestones and selenite lithofacies from the Miocene of northern Carpathian Foredeep: implications to the model of massive replacement of solid sulphates by calcium carbonates. *Chemical Geology* **164** 183-218.

Gehre M, Strauch G (2003) High-temperature elemental analysis and pyrolysis techniques for stable isotope analysis. *Rapid Communications in Mass Spectrometry* **17** 1497-1503.

Giese P, Reutter KJ, Jacobshagen V, Nicolich R (1982) Explosion seismic crustal studies in the Alpine Mediterranean region and their implications to tectonic processes. In: Berckhemer H, Hsü KJ (Eds.) Alpine Mediterranean Geodynamics. American Geophysical Union, Washington, DC, pp. 39-73.

Gill BJ, Lyons TW, Frank TD (2008) Behaviour of carbonate-associated sulfate during meteoric diagenesis and implications for the sulfur isotope paleoproxy. *Geochimica et Cosmochimica Acta* **72** 4699-4711.

Goldhaber MB, Kaplan IR (1974) The sedimentary sulphur cycle. In: Goldberg EB (Ed.) The sea. Wiley, New York, pp. 569-655.

Gray ND, Howarth R, Pickup RW, Gwyn Jones J, Head IM (1999) Substrate uptake by uncultured bacteria from the genus *Achromatium* determined by microautoradiography. *Applied and Environmental Microbiology* **65** 5100-5106.

Guido A, Jacob J, Gautret P, Laggoun-Défarge F, Mastandrea A, Russo F (2007) Molecular fossils and other organic markers as palaeoenvironmental indicators of the Messinian Calcare di Base Formation: normal versus stressed marine deposition (Rossano Basin, northern Calabria, Italy). *Palaeogeography, Palaeoclimatology, Palaeoecology* **255** 265–283.

Gunatilaka A (1989) Spheroidal dolomites - origin by hydrocarbon seepage? *Sedimentology* **36** 701-710.

Habicht KS, Canfield DE (1996) Sulphur isotope fractionation in modern microbial mats and the evolution of the sulphur cycle. *Nature* **382** 342-343

Habicht KS, Canfield DE (1997) Sulfur isotope fractionation during bacterial sulfate reduction in organic-rich sediments. *Geochimica et Cosmochimica Acta* **61** 5351–5361.

Habicht KS, Canfield DE, Rethmeier J (1998) Sulfur isotope fractionation during bacterial reduction and disproportionation of thiosulfate and sulfite. *Geochimica et Cosmochimica Acta* **62** 2585-2595.

Habicht KS, Canfield DE (2001) Isotope fractionation by sulphate-reducing natural populations and the isotopic composition of sulfide in marine sediments. *Geology* **29** 555-558.

Hardie LA (1987) Dolomitization; a critical view of some current views. *Journal of Sedimentary Petrology* **57** 166-183.

Harrison AG, Thode HG (1958) Mechanism of the bacterial reduction of sulphate from isotope fractionation studies. *Transactions of the Faraday Society* **54** 84-92.

Hartmann M, Nielsen H (1969) δ^{34}S-Werte in rezenten Meeressedimenten und ihre Deutung am Beispiel einiger Sedimentprofile aus der westlichen Ostsee. *Geologische Rundschau* **58** 621-655.

Harvey HR, McManus GB (1991) Marine ciliates as a widespread source of tetrahymanol and hopan-3-beta-ol in sediments. *Geochimica et Cosmochimia Acta* **55** 3387-3390.

Heider J, Spormann AM, Beller HR, Widdel F (1999) Anaerobic bacterial metabolism of hydrocarbons. *FEMS Microbiology Reviews* **22** 459-473.

Heindel K, Birgel D, Peckmann J, Kuhnert H, Westphal H (2010) Formation of deglacial microbialites in coral reefs off Tahiti (IODP 310). *Palaios* **25** 618–635.

Hentz TF, Henry CD (1989) Evaporite-hosted native sulfur in Trans-Pecos Texas: Relation to late-phase Basin and Range deformation. *Geology* **17** 400-403.

Hill C, Forti P (1997) Cave Minerals of the World - Second edition. National Speleological Society, Inc., Huntsville, 463p.

Hinrichs K-U, Hayes JM, Sylva SP, Brewer PG, DeLong EF (1999) Methane-consuming archaebacteria in marine sediments. *Nature* **398** 802-805.

Hinrichs K-U, Summons RE, Orphan V, Sylva SP, Hayes JM (2000) Molecular and isotopic analysis of anaerobic methane-oxidizing communities in marine sediments. *Organic Geochemistry* **31** 1685-1701.

Hoefs J (2004) Stable Isotope Geochemistry. Springer, Berlin, 244p.

Hoehler TM, Alperin MJ, Albert DB, Martens, CS (1994) Field and laboratory studies of methane oxidation in an anoxic marine sediment: Evidence for a methanogen-sulfate reducer consortium. *Global Biogeochemical cycles* **8** 451-463.

Hofmann M, Wolf-Gladrow DA, Takahashi T, Sutherland SC, Six KD, Maier-Reimer E (2000) Stable carbon isotope distribution of particulate organic matter in the ocean: a model study. *Marine Chemistry* **72** 131–150.

Holzer G, Oró J, Tornabene TG (1979) Gas chromatographic-mass spectrometric analysis of neutral lipids from methanogenic and thermoacidophilic bacteria. *Journal of Chromatography A* **186** 795-809.

Hora ZD, Hamilton WN (1992) Native sulfur resource potential of western Canada. In: Wessel GR, Wimberly BH (Eds.) Native sulfur developments in geology and exploration. Society for Mining, Metallurgy, and Exploration, Inc. Littleton, Colorado, pp. 51-57.

Hsü KJ, Cita MB, Ryan WBF (1973a) The origin of the Mediterranean evaporites. In: Ryan WBF, Hsü KJ, Dumitrica P, Lort JM, Maync W, Nesterov WD, Pautot G, Stradner H, Wezel FC (Eds.), Initial Reports of the Deep Sea Drilling Projects, Volume 13. US Government Printing Office, Washington, pp. 1203–1231.

Hsü KJ, Ryan WBF, Cita MB (1973b) Late Miocene desiccation of the Mediterranean. *Nature* **424** 240–244.

Hünger K-J, Henning O (1988) On the crystallization of gypsum from supersaturated solutions. *Crystal Research and Technology* **23** 1135-1143.

Huguen C, Foucher JP, Mascle J, Ondréas H, Thouement M, Gontharet S, Stadnitskaia A, Pierre C, Bayon G, Loncke L, Boetius A, Bouloubassi I, de Lange G and the NAUTINIL scientific party (2009) Menes caldera, a highly active site of brine seepage in the Eastern Mediterranean sea: "In situ" observations from the NAUTINIL expedition (2003). *Marine Geology* **261** 138-152.

Hunt WF (1915) The origin of the sulphur deposits of Sicily. *Economic geology* **10** 543-579.

Irwin H, Curtis C, Coleman M (1977) Isotopic evidence for source of diagenetic carbonates formed during burial of organic-rich sediments. *Nature* **269** 209-213.

Ivanov MV (1968) Microbial processes in the formation of sulfur deposits. Israel Program for Scientific Translations, Washington DC, 298 p.

Janaway TM, Parnell J (1989) Carbonate production within the Orcadian basin, northern Scotland: a petrographic and geochemical study. *Paleogeography, Palaeoclimatology, Palaeoecology* **70** 89-105.

Jassim SZ, Raiswell R, Bottrell SH (1999) Genesis of the Middle Miocene stratabound sulphur deposits of northern Iraq. *Journal of the Geological Society* **156** 25-39.

Johnston DT, Farquhar J, Wing BA, Kaufman AJ, Canfield DE, Habicht KS (2005a) Multiple sulfur isotopic fractionations in biological systems: a case study with sulfate reducers and sulfur disproportionators. *American Journal of Science* **305** 645-660.

Johnston DT, Wing BA, Farquhar J, Kaufman AJ, Strauss H, Lyons TW, Kah LC, Canfield DE (2005b) Active microbial sulfur disproportionation in the Mesoproterozoic. *Science* **310** 1477-1479.

Johnston DT, Farquhar J, Canfield DE (2007) Sulfur isotope insights into microbial sulfate reduction: When microbes meet models. *Geochimica et Cosmochimica Acta* **71** 3929-3947.

Johnston DT, Farquhar J, Habicht KS, Canfield DE (2008) Sulphur isotopes and the search for life: strategies for identifying sulphur metabolisms in the rock record and beyond. *Geobiology* **6** 425–435.

Jolivet L, Augier R, Robin C, Suc J-P, Rouchy JM (2006) Lithospheric-scale geodynamic context of the Messinian salinity crisis. *Sedimentary Geology* **188–189** 9–33.

Jones GE, Starkey RL (1957) Fractionation of stable isotopes of sulfur by microorganisms and their role in deposition of native sulfur. *Applied Microbiology* **5** 111-118.

Jørgensen BB (1982) Mineralization of organic matter in the sea bed – the role of sulphate reduction. *Nature* **296** 643-645.

Jørgensen BB (1990) A thiosulfate shunt in the sulfur cycle of marine sediments. *Science* **249** 152-154.

Joye SB, Samarkin VA, Bowles MW, Carini SA, Crespo-Medina M, Madigan MT (2009a) Patterns and controls on anaerobic oxidation of methane in extreme environments of varying salinity. *Geochimica et Cosmochimica Acta* **73** A 608.

Joye SB, Samarkin VA, Orcutt BN, MacDonald IR, Hinrichs K-U, Elvert M, Teske AP, Lloyd KG, Lever MA, Montoya JP, Meile CD (2009) Metabolic variability in seafloor brines revealed by carbon and sulphur dynamics. *Nature Geoscience* **2** 349-354.

Kahle CF (1965) Possible roles of clay minerals in the formation of dolomite. Journal of *Sedimentary Petrology* **35** 448-453.

Kaplan IR, Rittenberg SC (1964) Microbiological fractionation of sulphur isotopes. *Journal of General Microbiology* **34** 195-212.

Kasten S, Jørgensen BB (2000) Sulfate reduction in marine sediments. In: Schulz HD, Zabel M (Eds.) Marine Geochemistry. Springer, Heidelberg, pp. 263-281.

Kates M (1993) Membrane lipids of extreme halophiles: biosynthesis, function and evolutionary significance. *Experientia* **49** 1027-1036.

Kemp ALW, Thode HG (1968) The mechanism of the bacterial reduction of sulphate and of sulphite from isotope fractionation studies. *Geochimica et Cosmochimica Acta* **32** 71-91.

Kemp P, Lander DJ, Orpin CG (1984) The Lipids of the rumen fungus *Piromonas communis*. *Journal of General Microbiology* **130** 27-37.

Khalaf FI (1990) Occurrence of phreatic dolocrete within Tertiary clastic deposits of Kuwait, Arabian Gulf. *Sedimentary Geology* **68** 223-239.

Kirkland DW, Evans R (1976) Origin of limestone buttes, Gypsum Plain, Culberson County, Texas. *American Association of Petroleum Geologists Bulletin* **60**, 2005-2018.

Kleemann G, Poralla K, Englert G, Kjosen H, Liaaen-Jensen S, Neunlist S, Rohmer M (1990) Tetrahymanol from the phototrophic bacterium *Rhodopseudomonas palustris*: first report of a gammacerane triterpene from a prokaryote. *Journal of General Microbiology* **136** 2551-2553.

Klemmick GF (1992) Geology and mineralization of the Pokorny sulfur deposit, Culberson County, Texas. In: Wessel GR, Wimberly BH (Eds.) Native Sulfur – Developments in Geology and Exploration. Society for Mining, Metallurgy and Exploration, Inc., Littleton, Colorado, pp. 109-123.

Knittel K, Boetius A, Lemke A, Eilers H, Lochte K, Pfannkuche O, Linke P, Amann R (2003) Activity, distribution, and diversity of sulfate reducers and other bacteria in sediments above gas hydrate (Cascadia Margin, Oregon). *Geomicrobiology Journal* **20** 269-294.

Knorre Hv, Krumbein WE (2000) Bacterial calcification. In: Riding RE, Awramik SM (Eds.) Microbial Sediments. Springer, Berlin, Heidelberg, pp. 25–31.

Koga Y, Nishihara M, Morii H, Akagawa-Matsushita M (1993) Ether polar lipids of methanogenic bacteria: structures, comparative aspects, and biosyntheses. *Microbiological Reviews* **57** 164-182.

Koga Y, Morii H, Akagawa-Matsuchita M, Ohga M (1998) Correlation of polar lipid composition with 16S rRNA phylogeny in methanogens. Further analysis of lipid component parts. *Bioscience Biotechnology Biochemistry* **62** 230-236.

Könneke M, Widdel F (2003) Effect of growth temperature on cellular fatty acids in sulphate-reducing bacteria. *Environmental Microbiology* **5** 1064-1070.

Krijgsman W, Hilgen FJ, Meijer PT (2007) Chronological constraints and consequences for the Messinian Salinity Crisis. In: Briand F (Ed.) CIESM, 2007. The Messinian Salinity Crisis from mega-deposits to microbiology — A consensus report. CIESM Workshop Monographs 33, Monaco, pp. 39-44.

Krijgsman W, Hilgen FJ, Raffi I, Sierro FJ, Wilson DS (1999) Chronology, causes and progression of the Messinian salinity crisis. *Nature* **400** 652-655.

Krijgsman W, Garcés M, Agusti J, Raffi I, Taberner C, Zachariasse WJ (2000) The 'Tortonian salinity crisis' of the eastern Betics (Spain). *Earth and Planetary Science Letters* **181** 497-511.

Kroopnick P, Weiss RF, Craig H (1972) Total CO_2, ^{13}C, and dissolved oxygen-^{18}O at GEOSECS II in the North Atlantic. *Earth and Planetary Science Letters* **16** 103-110.

Ku TCW, Walter LM, Coleman ML, Blake RE, Martini AM (1999) Coupling between sulfur recycling and syndepositional carbonate dissolution: evidence from oxygen and sulfur isotope composition of pore water sulfate, South Florida platform, U.S.A. *Geochimica et Cosmochimica Acta* **63** 2529-2546.

Lalou C (1957) Studies on bacterial precipitation of carbonates in sea water. *Journal of Sedimentary Petrology* **27** 190-195.

Land LS (1998) Failure to precipitate dolomite at 25°C from dilute solution despite 1000-fold oversaturation after 32 years. *Aquatic Geochemistry* **4** 361-368.

Lee C, McKenzie JA, Sturm M (1987) Carbon isotope fractionation and changes in flux and composition of particulate matter resulting from biological activity during a sediment trap experiment in lake Greifen, Switzerland. *Limnology and Oceanography* **32** 83-96.

Lein AY, Samarkin VA, Zyakun AM, Matrosov AG, Kudryavtseva AI, Ivanov MV (1975) On the genesis of native sulfur in the Kerch Peninsula. *Geochemistry International* **12** 15-25.

Lloyd RM (1967) Oxygen-18 composition of oceanic sulfate. *Science* **156** 1228–1231.

Lloyd RM (1968) Oxygen isotope behavior in the sulfate–water system. *Journal of Geophysical Research* **73** 6099–6110.

Londry KL, Jahnke LL, Marais DJD (2004) Stable carbon isotope ratios of lipid biomarkers of sulfate-reducing bacteria. *Applied and Environmental Microbiology* **70** 745-751.

Lumsden DN (1979) Discrepancy between thin-section and X-ray estimates of dolomite in limestones. *Journal of Sedimentary Petrology* **49** 429-436.

Lyons TW, Walter L, Gellatly AM, Martini AM, Blake R (2004) Site of anomalous organic remineralization in the carbonate sediments of South Florida, USA: The sulfur cycle and carbonate-associated sulfate. In: Amend JP, Edwards KJ, Lyons TW (Eds.) Sulfur Biogeochemistry – Past and Present. The Geological Society of America Special Paper 379, pp. 161-176.

Machel HG (1992) Low-temperature and high-temperature origins of elemental sulfur in diagenetic environments. In: Wessel GR, Wimberly BH (Eds.) Native Sulfur – Developments in Geology and Exploration. Society for Mining, Metallurgy and Exploration, Inc., Littleton, Colorado, pp. 3-22.

Machel HG, Krouse HR, Sassen R (1995) Products and distinguishing criteria of bacterial and thermochemical sulfate reduction. *Applied Geochemistry* **10** 373-389

Machel HG (2001) Bacterial and thermochemical sulfate reduction in diagenetic settings – old and new insights. *Sedimentary Geology* **140** 143-175.

Madigan MT, Martinko JM (2009) Brock Mikrobiologie. Pearson Studium, München, 1203 p.

Manzi V, Lugli S, Roveri M, Schreiber BC (2009) A new facies model for the Upper Gypsum of Sicily (Italy): chronological and palaeoenvironmental constraints for the Messinian salinity crisis in the Mediterranean. *Sedimentology* **56** 1937–1960.

Manzi V, Lugli S, Roveri M, Schreiber BC, Gennari R (2010) The Messinian "Calcare di Base" (Sicily, Italy) revisited. Geological Society of America Bulletin, doi:10.1130/B30262.1.

McKenzie J (1981) Holocene dolomitization of calcium carbonate sediments from the coastal sabkhas of Abu Dhabi, U.A.E.: a stable isotope study. *Journal of Geology* **89** 185-198.

McKenzie JA (1985a) Stable-isotope mapping in Messinian evaporative carbonates of central Sicily. *Geology* **13** 851–854.

McKenzie J (1985b) Carbon Isotopes and Productivity in the Lacustrine and Marine Environment. In: Stumm W (Ed.) Chemical Processes in Lakes. Environmental science and technology. Wiley, New York, pp. 99-118.

Michaelis W, Seifert R, Nauhaus K, Treude T, Thiel V, Blumenberg M, Knittel K, Gieseke A, Peterknecht K, Pape T, Boetius A, Amann R, Jørgensen BB, Widdel F, Peckmann J, Pimenov NV, Maksim GB (2002) Microbial reefs in the Black Sea fueled by anaerobic oxidation of methane. *Science* **297** 1013-1015.

Mizutani Y, Rafter TA (1973) Isotopic behaviour of sulphate oxygen in the bacterial reduction of sulphate. *Geochemical Journal* **6** 183–191.

Nakai N, Jensen ML (1964) The kinetic isotope effect in the bacterial reduction and oxidation of sulfur. *Geochimica et Cosmochimica Acta* **28** 1893-1912.

Navarro Hervás F, Rodríguez Estrella T (1985) Caracteristicas morfoestructurales de los diapiros Triasicos de Hellín, Ontur, La Celia, Jumilla, La Rosa y Pinoso, en las provincias de Albacete, Murcia y Alicante. *Papeles de Geografica (Fisica)* **10** 49-69.

Nesse WD (2004) Introduction to Optical Mineralogy. Oxford University Press, New York, 348 p.

Newton RJ, Pevitt EL, Wignall PB, Bottrell SH (2004) Large shifts in the isotopic composition of seawater sulphate across the Permo–Triassic boundary in northern Italy. *Earth and Planetary Science Letters* **218** 331–345.

Niec M (1992) Native sulfur deposits in Poland. In: Wessel GR, Wimberly BH (Eds.) Native sulfur developments in geology and exploration. Society for Mining, Metallurgy, and Exploration, Inc. Littleton, Colorado, pp. 23-50.

Niederberger TD, Perreault NN, Tille S, Lollar BS, Lacrampe-Couloume G, Andersen D, Greer CW, Pollard W, Whyte LG (2010) Microbial characterization of a subzero, hypersaline methane seep in the Canadian High Arctic. *International Society for Microbial Ecology Journal* **4** 1326-1339.

Niemann H, Elvert M (2008) Diagnostic lipid biomarkers and stable carbon isotope signatures of microbial communities mediating the anaerobic oxidation of methane with sulphate. *Organic Geochemistry* **39** 1668-1677.

Nissenbaum A, Kaplan IR (1966) Origin of the Beeri (Israel) sulfur deposit. *Chemical Geology* **1** 295-316.

Nissenbaum A (1980) Sulfur occurrences in Israel and Northern Sinai. *Israel Journal of Earth-Sciences* **29** 85-91.

Oba M, Sakata S, Tsunogai U (2006) Polar and neutral isopranyl glycerol ether lipids as biomarkers of archaea in near-surface sediments from the Nankai Trough. *Organic Geochemistry* **37** 1643-1654.

Ohmoto, H., Rye, R.O., 1979. Isotopes of sulfur and carbon. In: Barnes, H.L. (Ed.), Geochemistry of Hydrothermal Deposits. John Wiley & Sons, pp. 509–567.

Oliveri E, Neri R, Bellanca A, Riding R (2010) Carbonate stromatolites from a Messinian hypersaline setting in the Caltanissetta Basin, Sicily: petrographic evidence of microbial activity and related stable isotope and rare earth element signatures. *Sedimentology* **57** 142–161.

Omoregie EO, Niemann H, Mastalerz V, de Lange GJ, Stadnitskaia A, Mascle J, Foucher J-P, Boetius A (2009) Microbial methane oxidation and sulphate reduction at cold seeps of the Eastern Mediterranean Sea. *Marine Geology* **261** 114-127.

Ono S (2008) Multiple-sulphur isotope biosignatures. *Space Science Reviews* **135** 203-220.

Orphan VJ, Hinrichs K-U, Ussler III W, Paull CK, Taylor LT, Sylva SP, Hayes JM, DeLong EF (2001a) Comparative analysis of methane-oxidizing archaea and sulphate-reducing bacteria in anoxic marine sediments. *Applied and Environmental Microbiology* **67** 1922-1934.

Orphan VJ, House CH, Hinrichs K-U, McKeegan KD, DeLong EF (2001b) Methane-consuming archaea revealed by directly coupled isotopic and phylogenetic analysis. *Science* **293** 484-487.

Orphan VJ, House CH, Hinrichs K-U, McKeegan KD, DeLong EF (2002) Multiple archaeal groups mediate methane oxidation in anoxic cold seep sediments. *Proceedings of the National Academy of Sciences of the United States of America* **99** 7663-7668.

Orphan VJ, Ussler WIII, Naehr TH, House CH, Hinrichs K-U, Paull CK (2004) Geological, geochemical, and microbiological heterogeneity of the seafloor around methane vents in the Eel River Basin, offshore California. *Chemical Geology* **205** 265– 289.

Ortí F, Rosell L, Anadón P (2003) Deep to shallow lacustrine evaporites in the Libros Gypsum (southern Teruel Basin, Miocene, NE Spain): an occurrence of pelletal gypsum rhythmites. *Sedimentology* **50** 361-386.

Ortí F, Rosell L, Anadón P (2010) Diagenetic gypsum related to sulfur deposits in evaporites (Libros Gypsum, Miocene, NE Spain). *Sedimentary Geology* **228** 304-318

Pancost RD, Sinninghe Damsté JS, de Lint S, van der Maarel MJEC, Gottschal JC and the MEDINAUT shipboard scientific party (2000) Biomarker evidence for widespread anaerobic methane oxidation in Mediterranean sediments by a consortium of methanogenic archaea and bacteria. *Applied and Environmental Microbiology* **66** 1126-1132.

Pancost RD, Bouloubassi I, Aloisi G, Sinninghe Damsté JS and the Medinaut Shipboard Scientific Party, 2001a. Three series of non-isoprenoidal dialkyl glycerol diethers in cold-seep carbonate crusts. *Organic Geochemistry* **32** 695-707.

Pancost RD, Hopmans EC, Sinninghe Damsté JS and the MEDINAUT shipboard scientific party (2001b) Archaeal lipids in Mediterranean cold seeps: Molecular proxies for anaerobic methane oxidation. *Geochimica et Cosmochimica Acta* **65** 1611-1627.

Pancost RD, Pressley S, Coleman JM, Talbot HM, Kelly SP, Farrimond P, Schouten S, Benning L, Mountain BW (2006) Composition and implications of diverse lipids in New Zealand Geothermal sinters. *Geobiology* **4** 71-92.

Pape T, Blumenberg M, Seifert R, Egorov VN, Gulin SB, Michaelis W (2005) Lipid geochemistry of methane-seep-related Black Sea carbonates. *Palaeogeography, Palaeoclimatology, Palaeoecology* **227** 31-47.

Pawlowski S, Pawlowska K, Kubica B (1979) Geology and genesis of Polish sulfur deposits. *Economic Geology* **74** 475–483.

Peckmann J, Paul J, Thiel V (1999a) Bacterially mediated formation of diagenetic aragonite and native sulphur in Zechstein carbonates (Upper Permian, Central Germany). *Sedimentary Geology* **126** 205-222.

Peckmann J, Thiel V, Michaelis W, Clari P, Gaillard C, Martire L, Reitner J (1999b) Cold seep deposits of Beauvoisin (Oxfordian; southeastern France) and Marmorito (Miocene, northern Italy): microbially induced authigenic carbonates. *International Journal of Earth Sciences* **88** 60-75.

Peckmann J, Goedert JL, Heinrichs T, Hoefs J, Reitner J (2003) The Late Eocene 'Whiskey Creek' methane-seep deposit (western Washington State) – Part II: Petrology, stable isotopes, and biogeochemistry. *Facies* **48** 241-254.

Peckmann J, Thiel V (2004) Carbon cycling at ancient methane-seeps. *Chemical Geology* **205** 443-467.

Peckmann J, Birgel D, Kiel S (2009) Molecular fossils reveal fluid composition and flow intensity at a Cretaceous seep. *Geology* **37** 847-850.

Pierre C (1985) Isotopic evidence for the dynamic redox cycle of dissolved sulphur compounds between free and interstitial solutions in marine salt pans. *Chemical Geology* **53** 191–196.

Pierre C, Rouchy JM (1988) Carbonate replacements after sulfate evaporites in the middle Miocene of Egypt. *Journal of Sedimentary petrology* **58** 446-456.

Pingitore NE, Meitzner G, Love KM (1995) Identification of sulfate in natural carbonates by X-ray absorption spectroscopy. *Geochimica et Cosmochimica Acta* **59** 2477-2483.

Pirlet H, Wehrmann LM, Brunner B, Frank N, Dewanckele J, van Rooij D, Foubert A, Swennen R, Naudts L, Boone M, Cnudde V, Henriet J-P (2010) Diagenetic formation of gypsum and dolomite in a cold-water coral mound in the Porcupine Seabight, off Ireland. *Sedimentology* **57** 786-805.

Playà E, Ortí F, Rosell L (2000) Marine to non-marine sedimentation in the upper Miocene evaporites of the Eastern Betics, SE Spain: sedimentological and geochemical evidence. *Sedimentary Geology* **133** 135-166.

Rabus R (2005) Biodegradation of hydrocarbons under anoxic conditions. In: Olliver B, Magot M (Eds.) Petroleum Microbiology. ASM Press, Washington, D.C. pp. 277-299.

Rashby SE, Sessions AL, Summons RE, Newman DK (2007) Biosynthesis of 2-methylbacteriohopanepolyols by an anoxygenic phototroph. *Proceedings of the National Academy of Sciences of the United States of America* **104** 15099-15104.

Riccioni RM, Brock PWG, Schreiber BC (1996) Evidence for early aragonite in paleo-lacustrine sediments. *Journal of Sedimentary Research* **66** 1003-1010.

Roberts HH, Aharon P (1994) Hydrocarbon-derived carbonate buildups of the northern Gulf of Mexico continental slope: A review of submersible investigations. *Geo-Marine Letters* **14** 135-148.

Rouchy JM, Taberner C, Blanc-Valleron M-M, Sprovieri R, Russell M, Pierre C, Di Stefano E, Pueyo JJ, Caruso A, Dinarès-Turell J, Gomis-Coll E, Wolff GA, Cespuglio G, Ditchfield P, Pestrea S, Combourieu-Nebout N, Santisteban C, Grimalt JO (1998) Sedimentary and diagenetic markers of the restriction in a marine basin: The Lorca basin (SE Spain) during the Messinian. *Sedimentary Geology* **121** 23-55.

Rouchy JM, Caruso A (2006) The Messinian salinity crisis in the Mediterranean Basin: a reassessment of the data and an integrated scenario. *Sedimentary Geology* **188–189** 35–67.

Roveri M, Lugli S, Manzi V, Gennari R, Iaccarino SM, Grossi F, Taviani M (2006) Field-trip itinerary. In: Roveri M, Lugli S, Manzi V, Gennari R, Iaccarino SM, Grossi F, Taviani M (Eds.) The record of Messinian events in the northern Apennines foredeep basins, R.C.M.N.S. Interim colloquium

'The Messinian salinity crisis revisited-II', Pre-congress field-trip. *Acta naturalia de "L'Ateneo Parmense"* **42**, Parma, pp. 38-65.

Roveri M, Lugli S, Manzi V, Schreiber C (2008a). The Messinian Sicilian stratigraphy revisited: new insights for the Messinian salinity crisis. *Terra Nova* **20** 483–488.

Roveri M, Bertini A, Cosentino D, Di Stefano A, Gennari R, Gliozzi E, Grossi F, Iaccarino SM, Lugli S, Manzi V, Taviani M (2008b) A high-resolution stratigraphic framework for the latest Messinian events in the Mediterranean area. *Stratigraphy* **5** 323–342.

Ruckmick JC, Wimberly BH, Edwards AF (1979) Classification and genesis of biogenic sulfur deposits. *Economic Geology* **74** 469-474.

Rueter P, Rabus R, Wilkes H, Aeckersberg F, Rainey FA, Jannasch HW, Widdel F (1994) Anaerobic oxidation of hydrocarbons in crude oil by new types of sulphate-reducing bacteria. *Nature* **372** 455-458.

Rütters H, Sass H, Cypionka H, Rullkötter J (2001) Monoalkylether phospholipids in the sulfate-reducing bacteria *Desulfosarcina variabilis* and *Desulforhabdus amnigenus*. *Archives of Microbiology* **176** 435-442.

Rütters H, Sass H, Cypionka H, Rullkötter J (2002) Phospholipid analysis as a tool to study complex microbial communities in marine sediments. *Journal of Microbiological Methods* **48** 149-160.

Sackett WM, Eckelmann WR, Bender ML, Bé AWH (1965) Temperature dependence of carbon isotope composition in marine plankton and sediments. *Science* **148** 235-237.

Sagemann J, Bale SJ, Briggs DE, Parkes RJ (1999) Controls on the formation of authigenic minerals in association with decaying organic matter: an experimental approach. *Geochimica et Cosmochimica Acta* **63** 1083–1095.

Salisbury BK (1992) Geophysical and geochemical surveys in Delaware basin sulfur exploration. In: Wessel GR, Wimberly BH (Eds.) Native sulfur developments in geology and exploration. Society for Mining, Metallurgy, and Exploration, Inc. Littleton, Colorado, pp. 81-90.

Samuelson SF (1992) Anatomy of an elephant. In: Wessel GR, Wimberly BH (Eds.) Native sulfur developments in geology and exploration. Society for Mining, Metallurgy, and Exploration, Inc. Littleton, Colorado, pp. 59-71.

Sánchez-Román M, McKenzie JA, de Luca Rebello Wagener A, Rivadeneyra MA, Vasconcelos C (2009) Presence of sulfate does not inhibit low-temperature dolomite formation. *Earth and Planetary Science Letters* **285** 131-139.

Sanz de Galdeano C (1990) Geologic evolution of the Betic Cordilleras in the Western Mediterranean, Miocene to the present. *Tectonophysics* **172** 107-119.

Sanz-Montero ME, Rodríguez-Aranda JP, García del Cura MA (2009) Bioinduced precipitation of barite and celestite in dolomite microbialites. Examples from Miocene lakustrine sequences in the Madrid and Duero Basins, Spain. *Sedimentary Geology* **222** 138-148.

Schneider A, Nielsen H (1965) Zur Genese des elementaren Schwefels im Gips von Weenzen (Hils). *Beiträge zur Mineralogie und Petrographie* **11** 705–718.

Schnellmann GA (1959) Formation of sulfur by reduction of anhydrite at Ras Gemsa, Egypt. *Economic Geology* **54** 889–894.

Schulz HN, Jørgensen BB (2001) Big bacteria. *Annual Review of Microbiology* **55** 105-137.

Schulz HN (2002) *Thiomargarita namibiensis*: Giant microbe holding its breath. *ASM News* **68** 122-127.

Schulz HN, Schulz HD (2005) Large sulfur bacteria and the formation of phosphorite. *Science* **307** 416-418.

Servant-Vildary S, Rouchy JM, Pierre C, Foucault A (1990) Marine and continental water contributions to a hypersaline basin using diatom ecology, sedimentology and stable isotopes: an example in the Late Miocene of the Mediterranean (Hellin Basin, southern Spain). *Palaeogeography, Palaeoclimatology, Palaeoecology* **79** 189-204.

Sharma T, Clayton RN (1965) Measurement of O18/O16 ratios of total oxygen of carbonates. *Geochimica et Cosmochimica Acta* **29** 1347-1353.

Shen Y, Buick R (2004) The antiquity of microbial sulfate reduction. *Earth-Science-Reviews* **64** 243-272.

Shen Y, Buick R, Canfield DE (2001) Isotopic evidence for microbial sulphate reduction in the early Archaean era. *Nature* **410** 77-81.

Slaughter M, Hill RJ (1991) The influence of organic matter in organogenic dolomitization. *Journal of Sedimentary Petrology* **61** 296-303.

Smith BN, Epstein S (1971) Two categories of $^{13}C/^{12}C$ ratios for higher plants. *Plant Physiology* **47** 380-384.

Soetaerd K, Hofmann AF, Middleburg JJ, Meysman FJR, Greenwood J (2007) The effect of biogeochemical processes on pH. *Marine Chemistry* **105** 30-51.

Sprott GD, Ekiel I, Dicaire D (1990) Novel, acid-labile, hydroxydiether lipid cores in methanogenic bacteria. *Journal of Biological Chemistry* **265** 13735-13740.

Sprott GD (1992) Structures of archaebacterial membrane-lipids. *Journal of Bioenergetics and Biomembranes* **24** 555-566.

Sprott GD, Dicaire CJ, Choquet CG, Patel GB, Ekiel I (1993) Hydroxydiether lipid structures in *Methanosarcina* spp. and *Methanococcus voltae*. *Applied and Environmental Microbiology* **59** 912-914.

Stabel HH (1986) Calcite precipitation in Lake Constance: Chemical equilibrium, sedimentation, and nucleation by algae. *Limnology and Oceanography* **31** 1081-1094.

Stadnitskaia A, Muyzer G, Abbas B, Coolen MJL, Hopmans EC, Baas M, van Weering TCE, Ivanov MK, Poludetkina E, Sinninghe Damsté JS (2005) Biomarker and 16S rDNA evidence for anaerobic oxidation of methane and related carbonate precipitation in deep-sea mud volcanoes of the Sorokin Through, Black Sea. *Marine Geology* **217** 67-96.

Stenni B, Longinelli A (1990) Stable isotope study of water, gypsum and carbonate samples from the Bannock and Tyro Basins, eastern Mediterranean. *Marine Chemistry* **31** 123–135.

Strickland-Constable RF (1968) Kinetics and mechanism of crystallization from the fluid phase and of the condensation and evaporation of liquids. Academic Press, London, New York, 347 p.

Suc J-P, Violanti D, Londeix L, Poumot C, Robert C, Clauzon G, Gautier F, Turon J-L, Ferrier J, Chikhi H, Cambon G (1995) Evolution of the Messinian Mediterranean environments: the Tripoli Formation at Capodarso (Sicily, Italy). *Review of Palaeobotany and Palynology* **87** 51–79.

Taberner C, Marshall JD, Hendry JP, Pierre C, Thirlwall MF (2002) Celestite formation, bacterial sulphate reduction and carbonate cementation of Eocene reefs and basinal sediments (Igualada, NE Spain). *Sedimentology* **49** 171–190.

Talbot MR (1990) A review of the palaeohydrological interpretation of carbon and oxygen isotopic ratios in primary lacustrine carbonates. *Chemical Geology* **80** 261-279.

Talbot MR, Kelts K (1990) Paleolimnological signatures from carbon and oxygen isotopic ratios in carbonates from organic carbon-rich lacustrine sediments. In: Katz BJ (Ed.) Lacustrine basin

exploration - case studies and modern analogs. American Association of Petroleum Geologists Memoir, Tulsa, pp. 99–112.

Taylor J, Parkes RJ (1983) The cellular fatty acids of the sulphate-reducing bacteria, *Desulfobacter* sp., *Desulfolobus* sp. and *Desulfovibrio desulfuricans*. *Journal of General Microbiology* **129** 3303-3309.

Taylor BE, Wheeler MC (1984) Stable isotope geochemistry of acid mine drainage: Experimental oxidation of pyrite. *Geochimica et Cosmochimica Acta* **48** 2669-2678.

Taylor J, Parkes RJ (1985) Identifying different populations of sulphate-reducing bacteria within marine sediment systems, using fatty acid biomarkers. *Journal of General Microbiology* **131** 631-642.

Teixidor P, Grimalt JO, Pueyo JO, Rodriguez-Valera F (1993) Isopranylglycerol diethers in non-alkaline evaporitic environments. *Geochimica et Cosmochimica Acta* **57** 4479-4489.

Tekin E, Varol B, Frieman GM, Dogan AU (1999) Elemental sulfur formation related to celestine reduction: An example of biomineralization of bacterial origin. *Carbonates & Evaporites* **14** 32-40.

Tekin E (2006) Elemental sulfur of bacterial origin in the lacustrine evaporites of the Polatli-Sivrihisar Neogene basin (Central Anatolia, Turkey). *Carbonates and Evaporites* **21** 33-39.

ten Haven HL, de Leeuw JW, Sinninghe Damsté JS, Schenck PA, Palmer SE, Zumberge JE (1988) Application of biological markers in the recognition of palaeo-hypersaline environments. In: Fleet AJ, Talbot MR (Eds.) Lacustrine petroleum source rocks. *Geological Society Special Publication* **40**, pp. 123-130.

ten Haven HL, Rohmer M, Rullkötter J, Bisseret P (1989) Tetrahymanol, the most likely precursor of gammacerane, occurs ubiquitiously in marine sediments. *Geochimica et Cosmochimica Acta* **53** 3073-3079.

Tenzer G, Meyers PA, Knoop P (1997) Sources and distribution of organic and carbonate carbon in surface sediments of Pyramid Lake, Nevada. *Journal of Sedimentary Research* **67** 884-890.

Thiel V, Peckmann J, Seifert R, Wehrung P, Reitner J, Michaelis W (1999) Highly isotopically depleted isoprenoids: Molecular markers for ancient methane venting. *Geochimica et Cosmochimica Acta* **63** 3959-3966.

Thiel V, Peckmann J, Richnow HH, Luth U, Reitner J, Michaelis W (2001) Molecular signals for anaerobic methane oxidation in Black Sea seep carbonates and a microbial mat. *Marine Chemistry* **73** 97-112.

Thiel V, Blumenberg M, Pape T, Seifert R, Michaelis W (2003) Unexpected occurrence of hopanoids at gas seeps in the Black Sea. *Organic Geochemistry* **34** 81-87.

Thode HG, Wanless RK, Wallouch R (1954) The origin of native sulphur deposits from isotope fractionation studies. *Geochimica et Cosmochimica Acta* **5** 286-298.

Thode HG, Monster J (1973) (reprint of 1965) Sulfur-isotope geochemistry of petroleum, evaporites, and ancient seas. In: Kirkland DW, Evans R (Eds.) Marine evaporites: origin, diagenesis and geochemistry. Benchmark Papers in Geology. Dowden, Hutchinson and Ross, Inc., Stroudsburg, Pennsylvania, pp. 363-373.

Tornabene TG, Langworthy TA (1979) Diphytanyl and dibiphytanyl glycerol ether lipids of methanogenic archaebacteria. *Science* **203** 51-53.

Utrilla R, Pierre C, Ortí F, Pueyo JJ (1992) Oxygen and sulphur isotope compositions as indicators of the origin of Mesozoic and Cenozoic evaporites from Spain. *Chemical Geology* **102** 229-244.

van Dam JA, Weltje GJ (1999) Reconstruction of the Late Miocene climate of Spain using rodent palaeocommunity successions: an application of end-member modelling. *Paleogeography, Palaeoclimatology, Palaeoecology* **151** 267-305.

van Lith Y, Warthmann R, Vasconcelos C, McKenzie J (2003) Sulphate reducing bacteria induce low-temperature Ca-dolomite and high Mg-calcite formation. *Geobiology* **1** 71-79.

van Stempvoort DR, Krouse HR, 1994. Controls of $\delta^{18}O$ in sulfate: review of experimental data and application to specific environments. American Chemical Society Symposium Series 550, 466–480.

Vasconcelos C, McKenzie J, Bernasconi SM, Crujic D, Tien AJ (1995) Microbial mediation as possible mechanism for natural dolomite formation at low temperatures. *Nature* **377** 220-222.

Vasconcelos C, McKenzie JA (1997) Microbial mediation of modern dolomite precipitation and diagenesis under anoxic conditions (Lagoa Vermelha, Rio de Janeiro, Brazil). *Journal of Sedimentary Research* **67** 378-390.

Vasconcelos C, McKenzie JA, Warthmann R, Bernasconi SM (2005) Calibration of the $\delta^{18}O$ paleothermometer for dolomite precipitated in microbial cultures and natural environments. *Geology* **33** 317-320.

Vidal Romani JR, Rodriguez MV (2007) Types of granite cavities and associated speleothems: genesis and evolution. *Nature Conservation* **63** 41-46.

Wagner M, Roger AJ, Flax JL, Brusseau GA, Stahl DA (1998) Phylogeny of dissimilatory sulfite reductases supports an early origin of sulfate respiration. *Journal of Bacteriology* **180** 2975-2982.

Wallace CSA, Crawford JE (1992) Geology of Culberson ore body. In: Wessel GR, Wimberly BH (Eds.) Native sulfur developments in geology and exploration. Society for Mining, Metallurgy, and Exploration, Inc. Littleton, Colorado, pp. 91-105.

Walter LM, Bischof SA, Patterson WP, Lyons TW (1993) Dissolution and recrystallization in modern shelf carbonates: evidence from pore water and solid phase chemistry. *Philosophical Transactions of the Royal Society of London Series A–Mathematical Physical and Engineering Sciences* **344** 27-36.

Wankel SD, Joye SB, Samarkin VA, Shah SR, Friederich G, Melas-Kyriazi J, Girguis PR (2010) New constraints on methane fluxes and rates of anaerobic methane oxidation in a Gulf of Mexico brine pool via *in situ* mass spectrometry. *Deep-Sea Research II* **57** 2022-2029.

Waples DW, Haug P, Welte DH (1974) Occurrence of a regular C_{25} isoprenoid hydrocarbon in Tertiary sediments representing a lagoonal-type, saline environment. *Geochimica et Cosmochimica Acta* **38** 381-387.

Warren J (2000) Dolomite: occurrence, evolution and economically important associations. *Earth-Science Reviews* **52** 1-81.

Weaver CE, Beck KC (1971) Clay water diagenesis during burial: how mud becomes gneiss. Geological Society of America, Special Paper 134. Geological Society of America, Boulder, 96p.

Werne JP, Baas M, Sinninghe Damsté JS (2002) Molecular isotopic tracing of carbon flow and trophic relationships in a methane-supported benthic microbial community. *Limnology and Oceanography* **47** 1694-1701.

Wessel GR (1994) Sulfur resources. In: Carr DD (Ed.) Industrial Minerals and Rocks. Society for Mining, Metallurgy, and Exploration, Inc, Littleton, Colorado, pp. 1011–1048.

Whiticar MJ (1999) Carbon and hydrogen isotope systematics of bacterial formation and oxidation of methane. *Chemical Geology* **161** 291–314.

Worden RH, Smalley PC, Oxtoby NH (1995) Gas souring by thermochemical sulfate reduction at 140°C. *American Association of Petroleum Geologists Bulletin* **79** 854-863.

Worden RH, Smalley PC, Fallick AE (1997) Sulfur cycle in buried evaporites. *Geology* **25** 643-646.

Wortmann UG, Bernasconi SM, Böttcher ME (2001) Hypersulfidic deep biosphere indicates extreme sulfur isotope fractionation during single-step microbial sulfate reduction. *Geology* **29** 647-650.

Wright DT (1999) The role of sulphate-reducing bacteria and cyanobacteria in dolomite formation in distal ephemeral lakes of the Coorong region, South Australia. *Sedimentary Geology* **126** 147-157.

Wright DT, Oren A (2005) Nonphotosynthetic bacteria and the formation of carbonates and evaporites through time. *Geomicrobiology Journal* **22** 27–53.

Wright DT, Wacey D (2005) Precipitation of dolomite using sulphate-reducing bacteria from the Coorong Region, South Australia: significance and implications. *Sedimentology* **52** 987-1008.

Youssef ESAA (1989) Geology and genesis of sulfur deposits at Ras Gemsa area, Red Sea coast, Egypt. *Geology* **17** 797-801.

Zander JM, Caspi E, Pandey GN, Mitra CR (1969) The presence of tetrahymanol in *Oleandra wallichii*. *Phytochemistry* **8** 2265-2267.

Zerkle AL, Farquhar J, Johnston DT, Cox RP, Canfield DE (2009) Fractionation of multiple sulfur isotopes during phototrophic oxidation of sulfide and elemental sulfur by a green sulfur bacterium. *Geochimica et Cosmochimica Acta* **73** 291-306.

Zheng Y-F (1999) Oxygen isotope fractionation in carbonate and sulfate minerals. *Geochemical Journal* **33** 109-126.

Ziegenbalg SB, Brunner B, Rouchy JM, Birgel D, Pierre C, Böttcher ME, Caruso A, Immenhauser A, Peckmann J (2010) Formation of secondary carbonates and native sulphur in sulphate-rich Messinian strata, Sicily. *Sedimentary Geology* **227** 37-50.

* „Die Sieben Gaben“, Text und Musik: Gerhard Schöne, veröffentlicht auf der CD „Die Sieben Gaben. Lieder im Märchenmantel.”, Buschfunk 1992.

9 - DANKSAGUNG

Mein allerherzlichster Dank geht an Jörn, zunächst mal dafür, dass er mich in seinen Vorlesungen und der Exkursion in den Harz auf den Geschmack gebracht hat, und dann natürlich dafür, dass er mir dieses Thema anvertraut, mich betreut und gefördert und zuletzt mit nach Wien genommen hat.

Außerdem möchte ich Daniel ganz herzlich danken, ohne den weder die Laborarbeit noch die Auswertung der Daten möglich gewesen wäre, ohne den mir der Sinn vieler Zacken im Chromatogramm für immer verborgen geblieben wäre und besonders auch für seinen Enthusiasmus und seine Zeit.

Ein ganz herzlicher Dank geht auch an Tim für die Übernahme der Zweitbegutachtung.

Danke Beno, für Deine Mühen, mir die Welt der Schwefelisotope näher zu bringen und mir zu zeigen, dass sogar Schwefelisotope gut schmecken können.

Je voudrais Jean Marie, Caterine et Marie-Madeleine exprimer toute ma gratitude. Grazie mille, Antonio. Thank you very much for bringing us to the right places, introducing me to the Messinian world, providing samples, discussing our results and offering such nice stays in Paris …

Ganz herzlich möchte ich mich auch bei Adrian bedanken, für seine Unterstützung beim Beproben der “Freaks”, inklusive der Rutschpartie beim Zwiesel, die tolle Zeit in Amsterdam und seine Unterstützung und Motivation.

Ein herzlicher Dank auch an alle anderen, die an der Entstehung dieser Arbeit mitgewirkt haben, Michael, Patrick, Christoph und viele mehr.

Vielen Dank auch an die gesamte Arbeitsgruppe der organischen Geochemie für die vielen schönen Treffen und Unternehmungen, besonders an Kai und Markus für die Hilfe im Labor und die Diskussionen rund um die Moleküle, und natürlich an Birgit, fürs da sein und die Hilfe bei all dem Papierkram.

Danke Solveig, mit Dir zu den Mädelsrunden zu gehen hat mir sehr gut getan und viel Mut gegeben!

Danke auch an die Hiwis und Laboranten, die mich bei der Laborarbeit unterstützt haben: Lars, Sarah, Karsten, Christine, Eva.

Meine ehemaligen Bürokollegen (Julio, Frauke, Arne, Rong), ich danke Euch ganz herzlich für die schöne Zeit mit Euch auf so engem Raum.

Ein ganz großer, lieber Dank geht an alle ehemaligen und noch aktuellen Mitglieder der sich leider auflösenden Super-Arbeitsgruppe Geobiologie, ganz besonders an Esther, Benni, Antonie, Tobi, Lars, Katrin, Henning, Sebastian, Yo und Moataz fürs füreinander da sein, die vielen gemütlichen Frühstücksrunden und anderen Treffen, den Austausch und die Unterstützung. Ich finde, wir waren echt ein tolles Team!

Am allermeisten danke ich aber meinen Eltern, die mich so gut vorbereitet und über die Jahre immer unterstützt haben, meinem Bruder, meinen Freunden und meiner großen Schwiegerfamilie für die Liebe und Herzlichkeit und natürlich meiner kleinen Familie: meinen Liebsten Elena und Marko. Marko, ohne Dich hätte das alles keinen Sinn gemacht und keinen Wert gehabt!

ERKLÄRUNG

Name: Simone Ziegenbalg

Anschrift: Bonygasse 55, 1120 Wien, Österreich

Hiermit erkläre ich, dass ich:

1) die Arbeit ohne unerlaubte fremde Hilfe angefertigt habe,

2) keine anderen, als die von mir angegebenen Quellen und Hilfsmittel benutzt habe

und

3) die den benutzten Werken wörtlich oder inhaltlich entnommenen Stellen als solche kenntlich gemacht habe.

Wien,

Simone Ziegenbalg